Reducing bowel toxicity for rectal cancer with CBCT-based online adaptive radiotherapy

Karoline Lewinsen

Master's Thesis in Medical Technology

Department of Physics and Technology
University of Bergen

June 2022

Acknowledgements

I would like to start by thanking my supervisor Sara Thörnqvist for granting me such an interesting project. This has been an incredibly exciting year, full of learning. Thank you for being so invested in this project, for sharing your knowledge, and for inspiring me with new ideas. I would also like to thank you for being so supportive, positive, and for all the good conversations during the past year.

I would also like to give a special thanks to my co-supervisor Johanna Austrheim Hundvin. Thank you for showing such interest in my work, and for sharing helpful thoughts and ideas on the project. Thank you for always giving thorough and patient explanations. I have really appreciated being able to call you when stuck with dose planning.

Thank you to everyone at Haukelandsbakken for making me feel so welcome. Thank you Liv Bolstad Hysing for showing me how to delineate bowel. I also wish to thank Jon Alfred Brennsæter for helping me get started with the simulation software, and for taking your time helping me when obstacles occurred.

Last but not least, thank you to my friends and family for motivating and supporting me, especially during the past year, but also throughout my whole degree. A special thanks to my fellow students Espen Folkedal and Trygve Birknes who have been with me through thick and thin all these five years. I also wish to thank the rest at room 534 for making the past year so amusing, and for always being so helpful and motivating.

Karoline Lewinsen

Bergen, June 2022

Abstract

Purpose: Daily motion of the rectum requires large safety margins for patients undergoing radiotherapy (RT) for their rectal cancer. Online adaptive RT (ART) using daily CBCT to adjust the plan to the anatomy of the day therefore has the potential to reduce safety margins and expose less normal tissue to RT. In this master, the purpose is to investigate online ART and optimize the beam angle setup to spare the bowel.

Methods: All IMRT dose plans were derived for short course RT 5 Gy x 5, motivated by the update in the national guidelines for rectal cancer. The CTV for standard RT was expanded by 8 mm in all directions except in the ventral direction where it was 10 mm. The PTV margins for the ART plans were based on literature. We used a 12-field class solution (CS) with gantry angles set to 64, 84, 100, 140, 160, 192, 220, 260, 272, 280, 292, and 300°and a 12-fields IMRT with equidistant (EQUI) angles, where the first gantry is sat to 0°, with 30°intervals. The dose optimization in the conventional treatment planning system (TPS) and the online ART TPS is different. Therefore, the plans with line objectives were generated in Eclipse TPS to benchmark the optimization of bowel sparing with Ethos TPS. The ART plans for both the CS and EQUI beam angle setup were simulated in the Ethos training software (Emulator). The IGRT plans for both the CS and EQUI beam angle setup were simulated in Eclipse TPS. The risk for Grade 3 (G3) diarrhea was quantified from a dose-response relationship for rectal cancer with the bowel volume receiving 10 Gy or more as input.

Results: Several steps were established to enable the implementation of the Emulator for online re-planning, such as defining safety margins and clinical goals. The safety margin was set to 4 mm isotropic, but safety margin recommendations were de-

pendent on the time required for delivery of a treatment fraction. The benchmarking plans showed no significant difference when compared to the ART plans with the derived clinical goals. There was a significant reduction in the toxicity risk for bowel from IGRT to ART for both the EQUI beam angle setup (p=0.0003) and the CS beam angle setup (p=0.01). There was no significant difference in the toxicity risk for the two angle beam setups for the ART treatments.

Conclusion: In the course of this project a workflow for daily adaptive RT in the Emulator has been established. Findings in this master thesis indicated that creating gender-specific treatments may lead to more efficient optimization of sparing dose to the bowel and avoidance of elevated dose outside of the target volume. This project gives a solid indication that online re-planning ART can improve treatment of locally advanced rectal cancer by reducing RT dose to healthy bowel. There was a significant reduction in toxicity risk for ART compared to IGRT treatments for both the EQUI and the CS beam angle setup.

Contents

Abbrevations

AI Artificial Intelligence

ART Adaptive Radiotherapy

BED Biologically Effective Dose

CBCT Cone Beam Computerized Tomography

COG Center Of Gravity

CRT Concurrent Chemotherapy and Radiotherapy

CS Class Solution

CT Computed Tomography

CTCAE The Common Terminology Criteria for Adverse Events

CTV Clinical Target Volume

DRE Digital Rectal Exam

DVH Dose Volume Histogram

D98%>95% 98% of the volume receiving over 95% of the prescribed dose.

ESMO European Society for Medical Oncology

EQUI Equidistant

GTV Gross Target Volume

HUH Haukeland University Hospital

ICRU International Comission on Radiation Units and Measurements

IGRT Image Guided Radiotherapy

IMRT Intensity-modulated radiotherapy

IOE Intelligent Optimization Engine

LARC Locally Advanced Rectal Cancer

LCRT Long Course Radiotherapy

LINAC Linear accelerator

LQ Linear Quadratic

MeV Mega electron Volt

MLC Multi Leaf Collimator

MRF Mesorectal Facia

MRI Magnetic Resonance Imaging

MV Mega volt

NCI National Cancer Institute

NTCP Normal Tissue Complication Probability models

OAR Organ At Risk

PET Positron Emission Tomography

PTV Planning Target Volume

QUANTEC Quantitative Analysis of Normal Tissue Effects in the Clinic

RAPIDO Rectal cancer And Preoperative Induction therapy followed by Dedicated Operation

RT Radiotherapy

SCRT Short Course Radiotherapy

TNT Total Neoadjuvant Therapy

TPS Treatment Planning System

V10Gy Volume receiving 10 Gy or more

List of Figures

List of Tables

Chapter 1

Introduction

In 2020, rectal cancer was ranked as the 7th most widespread form of cancer worldwide, estimating more than 730 000 new occurred cases annually [1]. The same year, the number of estimated deaths was almost 340 000, making rectal cancer the 10th most deadliest form of cancer. Norway is one of the countries with highest incidence of rectal cancer, and the prognosis indicates that the incidences of rectal cancer will increase [2]. Every year around 1100 men and women are diagnosed with rectal cancer in Norway [3]. This cancer normally do not occur until after the age of 40, with median ages at diagnosis of 69 years for women and 71 years for men [3]. Symptoms of rectal cancer are blood in the stool [4]. Another symptom is change in bowel habits in the form of alternation between loose stools and slow bowel movements. The relative 5-year survival after the diagnose is 72,6% [3]. This is based on numbers from the year 2016 to 2020 and includes all stages of the cancer.

The rectum is located in the pelvis region and extends 12-15 cm from the anal verge [5]. As illustrated in figure 1.1, the rectum makes up the last part of the digestive system above the anus [4]. If it is discovered that there is a distal extension lower than 15 cm from the anal margin, the patient is diagnosed with rectal cancer [6]. If however, the distal extension is larger than 15 cm from the anal margin, the patient is diagnosed with colon cancer. The cancer is furthermore categorized as low, middle and high rectal cancer. A distal extension up to 5 cm from anal margin is categorized as low rectal cancer, 5-10 cm is categorized as middle rectal cancer, and 10-15 cm is categorized as

high rectal cancer

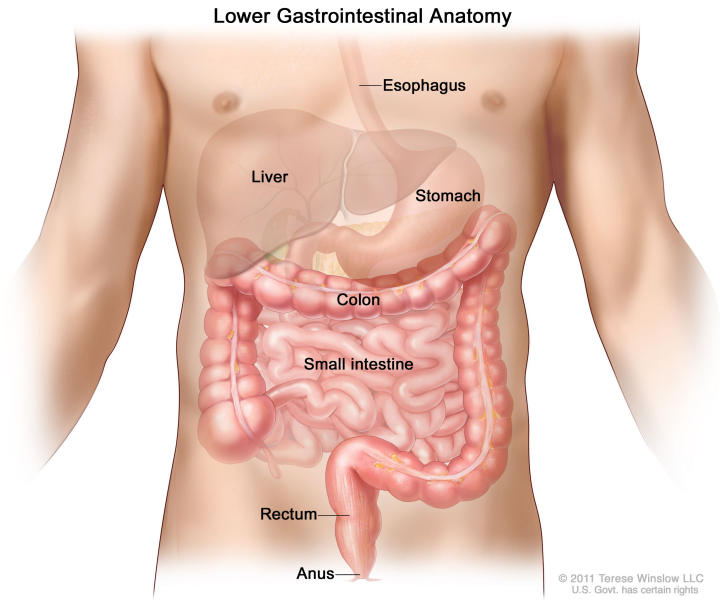

Figure 1.1: The anatomy of the lower gastrointestinal (Image from [4])

As with other cancers, the so-called TNM clinical classification is used to stage rectal cancer [6]. The T refers to the primary tumor, an overview is given in table 1.1, and the number in addition to the T indicates the severity of the ingrowth. The higher the number, the greater the invasion. The classification covers the stage where the small local tumors cannot be assessed to when the tumor invades submucosa and furthermore other organs and structures.

Metastasis is when the cancer cells spread from the origin site to another part of the body [7]. The cancer cells move through the blood and lymph system and form a new tumor in another part of the body. The N, with its additional number and letter, gives information about the presence and extent of nearby lymph node metastasis [6]. The different grades of N are listed in table 1.2. The M covers distant metastasis. The higher the additional number and letter, the more organs the tumor has metastasised to. The different classifications of the M are given in table 1.3.

Table 1.1: TNM Clinical Classification, T-Primary tumor. Table from [6]

TNM Clinical Classification	
T-Primary Tumor	
TX	Primary Tumor cannot be assessed
T0	No evidence of primary tumor
Tis	Carcinoma in situ: Invasion of lamina propria*
T1	Tumor invades submucosa
T2	Tumor invades muscularis propria
T3	Tumor invades subserosa or into nonperitonealised pericolic or perirectal tissues
T3a	Depth of invasion beyond the muscularis propria <1 mm
T3b	Depth of invasion beyond the muscularis propria 1-5 mm
T3c	Depth of invasion beyond the muscularis propria 6-15 mm
T3d	Depth of invasion beyond the muscularis propria >15 mm
T4	Tumor directly invades other organs or structures
T4a	Tumor perforates visceral peritoneum
T4b	Tumor directly invades other organs or structures

Table 1.2: TNM Clinical Classification, N-Regional Lymph Nodes. Table from [6]

TNM Clinical Classification	
N-Regional Lymph Nodes	
NX	Regional lymph nodes cannot be assessed
N0	No regional lymph nodes metastasis
N1	Metastasis in 1 to 3 regional lymph nodes
N1a	Metastasis in 1 regional lymph node
N1b	Metastasis in 2-3 regional lymph nodes
N1c	Tumor deposit(s), i.e satellites in the subserosa, or in non-peritonealised pericolic or perirectal soft tissue wuthout regional lymph node metastasis
N2	Metastasis in 4 or more regional lymph nodes
N2a	Metastasis in 4-6 regional lymph nodes
N2b	Metastasis in 7 or more regional lymph nodes

Table 1.3: TNM Clinical Classification, M-Distant Metastasis. Table from [6]

TNM Clinical Classification	
M-Distant Metastasis	
M0	No distant metastasis
M1	Distant metastasis
M1a	Metastasis confined to one organ (liver, lung, ovary non-regional lymph node(s)) without peritoneal metastases
M1b	Metastasis in more than one organ
M1c	Metastasis to the peritoneum with or without organ involment

The European Society for Medical Oncology (ESMO) presents guidelines for diagnosis and the treatment for rectal cancer [6]. According to ESMO, the digital rectum exam (DRE) is the first diagnostic exam. During the DRE the doctor examines the patient's lower part of the rectum by feeling for abnormal mass. This is followed up by rectoscopy and simultaneously histopathology. During rectoscopy, the rectum is examined using a lighted tube in order to get a clear view of tissue and abnormal mass [8].

The national guidelines refers to rectoscopy with biopsy for setting the primary diagnosis [2]. In addition to rectoscopy there are several other preoperative examinations needed to be done to set the treatment plan. The tumor level and whether or not the tumor has invaded the mesorectal fascia is crucial to both the prognosis and surgical method. Endorectal ultrasound is utilized to be able to determine if the tumor is to be classified as a T1 or T2 level tumor. This examination technique is also the best suited to distinguish between pre malignant and malignant tumors. For more advanced stages MRI is favorable. These preoperative examinations are also important to identify patients with increased risk of local recurrence and metastasis, such as patients with low tumors or tumors that invades the mesorectal facia. The left side on figure 1.2 shows an illustration of the different surrounding layers of the rectum. The right side of figure 1.2 is a illustration of the different tumor classifications and which layer that is invaded by the respective tumor.

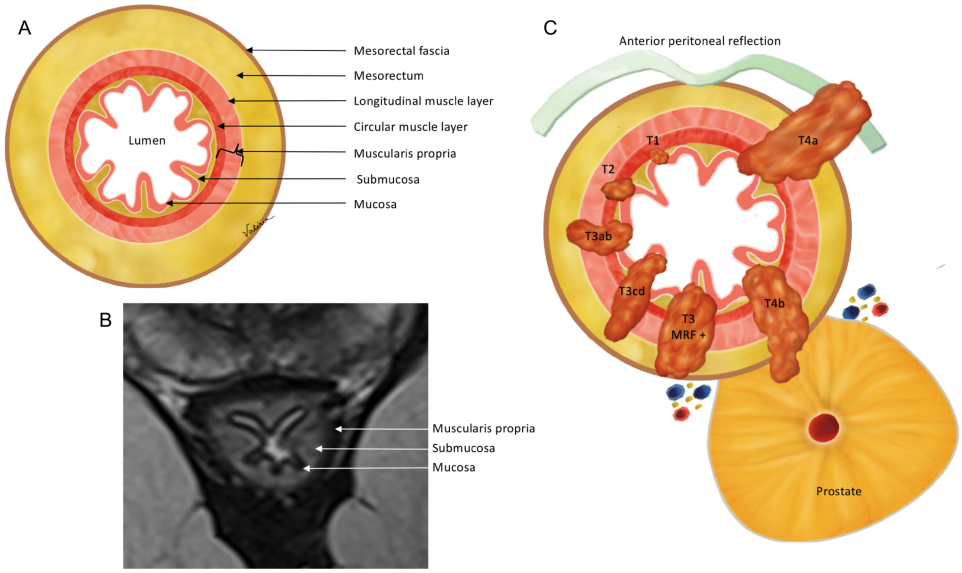

Figure 1.2: A: Illustration of the surrounding layers of the rectum. B: MR image of the muscularis propria, submucosa and mucosa. C: Illustration of the different primary tumors (T-stage) of rectal cancer. T3+ is when the tumor invades beyond the mesorectal fascia (MRF). (Image from: [9])

The different stages of tumors require different forms of treatment [2]. The small tumors with no regional lymph node metastasis (N0) and no distant metastasis M(0) to organs, might only require an operation. Locally advanced tumors are tumors that extends beyond the origin site. This definition includes tumors with greater stages than T3a (table 1.1), and extramural vascular invasion which is direct invasion of a blood vessel [10]. These tumors require an additional treatment to surgery.

1.1 The use of radiotherapy for curative treatment

Patients with locally advanced rectal cancer (LARC) have a large risk for recurrence [11]. The challenge is not local recurrence, but recurrence in the form of distant metastasis. Radiotherapy (RT) is utilized preoperative to shrink and potentially down-stage the tumor. This results in an increased probability of achieving radical surgery of local advanced tumors [2]. Radical surgery is when the surgery is curative and also reduces the chance of recurrence [12]. For rectal cancer it has been shown that RT reduces the risk of local recurrence after surgery with 50% [13]. Both long course RT (LCRT) and short course RT (SCRT) are recommended by ESMO as pre-operative treatment [10]. For LARC the dominant treatment in many countries has been LCRT in combination with chemotherapy and then surgery after 4-8 weeks [14]. LRCT consists of a total dose of 45-50.4 Gy delivered in 25-28 fractions [13], [14]. SCRT consists of a total dose of 25 Gy delivered in 5 fractions over a period of 1 week, following either an immediate surgery of a delayed surgery [13].

1.1.1 Recent advances in treatment of locally advanced rectal cancer

Several studies have shown that preoperative, also called neoadjuvant, chemotherapy has both better effect and less side effects than postoperative chemotherapy [2]. The standard in Norway has been to treat patients preoperative with concurrent chemotherapy and LCRT. Concurrent treatment is when chemotherapy and RT are given at the same time, also called chemoradiotherapy (CRT). Postoperative chemotherapy is prac-

ticed if any unexpected events occur after the surgery. This course of treatment is illustrated in figure 1.3 as standard-care. Larger fractions such as SCRT have been given to patients that are over the age of 75 and with other illnesses.

The Rectal cancer And Preoperative Induction therapy followed by Dedicated Operation (RAPIDO) trial studied if altering the treatment course would reduce the number of patients with distant metastases and following if it would reduce the disease-related treatment failure [11]. The treatment course consisted of SCRT, intensified chemotherapy, so-called total neoadjuvant therapy (TNT), and then surgery. The workflow is illustrated in figure 1.3.

The RAPIDO trial was a multicenter study and 54 centers from different countries participated [11]. The patients included in this trial were newly diagnosed with locally advanced rectal adenocarcinoma, staged as either T4a or T4b and N2. The patients recruited were randomly divided into two treatment groups: the SCRT followed by TNT group and the conventional LCRT. The timing for both the standard treatment and the experimental treatment is illustrated in figure 1.3.

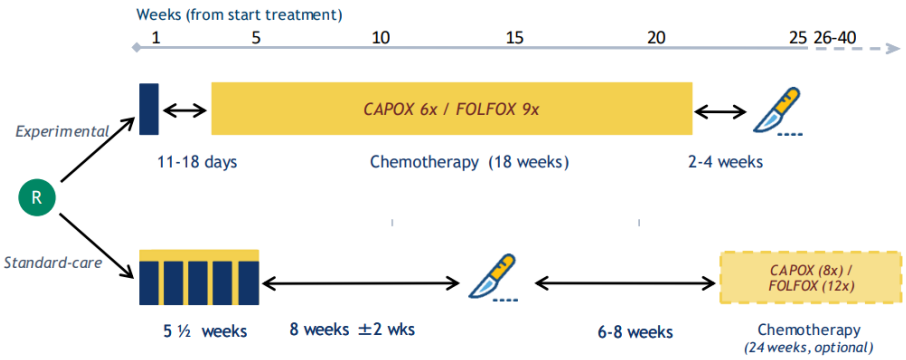

Figure 1.3: Illustration of the workflow for both the standard and experimental treatment. SCRT, week 1: 5 Gy x 5. CRT, week 1-6: 1.8 Gy x 28 or 2 Gy x 25. The black box illustrates one week of RT, knife illustrates surgery, CAPOX and FOLFOX are two types of chemotherapy. (Image from: [11])

The primary endpoint of this trial was disease-related treatment failure. The trial showed a significant difference in disease-related treatment failure between the two treatment courses. The follow-up time was 3 years. The number of patients with distant

metastasis were reduced significantly in the experimental treatment group compared to the standard care of treatment group, as illustrated in figure 1.4. The results from the trial showed that the amount of patients in the experimental treatment group that underwent surgery with curative intent was 92% [11]. In the standard of treatment group, 89% of the patients had surgery with curative intent. The experimental treatment had a longer course of chemotherapy which was mainly the reason for the fact that 15% stopped chemo in the experimental arm, compared to the 9% for patients undergoing CRT. Reduction of chemotherapy doses was made for 44% vs 6% in the experimental and CRT treatments respectively. The trial discovered a difference in pathological complete response, meaning disappearance of all signs of cancer, between the two groups. The pathological complete response rate of the patients in the experimental treatment group was 28%, compared to 14% in the standard of treatment group. However, the response of the of the remaining patients are not listed.

There is an ongoing discussion if whether the experimental arm in the RAPIDO trial should be implemented as the new standard treatment for patients with rectal cancer [15]. Some of the findings of the RAPIDO trial is hard to compare with other neoadjuvent trials for rectal cancer as the conclusion of the RAPIDO trial is based on an endpoint that has not been validated earlier. Though there was a significant reduction in number of patients with distant metastasis in the experimental group compared to the standard group, there were more adverse events in the experimental group than the standard group [11]. During preoperative treatment, Grade 3 or higher adverse events occurred in 219 (48%) of 460 patients in the experimental group, compared to 109 (25%) of 441 in the standard of care group and in 63 (34%) of 187 patients in the standard of care group during post-operative chemotherapy [11]. Severe diarrhea was the most common serious adverse event in both treatment groups. Severe diarrhea (Grade 3 or higher, figure 2.15), occurred for 18% of the patients in the experimental group and for 9% of the patients in the standard group.

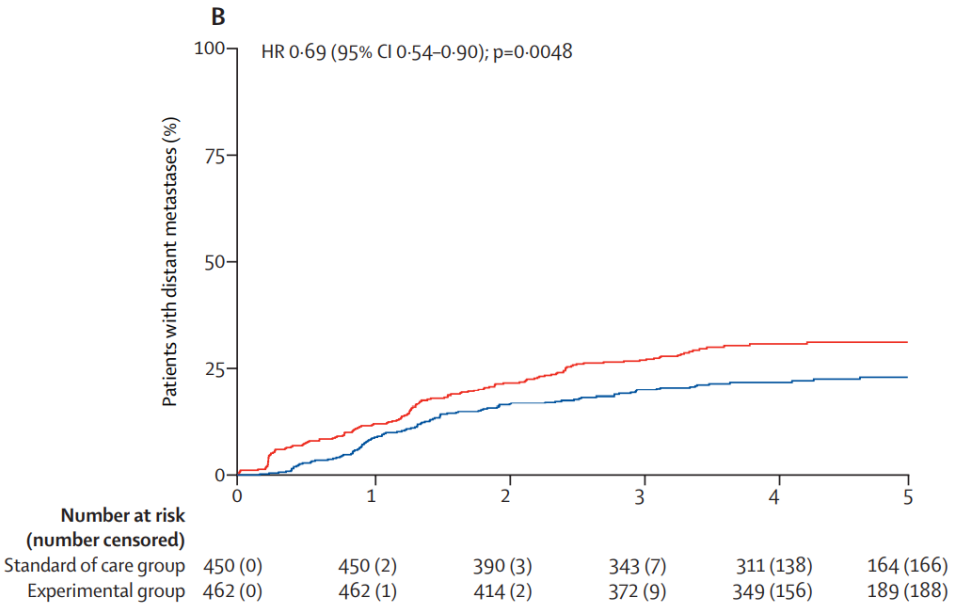

Figure 1.4: Percentage of patients with distant metastasis for both the standard of care group (red) and the experimental group (blue). (Image from: [11])

1.1.2 Project motivation

The purpose of this thesis is to investigate if daily adaption of the RT dose can reduce dose to the healthy bowel and thereby reduce the risk of severe diarrhea. Daily adaption of RT is available through the most recent investment in RT delivery, called the Ethos system, at Haukeland University Hospital (HUH). This is the first work with the Emulator, a virtual simulation software, to develop and evaluate a daily adaptive workflow. The goal is that the results can be contribute to a clinical implementation. The main objectives are:

(i) Prepare for daily adaptive RT by define margins for motion occurring within a treatment fraction (intrafractional) based on literature, and optimize RT beam angle setup to spare bowel.

(ii) Implement daily adaptive RT in the Ethos training software (Emulator) focusing on bowel sparing.

(iii) Evaluate the planning performance of the implementation in (ii).

(iiii) Compare the amount of bowel sparing for daily adaptive RT and current standard RT delivery.

The main part of this thesis involved generating treatment plans and simulating treatment in Eclipse treatment planning system and Ethos treatment planning system.

Chapter 2

The principles of radiation therapy

The fundamental principle of radiation therapy is to use ionizing radiation to destroy cancer cells, without causing intolerable damage to the adjacent healthy tissue [16]. This chapter presents the most relevant theory used in radiation therapy, including the physics of the radiation beams, their interaction with biological matter, and different dose delivery approaches.

2.1 Physical interactions of a photon beam

The most common type of RT is external RT, where treatment machines deliver radiation direct towards the cancer cite from outside the body [17]. Electromagnetic waves in terms of high energy x-rays, also referred to as photon beams, are mostly used [17]. These beams are capable of traveling through a cross section of the patient's body and are normally produced by a linear accelerator (Linac) [18]. The Linac accelerates charged electrons to a high-energy electron beam, which can be used directly for treatment or in the generation of a photon beam. When treating patients with photons, the accelerated electrons are directed toward a high atomic metal in the treatment head. Due to Coulomb forces of attraction, the electrons may interact and deflect from their paths and lose energy in terms of bremsstrahlung, producing a spectrum of high-energy x-rays. The maximum energy of the spectrum is approximately one-third [18]. Hence, the energy of the electron beam is discrete and can be expressed in mega electron volts (MeV), while the photon beam energies are expressed in terms of their maximum energy stated in megavolts (MV). Typical photon beam energies used in RT are 6 MV and

15 MV.

When a beam of photons passes through a medium, interactions between the photons and the matter may occur. The most important interactions for photons are the photoelectric effect, Compton scattering and pair production [18]. The photoelectric effect occurs at energies below 1 MeV and takes place when a photon is completely absorbed by an atom. As a result, one of the atom's orbital electrons is ejected with a kinetic energy of the photon energy minus the binding energy, E_{photon} - $E_{binding}$. The dominant mode of interaction in external beam radiation therapy is Compton scattering [16]. The predominant mode for Compton scattering in water is 30 keV to 24 MeV [18]. In this process the photon energy is much higher than the binding energy, resulting in an interaction with a bound electron as if it would be a free electron. The photon is scattered with a change in direction and reduced energy, while the electron receives energy and is emitted from the atom. Pair production takes place when photons convert into an electron-positron pair in interaction with the electromagnetic field of the atomic nucleus [18]. The rest mass of the electron is 0.51 MeV, meaning that photons with energies over the 1.02 MeV threshold can create an electron-positron pair by converting energy into mass, leaving the excessive energy as kinetic energy distributed between two particles.

Photons are indirectly ionizing, meaning that through interaction with matter the photons beam liberates electrons which are directly ionizing [18]. Ionization is when a neutral atom obtains a positive or negative charge, and excitation is when energy lost by an interacting particle isn't sufficient to eject an electron from the atom but raises the electrons to a higher energy level [18]. The energetic electrons that are liberated from the interactions mentioned above, transfer energy to the medium through ionization and excitation [18]. In other words, it is the liberated electrons that deliver the absorbed dose [16]. The mean energy, $d\bar{E}$, liberated to the mass dm constitutes the definition of absorbed dose as shown in equation 2.1. Absorbed dose is measured in

energy per mass (J/kg), using the unit gray (Gy).

$$D = \frac{d\bar{E}}{dm} \tag{2.1}$$

As the photons interact with matter, the photon beam attenuates [18]. The intensity of the photon beam as a function of distance within a given medium is described with equation 2.2, where *I(x)* is the intensity after a distance, x cm the medium. I_0 is the initial intensity, μ is the attenuation coefficient and x is the thickness.

$$I(x) = I_0^{-\mu x} \tag{2.2}$$

The attenuation coefficient varies with the absorbing matter, and can also be referred to as the probability that an atom will interact with one of the photons in the beam [19]. The attenuation coefficient for water decreases with photon energy as illustrated in figure 2.1, hence the higher the energy of the photon beam, the greater the penetration power in the patient [18].

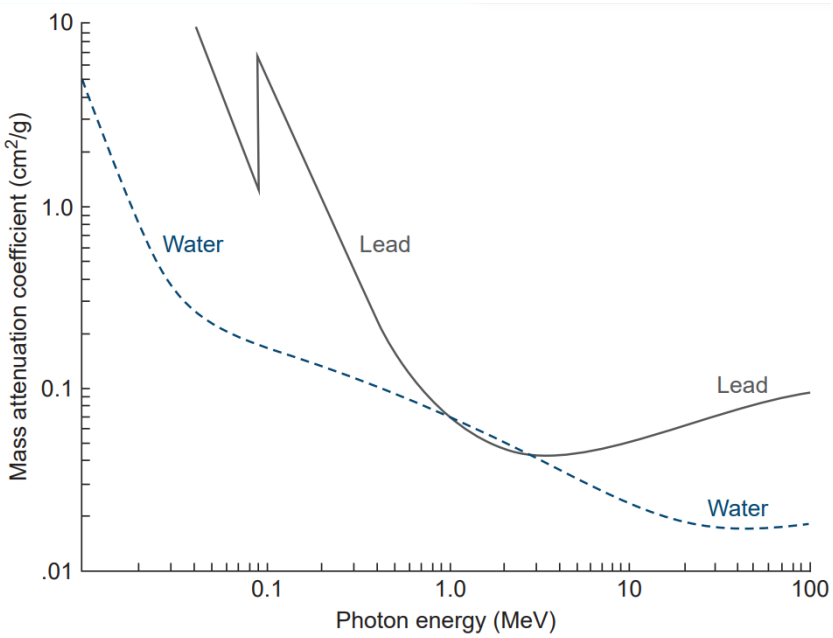

Figure 2.1: The mass attenuation coefficient of water and lead as a function of the photon energy. Image from [18]

Increasing energy also results in an increase in depth of the dose maximum [16]. Figure 2.2 illustrates how the dose maximum appears at an increased depth for a 15 MV photon beam compared to a 6 MV photon beam. The 6 MV photons have a higher entrance

dose and the 15 MV photons have a higher exit dose. Both curves show an initial build-up prior to the peak. This is due to the fact that when photons beams enter the patient, electrons are liberated caused by the interaction between the photons and the body tissue. The number of electrons increases for each passing layer within the patient's body until electron equilibrium is reached. The electron equilibrium is characterized as the range of the electrons and is where the dose maximum is obtained. As the electron equilibrium is within the patient, this is also called the skin-sparing effect. Due to the attenuation of photons, the absorbed dose decreases with distance beyond the dose maximum.

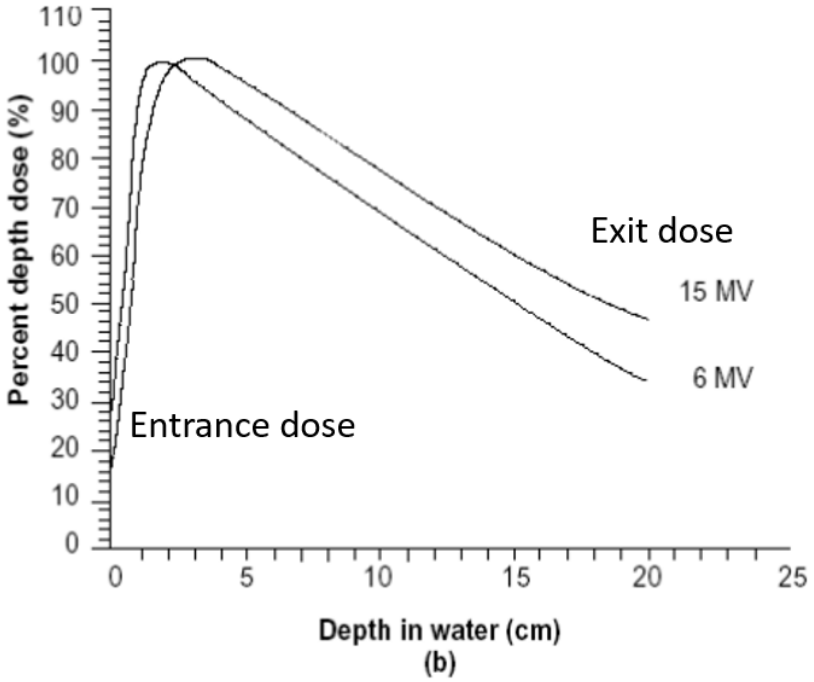

Figure 2.2: Dose depth curve for 6 MV photons and 15 MV photons. Dose is expressed in % and distance is expressed in cm. Image from [20]

2.2 Radiobiology

Radiobiology is the study on how ionizing radiation affects the biology of organisms [21].

2.2.1 The target of Radiotherapy

The target of RT is the DNA in the cells, more specifically, the intention is to deliver radiation to destroy the cancer cells' ability to reproduce [21]. The DNA consists of two strands held together by hydrogen bonds between pairs of bases. Irradiation of the cells can result in single-strand breaks, yet this does not necessarily cause permanent damage. As the DNA consists of two strands, it can copy the opposite strand and repair the damage. However, if the radiation causes a double-strand break of two opposite strands, it is more likely to result in permanent damage as the DNA no longer has the ability to copy the opposite strand.

2.2.2 Cell Cycle and damage from irradiation

Clonogenic cells have the ability to proliferate [16]. The time from a cell proliferates to the next generation of cells do the same is known as the cell cycle time, T_c [21]. The cell cycle consists of different phases and is illustrated in figure 2.3. Mitosis, also known as cell division, is the phase where the division of the chromosomes and two daughter cells occur. This is followed by the gap G1, where there is low activity. The next phase is the S phase, the synthesis of the DNA. During this phase, the DNA is replicated. The synthetic phase is then followed by another gap with low activity, G2.

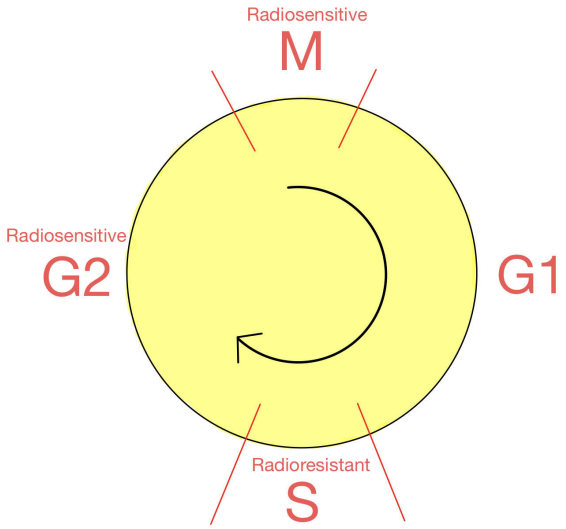

Figure 2.3: Illustration of the cell cycle. The S phase is a radioresistant phase, while the G2 and M phases are when the cells are the most radiosensitive.

The radiosensitivity of the cell varies with the different phases. The cell is most radiosensitive close to and at the mitosis phase, and most radioresistant in the synthesis phase. It is believed that the reason for the cell being more radioresistant in the synthesis phase is because in this phase the DNA is duplicated [21]. In case of any destruction of the DNA, it is more likely to be able to copy an opposite string [21].

Normal cells have control of the production and release of the signals that stimulate growth and the different phases in the cell cycle [22]. This results in the preservation of the function of the cells, and also stability in the number of cells. For cancer cells, on the other hand, this control has been disrupted through mutations [22]. This gives the cancer cells the ability to proliferate at a much higher rate than normal cells. However, the cancer cells may not evolve properly and the ability to detect and repairing damage to the DNA can be disrupted. Hence, when damaged by irradiation, normal cells can potentially regenerate the normal tissue more rapidly than the altered tumor cells composing the cancer. The difference is fundamental in RT.

2.2.3 The Linear Quadratic model

The linear quadratic (LQ) model is a preferred model when calculating cell survival for different dose per fraction used in RT [23]. The LQ model is based on the fact that there are two parameters, single and double strand-breaks, when it comes to killing cells by radiation [21]. One, α, is proportional to dose, and the other, β, is proportional to the square of dose. The model is given in equation 2.3, where S is the survival probability of a cell following exposure to a single dose, D, where α and β are constants.

$$S = e^{(-\alpha D - \beta D^2)} \tag{2.3}$$

When the linear contribution to cell killing (αD) equals the quadratic contribution (βD^2), the dose can be expressed as the ratio of the constants.

$$\alpha D = \beta D^2 \tag{2.4}$$

$$D = \frac{\alpha}{\beta} \tag{2.5}$$

Early responding tissue has a higher $\frac{\alpha}{\beta}$ ratio. This is illustrated in figure 2.4, where the cell survival curve for a low $\frac{\alpha}{\beta}$ ratio is more curved compared to the higher $\frac{\alpha}{\beta}$ ratio, due to the different contribution from the quadratic component. The $\frac{\alpha}{\beta}$ ratio has been calculated for different tissues, but the standard $\frac{\alpha}{\beta}$ values for early and late responding tissue are respectively 10 Gy and 3 Gy.

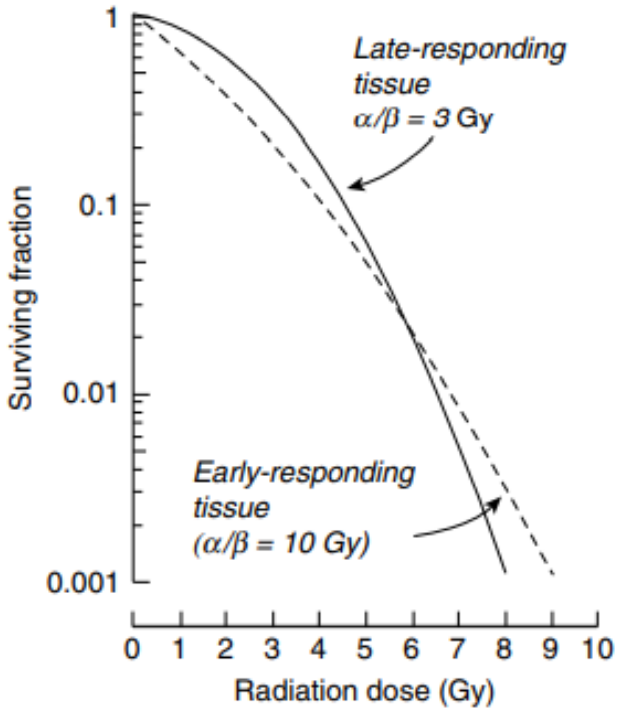

Figure 2.4: Illustration of the cell survival fraction as a function of the radiation dose. (Image from [16])

The $\frac{\alpha}{\beta}$ ratio also expresses the dose-per-fraction sensitivity of the tissue [23]. Late responding tissue has shown to be sensitive to changes in dose per fraction. Figure 2.5 illustrates how the curves of low α/β ratio are much steeper and curved than the curves of high α/β ratio. In other words, tissues with a low α/β ratio are far more resistant to low dose per fraction than tissues with high a α/β ratio [24]. As the α/β ratio of normal tissue may differ from the α/β ratio of tumors, the various types of tissues will benefit from the different doses per fraction [24].

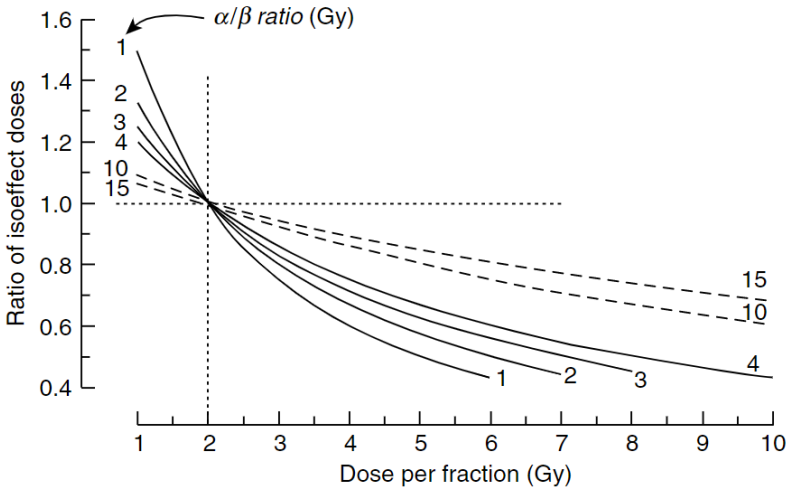

Figure 2.5: Illustration of how the total dose needs to be altered in order to maintain a constant level of effect when adjusting the dose per fraction (Image from [16], page 168)

2.2.4 Fractionation

The different radiobiological mechanisms of tumors and late responding tissue are exploited in fractionation. Fractionation is dividing the total prescripted dose into smaller fractions, distributing the dose over a period of time [18]. The linear quadratic approach on fractionation illustrates how this strategy increases cell survival [21]. As illustrated in figure 2.6, the shoulder of the cell survival curve is repeated for each fraction. This is because the time interval between each fraction allows for sublethal damage repair, which results in increased survival of normal cells and hence reduction in damage to normal tissue. Still, there needs to be a balance between sparing normal tissue and preventing the surviving tumor cells to repopulate.

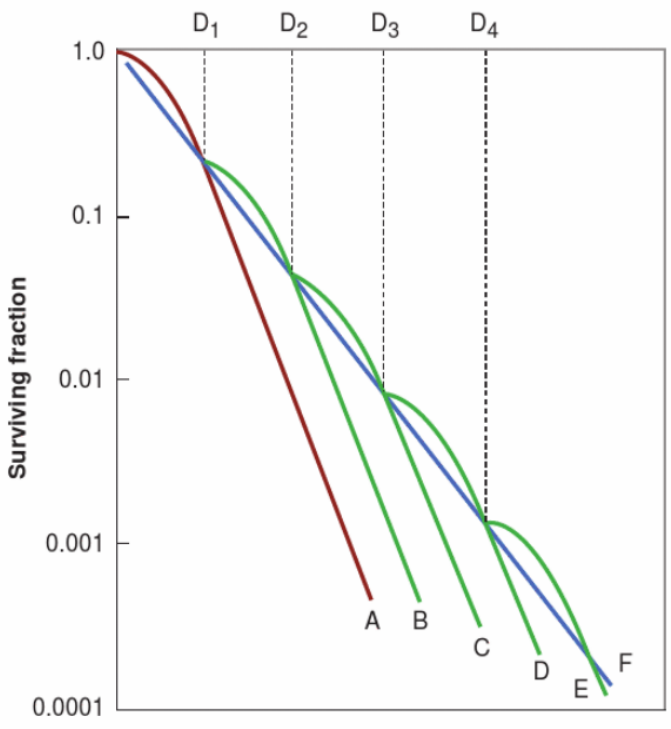

Figure 2.6: Illustration of the survival curve for a multifractional regimen. The y-axis represents the surviving fraction, and the x-axis represents the fraction doses. Image from [21]

Table 2.1: Short abbreviation of the different fractionation schemes utilized in RT.

Fractionation schemes	
Conventional treatment	Conventional fractionation is given in 1.8-2 Gy per fraction [16]. The delivery period is normally 5-7 weeks.
Hyperfractionation	The dose per fraction is below the conventional level of 1.8-2 Gy [16]. Combined with accelerated fractionation, which involves delivery of more than once fraction per day.
Hypofractionation	In comparison to conventional fractionation, the dose per fraction is increased, and the number of fractions are decreased [16].

Both conventional fractionation and hypofractionation listed in table 2.1, are used in rectal cancer treatment. The biologically effective dose (BED) is often used to compare the different fractionation schemes as it is a measure of the biological effect. The BED equation is given in equation 2.6, where n is the number of fractions, d is the dose per fraction, and D is the total dose delivered. The α/β value is set to 10 Gy for the rectal tumor.

$$BED = nd[1 + \frac{n}{(\frac{\alpha}{\beta})}] = D[1 + \frac{d}{(\frac{\alpha}{\beta})}] \tag{2.6}$$

2.3 Dose prescription and plan evaluation

Prior to the course of RT, there needs to be sat a diagnosis which is done by biopsy and medical imaging [16]. The procedures for these can be different from different tumor sites, and information specific to rectal cancer was given in chapter 1. The pre-RT workup starts with obtaining CT scans of the patient in treatment position, in addition to MRI scans and also PET-scans if needed.

2.3.1 Tumor Volume Definition in treatment of rectal cancer

The International Commission on Radiation Units and Measurements (ICRU) reports specifies the terminology and the characteristics of the volumes that are relevant to RT [16]. The ICRU stipulates two tumor volume definitions, gross target volume (GTV) and clinical target volume (CTV). The GTV and CTV are defined by oncologists, as is the prescribed dose. The GTV and CTV can be defined either as a whole organ or more commonly as part of an organ. Bladder and prostate cancer are examples of cancer types where the whole organ previously was considered a GTV, due to poor visibility

of tumor on CT. Another important volume is the planning target volume (PTV), which is a margin-related volume [25]. These three-volume definitions are visualized in figure 2.7.

GTV is the tumor volume as detected on images, the macroscopic tumor [2]. When it is the *primary tumor* that is drawn, the structure may be entitled GTVp. The GTVp is illustrated in figure 2.7. The CTV includes the GTV in addition to subclinical diseases, which are not detected on images [26]. For CTV there are practiced elective volumes and boost volumes. The elective volume includes the lymph node regions. The elective CTV structure is named CTVe_46 or CTVe_25, depending on the amount of total dose delivered. The boost volume, CTVp_50, receives a higher dose than the rest of the target. The elective CTV and boost CTV are illustrated in figure 2.7. In order to cure cancer, the sub-clinical spread needs adequate treatment as well as the tumor volume [18].

The ICRU stipulates that the CTV should be expanded with a safety margin, creating the PTV, in order to ensure that the planned dose actually reaches the CTV [25]. In RT there are execution uncertainties that need to be taken into account when planning the dose delivery [27]. These uncertainties can be divided into systematic errors and random errors. The systematic errors cause a shift in the dose distribution while the random errors unfocus the dose distribution. Both the systematic and random errors can have the same source. One important source of error is organ motion. The drawn PTV is named PTVe_46 or according to the national guidelines, and the PTV of the boost volume is named PTVp_50 [2]. These structures are illustrated in figure 2.7.

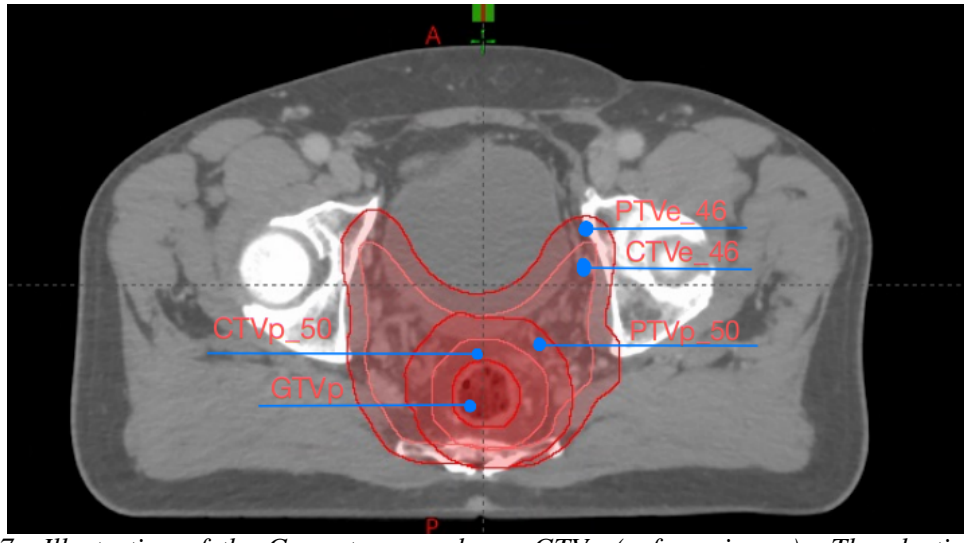

Figure 2.7: Illustration of the Gross tumor volume, GTVp (p for primary). The elective volumes CTVe_46 and PTVe_46, 46 for receiving 46 Gy. The primary volumes CTVp_50 and PTVp_50 receiving 50 Gy.

It is not possible to identify the systematic and random errors for the individual patient until after completed treatment. However, the error data from former patients in a similar treatment group may be assessed [28]. This population data is used when calculating the sufficient PTV margin. Van Herk et al. developed a margin recipe that guarantees that 90% of the population receives a minimum of 95% of the prescribed dose to the CTV [27]. This function is given in equation 2.7, where M is the margin, Σ is the systematic error and σ is the random error. As the equation shows, the systematic errors are weighted more as they can result in the same volume being underdosed.

$$M = 2.5\Sigma + 0.7\sigma \tag{2.7}$$

The ICRU 83 rapport recommends that 98% of the PTV volume, D98%, should receive 95% of the prescribed dose and that no more than 2% of the PTV volume, D2%, should receive over 107% of the prescribed dose [29].

Organs at risk (OARs) are non-target organs surrounding the PTV which may sustain damage from the radiation [16]. In addition to the target volume it is also procedure to delineate the surrounding OARs. This allows assessing the dose distribution to normal tissue and imposing restrictions on the amount of dose the OARs can receive in order to avoid side effects from treatment.

Figure 2.8: Illustration of a structure set for a patient diagnosed with rectal cancer. The red structures are the target volume structures. The yellow structure is the bladder, the magenta is bowel bag, and the green structure is the rectum.

2.3.2 External beam

The data from the CT scan is implemented in a treatment planning system (TPS). The TPS gives complex information about the dose distribution within the patient using the desired treatment field setup [16]. Three-dimensional Conformal RT, Intensity-modulated RT (IMRT), and Volumetric Modulated Arc Therapy (VMAT) are three developed RT techniques that utilize 3D-anatomic information [30]. In order to fit the high dose to the target volume, and at the same time spare the normal tissue, these techniques use a multileaf collimator (MLC) [31]. MLC consists of two opposite banks of multiple attenuating leaves that are made out of tungsten alloy. These are controlled by a computer, allowing for shaping the beams to the target volume as illustrated in figure 2.9.

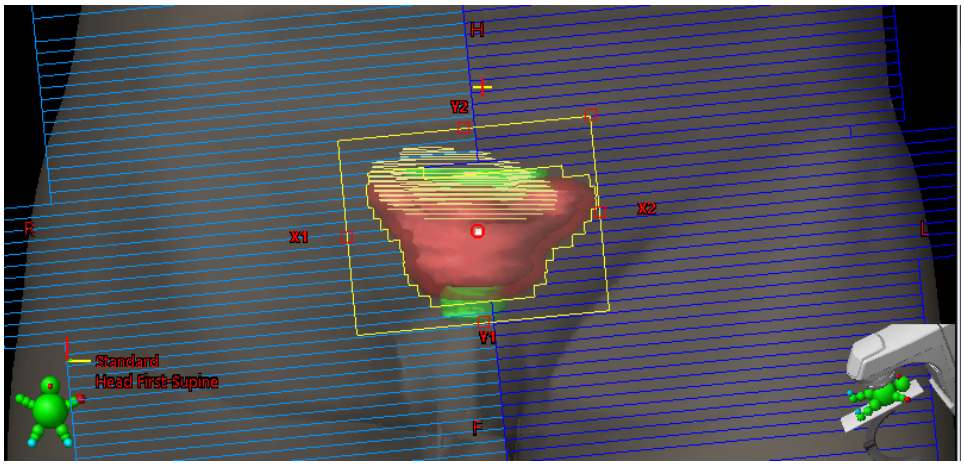

Figure 2.9: The MLC are used in 3D-Conformal RT, IMRT and VMAT. The MLC consists of two opposite banks with attenuating leafs which are outlined in blue. The target is delineated in red.

Forward-planning treatment technique

The 3D-Conformal RT treatment technique utilizes a 3D-TPS. This allows for viewing and planning 3D images and 3D-beam alignments [31]. In the conventional forward-planning system the beam directions, number of fields, beam weights, and intensity modifiers are chosen on a trial-and-error basis [18]. This planning technique can therefore become very time-consuming. In 3D-Conformal RT the beams are delivered with uniform intensity across the field [32]. The concept of 3D-Conformal RT is to align often multiple fields to shape the beam to deliver a uniform and heightened dose to the target volume, while simultaneously sparing the OARs and normal tissue.

As mentioned earlier and illustrated in figure 2.2 the dose distribution of a field is higher closer to the skin than further into the patient. Using several beams makes it possible to deliver a high dose to the target volume as overlapping beams result in a higher deposited dose, illustrated by two opposite beams in figure 2.10. The greater amount of beams, the better fitting of the dose to the target volume, quality of the dose distribution termed *dose conformity*. The dose plan with 4 fields in figure 2.11 shows a more conform dose distribution compared to the plan consisting of 2 fields, as it gives a better fitting of the high dose to the target volume, at the expense of a larger volume receiving low dose from the fields.

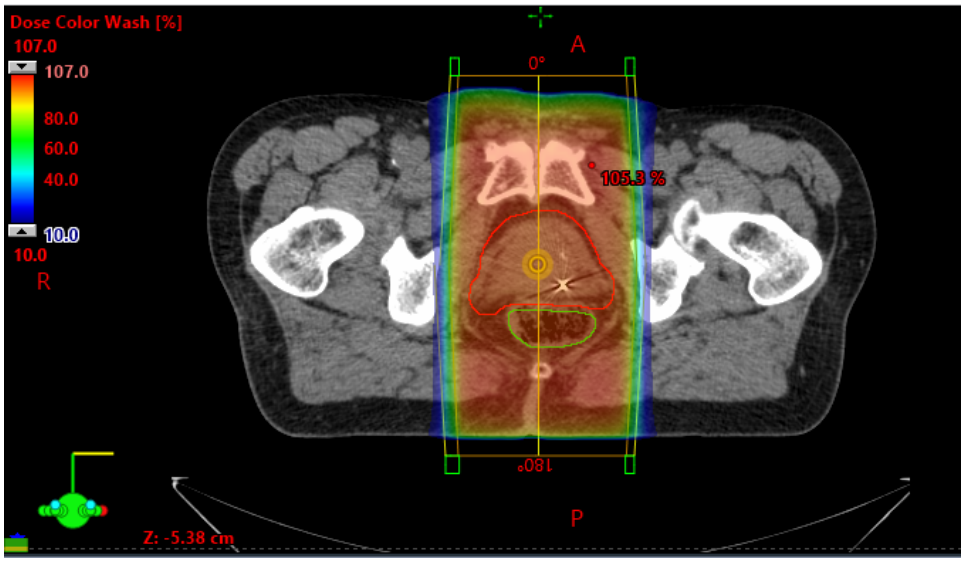

Figure 2.10: Dose distribution from the 3D planning system Eclipse. The dose scale in the left of the figure illustrates that high dose is represented as red and lower dose is in the blue color scale.

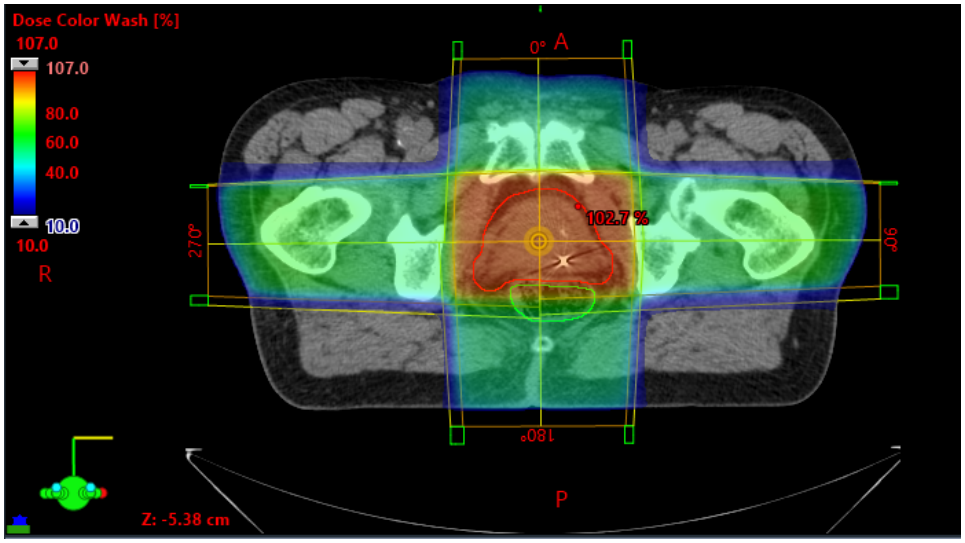

Figure 2.11: Dose distribution from the 3D planning system Eclipse. Utilizing 4 beams results in a better fit of the target volume.

Inverse planning treatment technique

Both VMAT and IMRT are inverse planning techniques and enable the possibility of a nonuniform beam intensity across the radiation field [32]. In contrast to the 3D-Conformal RT technique, where the fields are adjusted to find the optimal dose distribution, the desired optimal dose distribution is the inverse planning technique's starting point. This means that the prescribed dose to the targets and accepted dose to OARs are defined by the dose planner, as well as the field setup, and then the TPS strives to fulfill these criteria by adjusting the fluence of the given fields. IMRT involved a specific set of beam angles, typically less than 10, while VMAT rotates the gantry around the patient during beam delivery [18]. Figure 2.12 shows dose distribution with 9 fields.

Compared to the 3D-Conformal RT technique, IMRT spares more normal tissue delivering a higher dose to the target volume. This can also be illustrated with the dose line profile for the treatment plan in figure 2.13, where the IMRT plan with 9 equidistant beams generates a difference of about 50-60% between the maximum dose to the target and the low dose in normal tissue in the given cross-section.

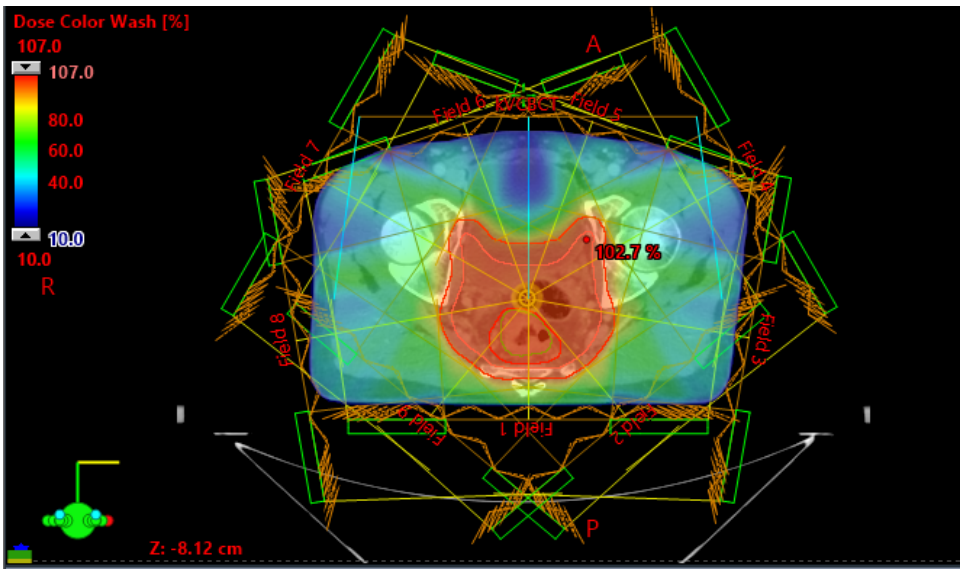

Figure 2.12: Dose distribution for an IMRT-plan from the 3D planning system Eclipse. The treatment plan consists of 9 different gantry angles.

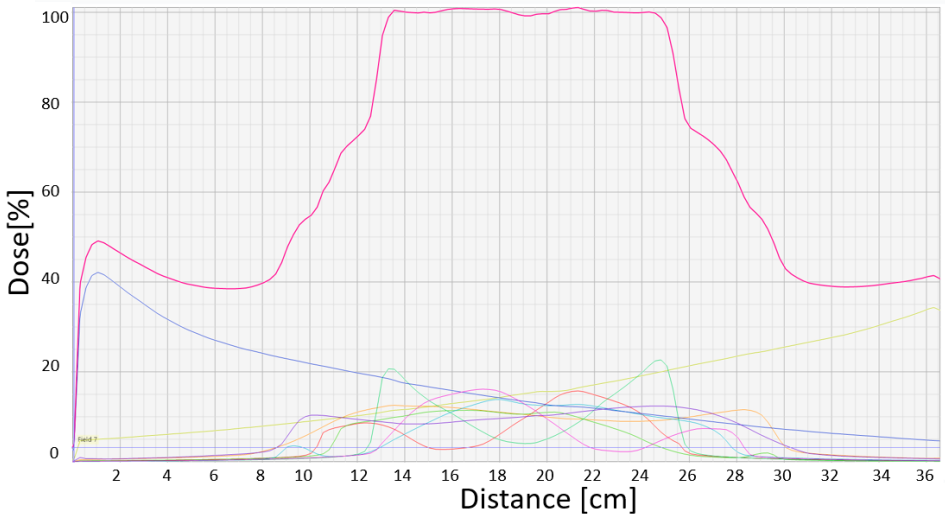

Figure 2.13: The Dose line profile for an IMRT plan with 9 equidistant beams.

2.3.3 Dose Response

When planning the acceptable dose distribution, the decision-making is based on measuring the risk up against the benefit for the individual patient. The effects of RT can be divided into two categories, early and late effects [21]. When planning the dose, fractions, and treatment period one needs to consider both. Prolonging the treatment time spares early reacting tissues, while this has little effect on late-reacting tissues. The size of the fractions will however influence the late effects.

Dose-volume histogram (DVH) is a graph that gives quantitative information about the amount of dose distribution to the structures of interest [16]. This makes DVH a useful tool when wanting to compare potential dose distributions. Figure 2.14 shows an example of a DVH. The ratio of total structure volume is given in percentage on the y-axis and the dose level is given on the x-axis. However, the DVH does not give any prediction of the toxicity risk, but the DVH can be utilized as input to Normal tissue complication probability models (NTCP). The NTCP connects different dose levels to a toxicity endpoint for a population [33]. One NTCP model that is frequently used in studies when wanting to calculate the toxicity risk is done by taking a dose-volume cut-off point from the DVH.

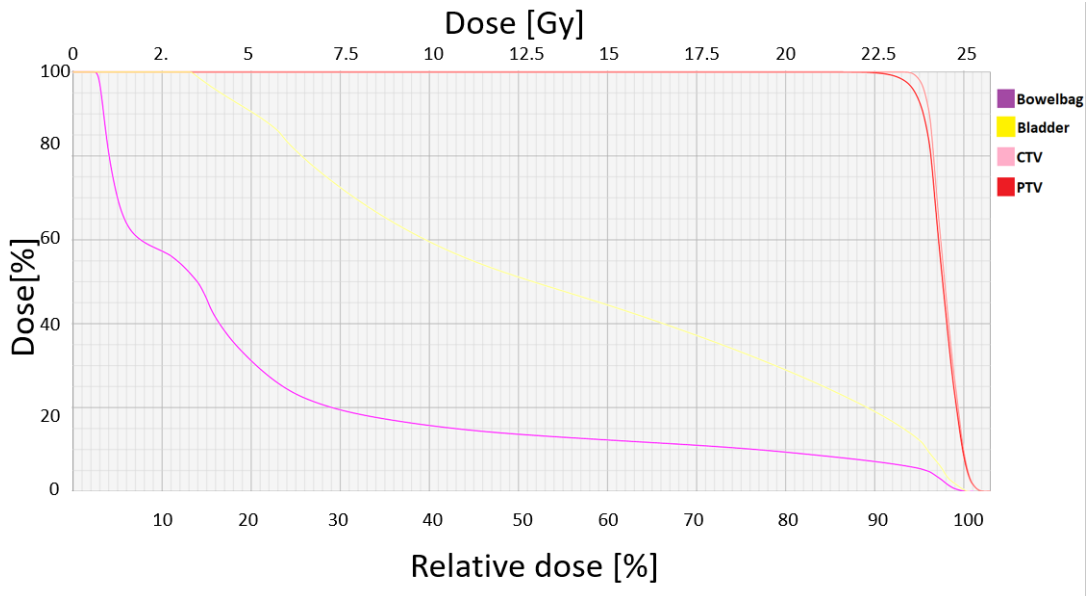

Figure 2.14: Dose Volume Histogram showing amount of dose distributed to the structures bowel bag, bladder, CTV and PTV.

When prioritizing normal tissue, it would be ideal to be able to predict the toxicity in regard to dose exposure. The Quantitative Analysis of Normal Tissue Effects in the Clinic (Quantec) has been reviewing various studies for data about normal tissue complications as followed by RT treatment. The overview of the normal tissue complications is mostly listed as dose to volume and the following risk of a specific grade of complication. The Common Terminology Criteria for Adverse Events (CTCAE) released by the National Cancer Institute (NCI) is an internationally accepted standard for defining and categorizing adverse events [34]. An adverse event is defined as a symptom or disease that may have occurred as a result of medical treatment such as RT. The CTCAE consists of a definition of the adverse event and the severity listed as grades. Grade 1 is described as mild, and the patient is either asymptomatic or has mild symptoms of the adverse event. Grade 1 is often found as a negligible clinical consequence and rarely scored in the RT-induced toxicity reports [35]. Grade 2 is moderate, Grade 3 severe, Grade 4 life-threatening, and Grade 5 is when the adverse event is the cause of death [34]. Each adverse event has a description of the symptoms of the different grades, which makes a well-guided reporting system. An example of an adverse event and definition of the severity grades is presented in figure 2.15.

Gastrointestinal disorders					
CTCAE Term	**Grade 1**	**Grade 2**	**Grade 3**	**Grade 4**	**Grade 5**
Diarrhea	Increase of <4 stools per day over baseline; mild increase in ostomy output compared to baseline	Increase of 4 - 6 stools per day over baseline; moderate increase in ostomy output compared to baseline; limiting instrumental ADL	Increase of >=7 stools per day over baseline; hospitalization indicated; severe increase in ostomy output compared to baseline; limiting self care ADL	Life-threatening consequences; urgent intervention indicated	Death
Definition: A disorder characterized by an increase in frequency and/or loose or watery bowel movements.					
Navigational Note: -					

Figure 2.15: Description of the symptoms occurring in the different grades of the adverse event diarrhea. (Image from [34])

In order to utilize the DVH to minimize the risk of specific normal tissue complications, the tolerance needs to be quantified. As the focus of this thesis is to reduce the toxicity of the bowel, I have only included a section about the small bowel.

Small bowel

When the target volume is located in the torso, the stomach and small bowel are often exposed for irradiation. Acute and late RT-induced complications can be nausea, diarrhea, obstruction, bleeding/ulceration, weight loss, and fistula [35].

Based on an analysis of patients that had undergone conventional-fractionated RT for rectal cancer, Baglan et al. discovered a significant correlation between the different absolute volumes and Grade 3 acute toxicity [36]. Patients that did not experience Grade 3 toxicity had a mean absolute volume of 127 cc that received 15 Gy (V15 Gy). For the patients that did experience Grade 3 toxicity the mean V15 Gy was 319 cc. The Baglan-Robertson model is shown in figure 2.16. Patients below the curve have a low risk of toxicity, which constitutes to 10% of Grade$\geq$3 acute toxicity. The patients above the curve have a high risk, approximately 40%, of Grade $\geq$3 acute toxicity.

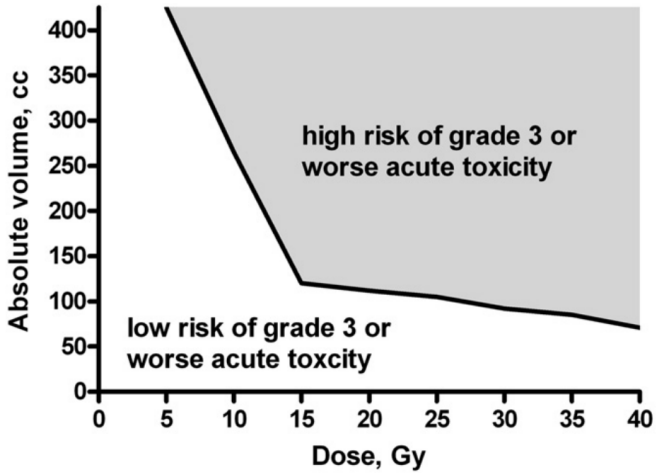

Figure 2.16: The Baglan-Ropertson model which shows the threshold for the risk of acute small-bowel toxicity. (Image from [35])

The cutoff point of the Baglan-Roberston model was 120 cc receiving 15 Gy [35]. It is important to remark that Bagland and Roberton delineated the bowel loops only. Roeske et al. on the other hand delineated the whole bowel cavity, which is the whole area where the bowel loops potentially can be located [37]. This resulted in a much higher absolute volume threshold. The volume of the bowel cavity receiving 45-50 Gy should be lower than 195 cc. These and other studies led to Quantec setting two different guiding clinical goals to withhold to minimize the risk for Grade $\geq$3 acute toxicity for small-bowel [33]. If the small bowel is delineated as individual loops then V15 Gy < 120 cc. If the small bowel is delineated as a bowel cavity then V45 Gy < 195cc.

In 2019, Holyoake et al. did a meta-study on small bowel dose-volume for conventional-fractionated rectal cancer RT [38]. The results showed that for patients with Grade$\geq$3 toxicity the dose-volumes V5 Gy - V40 Gy, volumes receiving 5 Gy - 40 Gy, were sig-

nificant. The DVH parameter with the strongest significance for predicting toxicity risk was V10 Gy.

2.4 Radiation therapy delivery

To make the setup position fixed, there are fixation devices to stabilize the patient in a comfortable position [16]. Fixation devices may be sandbags for general support, knee supports or headrests made of hard plastic, vacuum bags, or thermoplastic casts. It is important that the fixation devices are made of material that will not cause too much disturbance to the dose distribution. The CT scans are used to define and delineate the tumor volume and OARs. There have been advances in treatment delivery technology that allows for a higher dose distribution to the target volume while simultaneously sparing the normal tissue surrounding the target. Two of these delivery techniques are Image guided RT (IGRT) and adaptive RT (ART) which will be represented in this subchapter.

ART, also commonly IGRT, utilizes so-called cone-beam CT (CBCT) during treatment fractions. Conventional CT utilizes 2D-shaped fan beams [39]. Each image slice requires one rotation around the patient. Several slices need to be acquired to construct a 3D image. The CBCT on the other hand, utilizes a cone shaped beam. The CBCT consists of a beam source and an opposing detector. The beam is aimed at the middle of the area of interest and then reaches the target on the other side. In contrast to the conventional CT, the CBCT only requires one rotation around the patient as the cone-shaped beam covers the area of interest. This makes CBCT a more rapid image acquisition technique compared to conventional CT. It does however result in uncertainties and artifacts. Due to the geometry of the CBCT beam, more scattered radiation is detected which results in increased noise. This is worsened the larger the field of interest, as larger amounts of scattered radiation are detected. Adding corrections for effects such as scattering makes CBCT sufficient for certain use [18]. Figure 2.17 illustrates the difference in image acquisition and image quality of conventional CT and CBCT. Figure 2.18 shows the Linac with the CBCT system integrated.

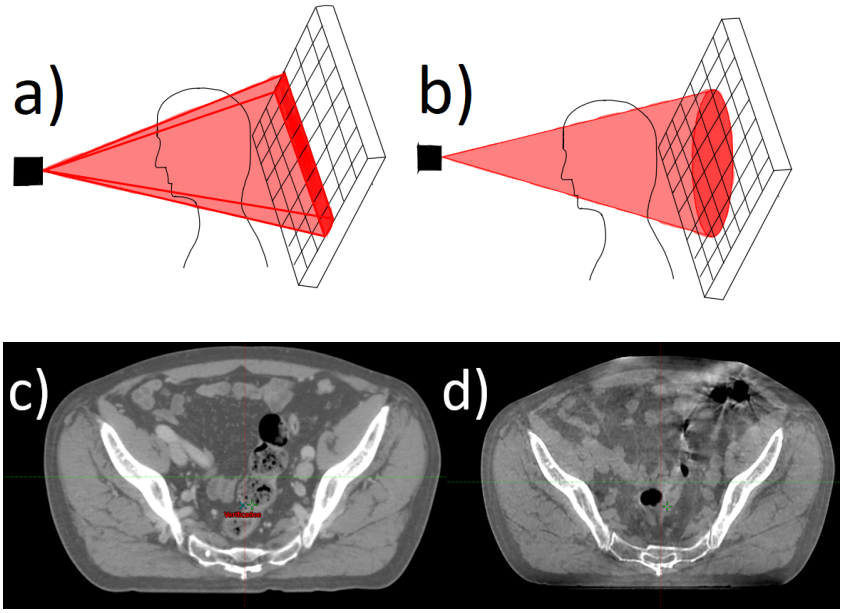

Figure 2.17: a) Conventional CT, one rotation covers one image slice. b) CBCT, one rotation covers enough voxel to construct a 3D-image. c) Planning CT. d) CBCT

2.4.1 Image guided radiotherapy

IGRT utilizes imaging technology to adjust the position of the patient to match the anatomy of planning CT [16]. [18].

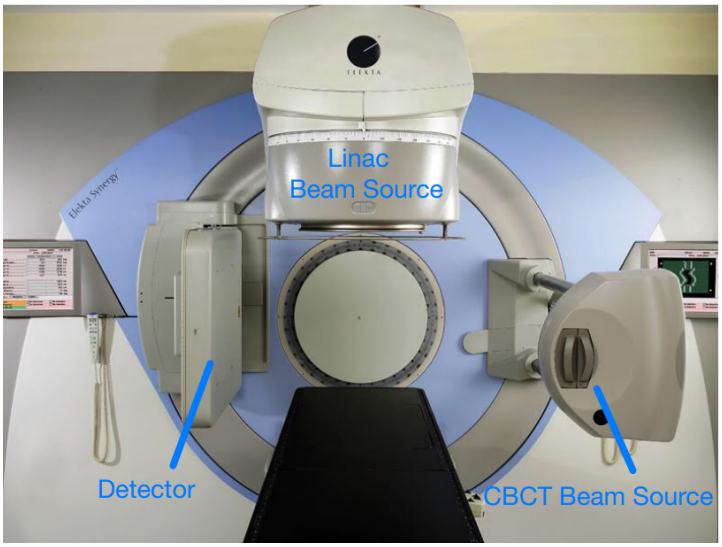

Figure 2.18: Illustration of a Linac with a CBCT system integrated. (Image from [40])

The CBCT is acquired at the start of the fraction when the patient is in treatment position. This CBCT is then compared or fused to the planning CT and the patient setup is adjusted so that the treatment area on the CBCT matches the treatment area on the CT. The adjustment is often in the form of adjusting the treatment table. When the patient setup is adjusted the scheduled dose is delivered as planned. The workflow of IGRT is

illustrated in the flowchart in figure 2.19.

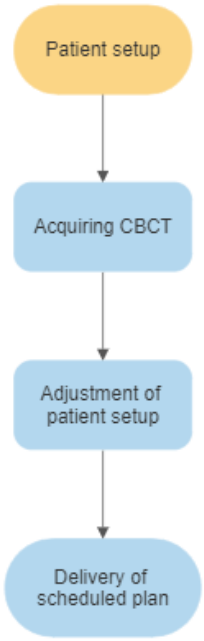

Figure 2.19: Flow chart illustrating the workflow of IGRT

Bones are often used as reference markers to match the CT and CBCT and to help guide the placement of the radiation beam [41]. This is not always ideal as some targets move independently of the skeleton. For these targets it is possible to implement fiducial markers. Fiducial markers are metal objects such as for example gold, which are placed nearby or in the tumor [42]. This makes it easier to localize the tumor and adjust the radiation beam accordingly. This technique is often used with prostate cancer patients [41].

2.4.2 Adaptive Radiation Therapy

As the scans and the treatment plan made prior to the treatment are used throughout the treatment, it does not allow for accurate adjustments according to geometric alternations. The individual patients have unique differences in shape and organ motion [43]. The procedure today is to expand the CTV to PTV margin based on population data. For the rectum, bladder, uterus, and cervix there has been recommended a margin of 1cm or greater. However, within the population-based margin there can be large margin variation for the patients [44]. Since the PTV expansion is based on outliers (90%) of the population, patients that actually have a smaller margin receive dose to a larger

area of surrounding tissue than necessary, also resulting in a missed opportunity for dose escalation. Patients that have an undetected larger motion don't receive dose to an adequate area of tissue.

Yan et al. presented ART in 1997 [44]. This radiation treatment process uses systematic feedback of measurement to modify the treatment plan. ART makes it possible to customize the treatment plan to the motion uncertainties of the individual patient. It opens up for modification of parameters such as field shape, beam intensity, and geometry guided by in treatment acquired images. Offline ART and online ART are two different strategies within the ART treatment technique. With offline-ART new treatment plans are made when the patient is off the treatment couch. Online ART, on the other hand, means adjusting the plan to the anatomy of the day while the patient is on the treatment couch. Offline ART considers the systematic alterations, while online ART has the potential to adjust for both systematic and random variations [45].

Online ART

Geometrical changes, especially organ movements, are hard to predict. With a more frequent adaption, it could lead to reducing the PTV margin even further. ART requires a large number of resources, and several solutions have been introduced to the clinical workflow. In this part two different variants of online ART will be introduced, Daily adaptive plan selection and Online re-planning.

Daily adaptive plan selection

The daily variation in organ size can be accounted for by developing a plan selection library [46]. This library consists of a number of customized treatment plans for different anatomical scenarios. On the day of the dose delivery a new CBCT is acquired. This CBCT is set up against the different dose plans in the plan selection library. The plan that best covers the target volume that day is selected for treatment. This process is repeated for all the remaining fractions.

Online re-planning

Online re-planning means that the original plan is adjusted to the specific anatomy of each fraction. The ideal of online re-planning is therefore automated organ segmentation, and automated treatment planning [47]. This requires 3D images and there exists both kVCBCT solutions (Ethos by Varian), and MR-RT machines (MRIdian vy ViewRay, Utility by Elekta) ([48], [49]). Figure 2.20 illustrates the workflow of online adaptive RT.

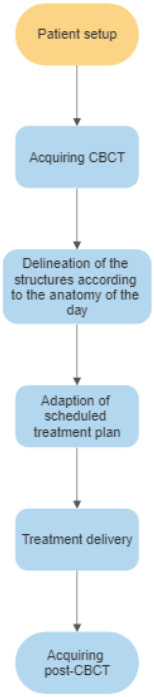

Figure 2.20: Flow chart illustrating the workflow of online adaptive RT

De Jong et al. simulated plan selection and the online ART strategy [50]. For the plan selection strategy there was created a library containing two plans, while for online ART a new treatment plan was created prior to each fraction. Automated planning was utilized for both the plan selection strategy and online ART. The online ART strategy allowed for the use of smaller margins [50]. This resulted in a smaller amount of normal tissue being irradiated. The median volume of normal tissue receiving 95% of the prescribed dose or more decreased from $642cm^3$ to $237cm^3$ with the simulation of online ART. Figure 2.21 shows how the simulated online ART resulted in a lower dose to the bowel bag for all dose levels compared to the plan selection strategy. This is illustrated for both LCRT and SCRT.

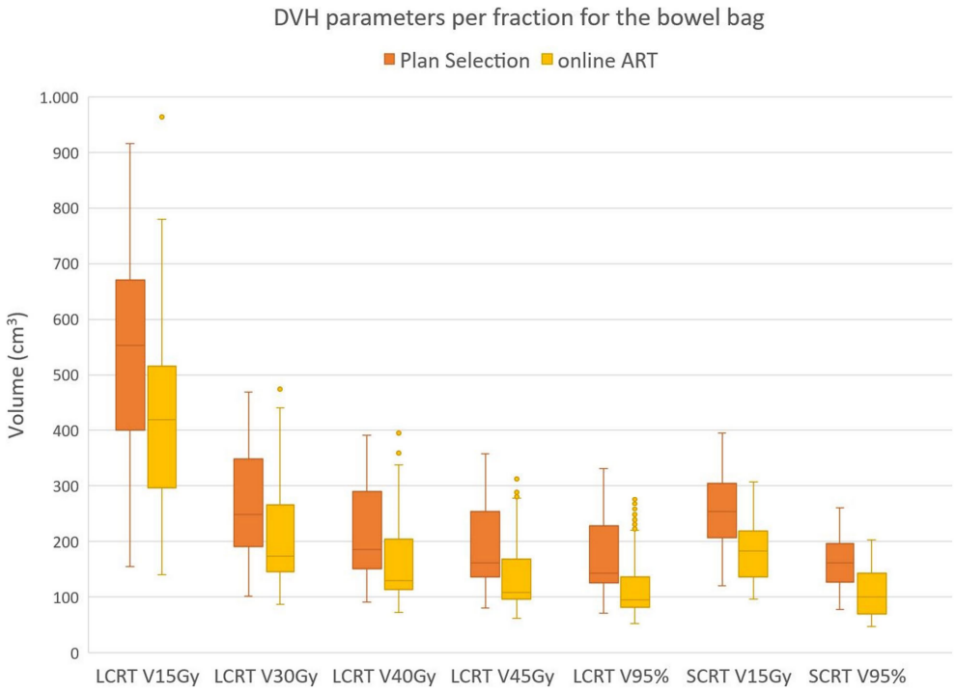

Figure 2.21: Amount of dose received by bowel bag for different dose levels. (Image from: [50])

There is a machine that can carry out the whole workflow with CBCT, treatment planning, and treatment delivery. Varian Ethos utilizes artificial intelligence (AI) and machine learning to solve challenges that exist within RT [51]. AI makes it possible to train a computer to execute a task that normally would require human intelligence [52]. Implementing online ART workflow without AI has been challenging as treatment planning requires time and accuracy. Varian has developed different algorithms to automate the treatment planning [53]. Structures such as the body and bones are segmented by segmentation algorithms that are based on different tolerance ranges. AI segmentation is utilized in order to delineate the organs close to the target, called influencers. For different anatomical sites, there are made different AI segmentation models with a predetermined set of influencers. The CTV is delineated through image matching. The target propagation algorithm produces a CTV based on the planning CT and the session image. They have also developed the Intelligent Optimization Engine (IOE), an algorithm that manages the plan optimization. The IOE is used by the automated planning algorithm. These are some of the algorithms that make the treatment planning with Varian Ethos highly automated. In this thesis, the Ethos machine and the TPS are utilized to spare bowel.

A study by Sbholt et al. on clinical implementation of online ART with Varian Ethos in the pelvis region, showed that the online adaptive re-planning procedure took on average 17.6 minutes, measured from the approval of the CBCT to the treatment delivery [47]. De Jong et al also completed an online adaptive workflow for patients with rectal cancer with Varian Ethos [54]. The online adaptive procedure which included acquiring pre-CBCT, contouring adjustments, plan calculation and the second verification CBCT took on average 20 minutes. The total workflow was estimated to be an average of 26 minutes. This is longer than a conventional RT segment. For some patients this can be experienced as stressful.

An overarching goal is to reduce the dose to healthy tissue. In order to deliver the prescribed dose to rectum cancer, the oncologist has to accept a certain dose to the adjacent healthy tissue. The use of IGRT and ART may result in a lower dose to the small bowel, and hence a lowered probability of later suffering from severe diarrhea during the chemotherapy regimen, illustrated in figure 2.22. This can further lead to an increased amount of patients that complete scheduled chemotherapy and improve their prognosis.

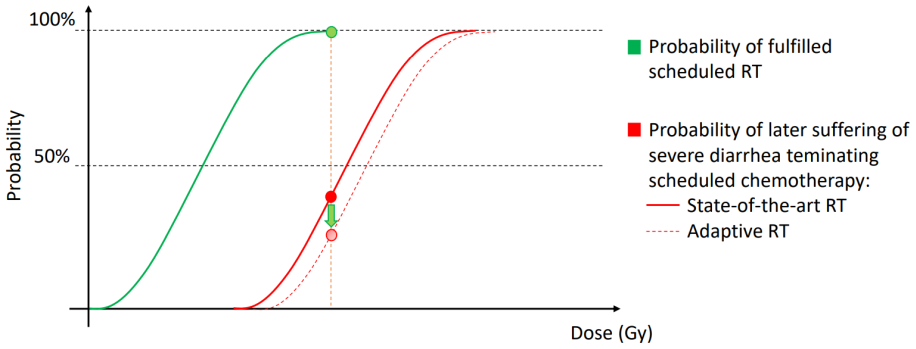

Figure 2.22: Illustration of the therapeutic window for both state-of-the-art RT and Adaptive RT.

Chapter 3

Materials and methods

This chapter presents the patient data, the steps done in preparation for an online re-planning workflow, including selection of PTV margins and dose optimization as well as performing treatment simulation. The model utilized to calculate the toxicity risk and the statistics utilized to compare IGRT and ART delivery are also presented in this chapter.

3.1 Patients

The patients included in this master study were treated for rectal cancer with image-guided IMRT. Prior to the start of RT all included patients consented to inclusion in an observational study approved by the regional ethical committee (REK-id205367). The patients were anonymized. There were taken a CBCT prior to the fraction (pre-CBCT) and one CBCT post fraction (post-CBCT). The pre-CBCTs were utilized in order to simulate the delivery of SCRT for both IGRT and online re-planning ART. Only the first five pre- and post-CBCTs were included for the patients that underwent LCRT. More detailed information about the patients is given in table 3.1.

Table 3.1: Overview of the gender, tumor location and treatment course of the patient group. SCRT (5 Gy x 5), LCRT (2 Gy x 25).

Patient	Gender	Tumor location	Treatment course
Patient 1	Male	Intermediate	SCRT
Patient 2	Male	Upper	SCRT
Patient 3	Male	Intermediate	LCRT
Patient 4	Female	Intermediate	LCRT
Patient 5	Female	Intermediate	LCRT
Patient 6	Male	Intermediate	LCRT
Patient 7	Male	Intermediate	LCRT

3.1.1 Defined structures

On the planning CT, the CTV and GTV were defined by oncologists. The CTV was expanded by 8 mm in all directions except the ventral direction where it was expanded by 10 mm. The BowelBag, bladder, and rectum structures were delineated by radiotherapists. At HUH the BowelBag is outlined from the cranial part of the fourth lumbar vertebra (L4) to the most inferior small or large bowel loop. The optimization volume, zBowelBagOut, for bowel was delineated by cropping 5 mm of the bowel volume from the PTV_{25}. The same was applied for the optimization volume of the bladder, zBladderOut. This is to take the dose gradient into an account and is used in procedures for Eclipse TPS at HUH. The clinical goals for the structures are listed inn table 3.2 with weighted priority. These clinical goals are given in the existing clinical procedure for rectal cancer treatment planning at HUH. As the aim of this master thesis is to look at the toxicity to the bowel I delineated the bowel loops on the planning CT for each individual patient.

Type	Structure	Limit	Vol [%]	[Gy]	Priority
Mean	**zBowelBagOut**			2.00	50
Mean	**zBladderOut**			10.00	50
Point	**PTV_25**	Upper	0.0	25.30	130
Point	**PTV_25**	Lower	100	24.70	130
Point	**CTV_25**	Upper	0.0	25.30	130
Point	**CTV_25**	Lower	100	24.80	140

Table 3.2: The clinical criteria for zBowelBagOut, zBladdderOut, PTV_{25} and CTV_{25}

3.2 PTV margins in IGRT and online ART

The clinically applied PTV-margins for rectal cancer treated with IGRT according to the clinic at HUH is 8 mm in all directions except 10 mm in the ventral direction. Online ART makes it possible to adjust according to the inter-fractional motion, which will affect both the random and systematic errors. In order to decide on margins for use for online adaptive treatments in rectal cancer, studies on intra-fraction motion was identified from PubMed search (mesh words: [rectal cancer AND intra-fraction motion NOT prostate]), as well as studies referenced by the identified papers. From the studies that were deemed presenting relevant information, patients, input motion, quantification of margin, and intrafraction time interval were retrieved from each study.

3.3 Optimizing sparing of normal tissue

3.3.1 Beam angle selection

At HUH VMAT has recently been introduced for these patients. VMAT in an online re-planning workflow has however a longer delivery time. For patient treated on the Ethos system at HUH, IMRT is standard for both ART and IGRT. We therefore used IMRT in the ART workflow. In order to reduce dose exposure of the bowel, IMRT plans using different beam angle setup were constructed. My planning was based on the clinical procedure for RT planning of rectal cancer at HUH.

For each patient, it was produced treatment plans for two different beam setups. The conventional beam selection is based on experience and is identical for all patients. The EQUI beam setup consists of equal angular distance between the gantry angels. The plan types supported in Ethos TPS are equidistant IMRT fields [53]. The Ethos TPS does not support the user defining custom beam angles. Based on a recent study by Bijman et al. the Class solution (CS) was chosen as on of the beam setups [55]. The Class solution (CS) beam setup is a computerized beam angle selection, developed for greater sparing of OAR by exploring several beam angle solutions in a population.

The beam angles are automatically generated, making the treatment planning more efficient. In order to document the effect of the CS, the equi-angular (EQUI) beam setup was also used as these are pre-defined by Ethos TPS. Initially there were made plans with 9-fields, because more fields results in longer planning time and longer delivery time. These are factors which must be considered in online ART. However the supplementary material from, Bijman et al. showed a tendency of increased sparing dose to the bowel when generating plans with 12-fields compared to 9-fields [55]. Therefore, 9-fields and 12-fields CS beam were initially compared for target coverage and bowel sparing. The gantry angles for the CS and EQUI beam setup are illustrated in figure 3.1.

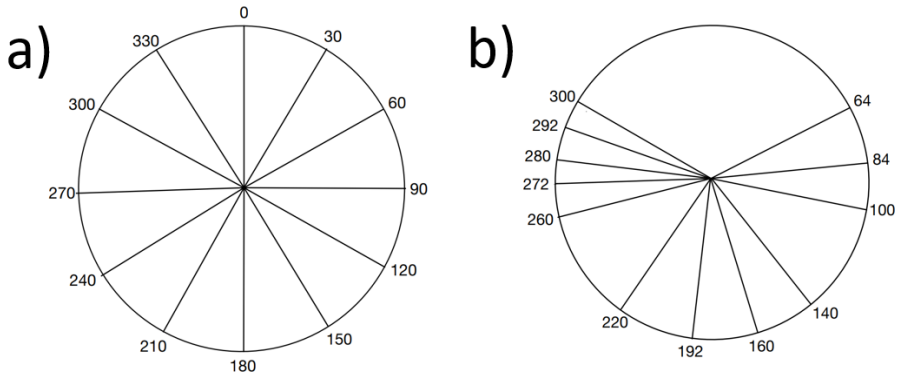

Figure 3.1: a) Illustration of the beam setup for 12-field class solution plans. b) Illustration of the beam angles for 12-field equidistant plans)

3.3.2 Line objective

In the clinic at HUH there is implemented one clinical goal for the BowelBag structure when treating rectal cancer in IGRT mode with the Ethos TPS. This clinical goal is a mean dose (see table 3.2). The goal of this master thesis was to see if the dose to bowel could be reduced even further. The approach was to implement more restrictions on the dose to the $zBowel_{ART}$ for the adaptive plan in the Eclipse TPS. This was done by constructing a line objective. A line objective is a drawn geometrical line between several selected points on a DVH with a common priority. This is a more efficient method than using numerous more or less independent point objectives each with different priorities. The location of the points was decided by looking at the DVHs for all seven patients. An upper limit was set for volume and the respective dose, meaning the maximum dose the respective volume could receive. This was a trial and error method,

where different values were tested and then optimized and evaluated to check such that the line objective didn't affect the coverage of the PTV negatively. The D98%>95% was used to evaluate the PTV coverage. In agreement with the clinical procedure at HUH, the PTV coverage was prioritized over bowel sparing. In the scenarios where the coverage of the PTV were lower than the evaluation threshold, the line values were adjusted to be less restrictive. This was done until there was found a balance between a lower dose to the bowel and an acceptable coverage of the PTV. The constructed line objective is visualized in the DVH on figure 3.2. The figure illustrates how the line objective is interpolated between the different set of values displayed as squared. For the remaining OARs, there were utilized clinical criteria which are listed in table 3.2. The dose plans with line objective was used to evaluate the optimization of the ART plans generated in the Ethos TPS (see details in section 3.4 and 3.4.1)

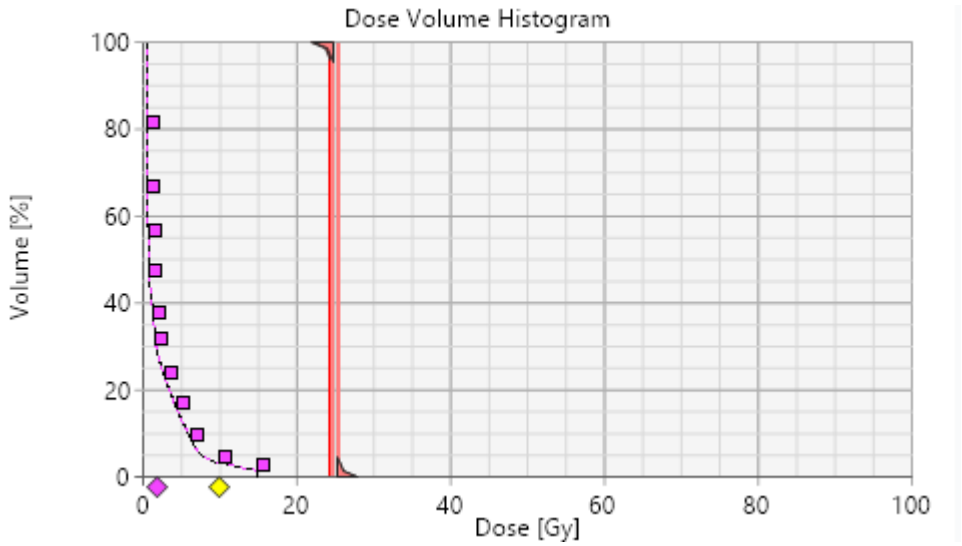

Figure 3.2: The line objective designed for the $zBowel_{ART}$ optimization structure. The line objective is calculated from the values that are displayed as squared, as illustrated on the DVH on the figure. The two red lines illustrates the lower and upper dose limit of the PTV.

3.4 The Ethos system

For this master thesis the online adaptive treatment was simulated using a virtual simulation software of the Ethos machine (Emulator) that is normally used for training. This allows for treatment planning and simulating an online adaptive workflow in previously treated patients. The patients were exported from Eclipse TPS to the Emulator. This was done by my supervisor. Each patient were registered in the program Physicians intent. The flow chart of the emulator workflow is given in figure 3.3.

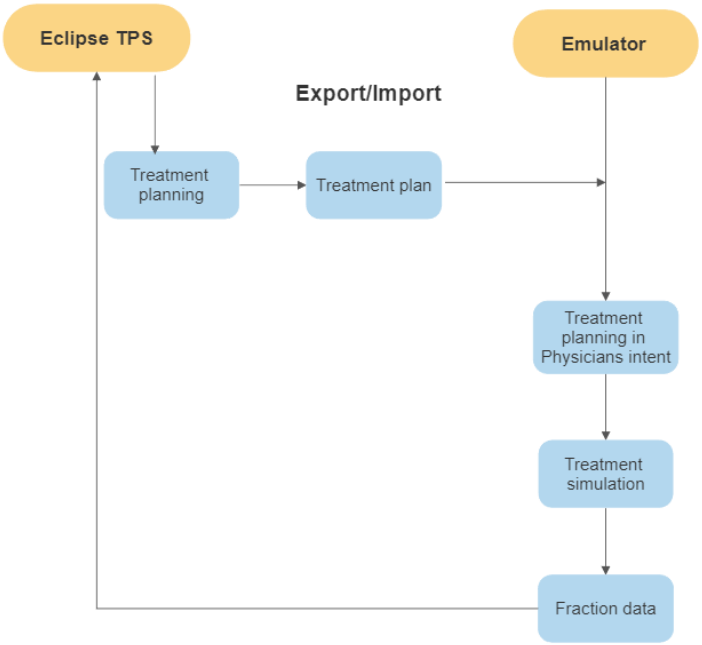

Figure 3.3: Illustration of the workflow of exporting and importing data between Eclipse TPS and the Emulator with Ethos TPS.

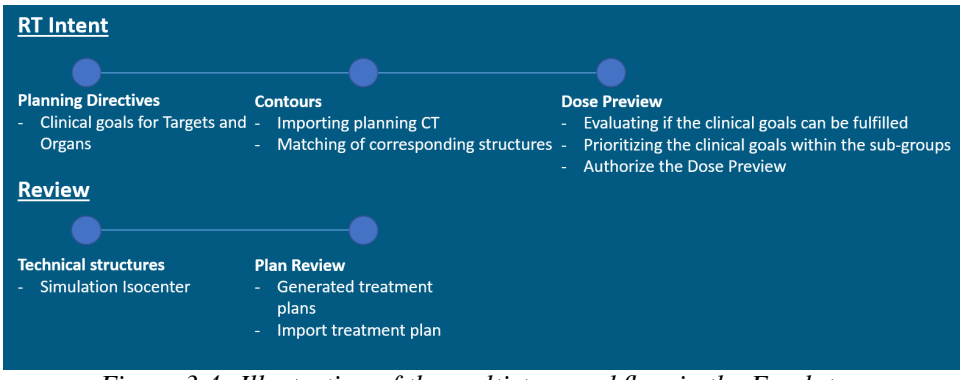

Figure 3.4: Illustration of the multistep workflow in the Emulator.

The steps in the Emulator workflow are visualized in figure 3.4. The automated planning algorithm generates the clinical plans based on the clinical goals set by the user, the IMRT technique, and the number of fields. The Ethos utilizes 6 MV FFF photon beams. In the planning directives, I stated the clinical goals that were used by the automated planning algorithm when deriving the treatment plan. The planning CT and the following structure set were inserted in the Contours section. In order for the Emulator to utilize the structure set from Eclipse TPS, it had to be matched with the corresponding structures in the Emulator. The body was automatically segmented in the Contours section. For the different anatomical regions there exists different segmentation models and influencers [53]. For the anatomical site that includes the rectum, the influencers created via AI segmentation are the rectum, bladder, and bowel. In the Dose Preview, I prioritized the clinical goals in the groups Most Important, Very Important, Important, and Less Important. It is important to note that there is both a priority group and also a sub-priority within the group. The structures that are listed highest in the group are higher prioritized.

The optimization is divided into several steps. The clinical goal of the highest prioritized structure is met before moving on to the following structure. When all goals are met, the optimization process continues to reduce dose to organs if possible. If a structure overlaps with another structure of higher priority and a conflicting goal, these are cropped within the system to fulfill the clinical goal of the higher prioritized structure. So if the PTV overlaps with an organ of lower rank, the organ will be cropped in order to get sufficient dose coverage of the target. The clinical goals and the acceptable variation of the PTV and CTV are listed in table 3.3. These clinical goals are currently used as a template at HUH for rectal cancer patients treated in IGRT mode with the Ethos TPS. In the Dose Preview section, an approximate dose distribution of a 9-field IMRT without the leaves motion was generated. This allowed for checking if the clinical goals were to be achieved.

Table 3.3: Clinical goals of the PTV and CTV used in the emulator.

PTV	
Clinical goal	D98% $\geq$95%
Acceptable variation	D98% $\geq$94%
Clinical goal	Dmax(0.10cm3)< 105%
Acceptable variation	Dmax(0.10cm3)$\leq$107%
CTV	
Clinical goal	D99.5% > 98%
Acceptable variation	D99.5% $\geq$95%

In the Plan Review section there is given an overview of how the different plans have succeeded in fulfilling the target coverage and the clinical goals. The most fitting plan for delivery is then approved by the user. The auto-generated plans are 7-field IMRT, 9-field IMRT, 12-field IMRT and a VMAT plan. These plans have fixed equidistant beam angles and it is not possible to modify them. The Ethos TPS support import of plans that are generated in the clinical TPS which is how it was possible to generate CS plans in Ethos TPS.

The treatment plan with the EQUI beam setup and the treatment plan with the CS beam setup were both imported into the Emulator for treatment simulation. As the plans were imported, the system generated two treatment plans: one recalculated plan, and one recalculated and reoptimized plan with the imported plan geometry. The recalculated plan is recalculated with the Acuros XB dose calculation algorithm used in Ethos TPS. The recalculated and reoptimized plan keeps the isocenter and beam angle setup from the imported plan, but reoptimizes the MLC-movement based on the clinical goals defined in RT intent. The recalculated and reoptimized plan is also normalized to the normalization goals defined in RT intent. The normalization defined in RT intent is the same as the defined normalization in Eclipse TPS. The plan review window allows for visualizing the dose distribution, and each plan has its own plan report with the DVH and quantified information about the dose distribution (see Appendix B). As the recalculated and reoptimized plan had the best clinical goal score, this version of the imported plan was approved for all patients.

3.4.1 Constructing clinical goals

The EQUI plans with the line objectives generated in Eclipse TPS were used as benchmarking plans in order to set clinical goals for the treatment with the Ethos TPS. The EQUI plans generated in Ethos TPS had no clinical goals to the bowel as we wanted to study how well the Ethos TPS optimization process restricted dose to bowel when no clinical goals were added. The relative volume of the bowel exposed to 9 different dose levels, distributed over 25 Gy, were acquired from the DVH. The corresponding treatment plans were then compared in a DVH. This optimization process was the starting point of constructing the clinical goals.

The variation in dose to the bowel for the 9 dose levels was studied for all seven patients. The median value of the dose levels was utilized in the first attempt to calculate clinical goals. This was done to calculate an indication of what could be tolerable clinical goals. The initial clinical goals were then modified by a trial and error method. This was done by simulating one fraction of all patients, starting with the initial clinical goals. This allowed for testing if the Ethos TPS was able to fulfill the defined threshold in addition to the clinical goal of the PTV. The clinical goals were found satisfying when the clinical goals of the bowel and the clinical goal of the PTV were fulfilled for the patients with the largest bowel volume. The clinical goals that were found for the EQUI plans were applied to all CS plans.

The extent of the CBCT is reduced as compared to the volume imaged on the planning CT, as illustrated in figure 3.5. This shows the bowel structure from the planning CT overlayed on a daily CBCT. The structure delineated on the planning CT extends outside the CBCT. In addition to this, the total bowel volume of the patients varies to a great extent. Therefore, a relative dose criteria will be very imprecise and vary for each individual patient.

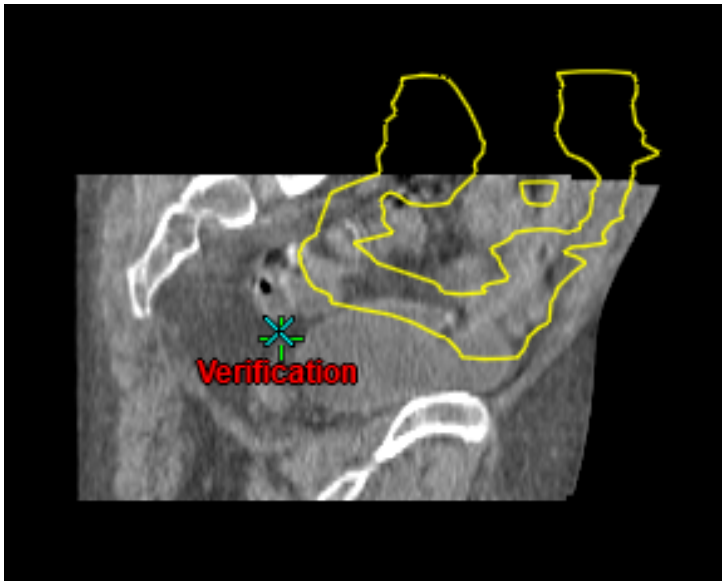

Figure 3.5: A CBCT segmentation illustrating how the bowel structure from the planning CT extends outside the session CBCT

3.4.2 Evaluating the clinical goal against the line objective

When the clinical goals were found for bowel, the final treatment plans for all patients for both the EQUI and the CS beam angle setup were generated. The EQUI plans with implemented clinical goals generated in Ethos TPS were compared to the EQUI plans with the line objectives from Eclipse TPS. This was done to secure the plan optimization for bowel sparing. The bowel sparing was compared by acquiring dose-levels from the DVH. In addition to the comparison of the bowel sparing, the PTV D98% was also compared.

3.5 Simulation of treatment delivery

3.5.1 Online re-planning in Ethos

Both treatment plans using CS and EQUI beam setup were simulated in this master project. In order to simulate these two beam setups for the same patient, the patient were registered twice as two different patients. The patient ID and name needed to be identical as the one given in the anonymization process in order for the emulator to be able to connect the imported patient data. The treatment plans were imported into the emulator into a file name with the patient ID. The structures were used as templates for

the second round of simulation of the treatment with the EQUI beam angle setup, and the simulation of the CS beam angle setup.

As the treatment plan was approved in Physicians intent it became available in the treatment simulation program. The treatment was simulated fraction by fraction. After opening a fraction the program needed a pre-CBCT as input. This is to detect the daily anatomy. Subsequently the bladder, rectum, and bowel were automatically delineated on the session-CBCT by the AI-enhanced image segmentation. I then did manual adjustments to the delineation of these influencers and target volumes if needed. The review of influencers were approved by the supervisor. Every influencer needed to be reviewed and approved in order to move further in the workflow. The next step was the Target section. The target volumes GTV and CTV were delineated automatically on the CBCT. I did adjustments to the GTV and CTV overviewed by the supervisor, and using the target structures for the planning CT displayed from the Eclipse TPS as reference. The PTV was automatically generated by expanding the adapted CTV by 4 mm isotropically.

With consideration of the initial treatment plan, an AI-planning algorithm generates an adaptive plan based on the daily anatomy. This results in the user having the choice between two treatment plans for delivery, the scheduled plan or the adaptive plan (see figure 2.20). The target coverage and the clinical goals were checked against their pre-set reference values as illustrated in figure 3.6. Any deviation were noted, but the adaptive plan was always chosen in order to compare online re-planning with IGRT (see 3.6.1). The treatment details became available in Physicians intent after the delivery of each fraction. The data generated for each delivered fraction was exported from the Emulator to the patient in Eclipse TPS in order to study the dose distribution, the structures and the DVH data. Examples of DVHs are given in Appendix A.

Figure 3.6: Illustration of the Plan Selection section. The achieved clinical goals, the dose distribution and the DVH can be studied for both the Scheduled Plan and the Adapted Plan before treating the patient with the selected plan. Image from [56]

3.5.2 IGRT

The structure sets generated for each CBCT, consisting of the CTV, bowel, and bladder was utilized to simulate IGRT treatment. This was done so that the IGRT treatment and online ART had identical structures when comparing these delivery options. The IGRT treatment was simulated in Eclipse TPS for both the CS and EQUI beam setup. Using image registration the planning CT and the CBCT for each session were co-registered based on bony anatomy auto-matching. The registration results were visually inspected. Figure 3.7 shows a co-registration for a patient. This was done for each session CBCT to simulate the pre-CBCT that is taken prior to the treatment fraction.

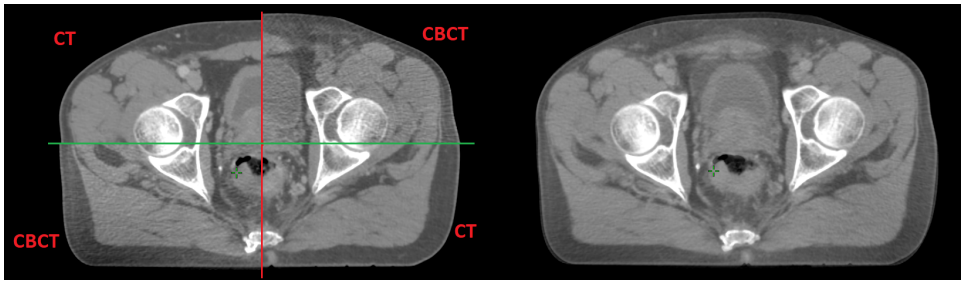

Figure 3.7: Illustration of the co-registration of the planning CT and the CBCT.

To simulate an IGRT treatment with identical photon fluence as for the plan, a verification plan was created. The registration were used to copy the verification plan onto each of the five CBCTs for each session.

3.6 Evaluation

3.6.1 Statistical considerations

Due to few sample sizes the median is utilized as the quantitative measurement for summarizing the data. The Wilcoxon matched pairs test is used to compare two different treatment techniques of the same patient group when there are assumptions that the observations are not normally distributed [57].

- The difference between the paired observations x_{1i} and x_{2i} come from a population with a symmetric distribution
- The difference between the paired observations x_{1i} and x_{2i} are independent of each other.

The significance level (α) was sat to 0.05. The result is statistically significant when the p-value is less than α. The null hypothesis is that there are no median difference in the population.

To compare the toxicity risk for each fraction for each patient within EQUI for IGRT and ART as well as CS for IGRT and ART, the paired t-test was evaluated. The paired t-test is valid for the following assumptions:

- The difference between the paired observations x_{1i} and x_{2i} are plausibly Normally distributed.
- The difference between the paired observation x_{1i} and x_{2i} are independent of each other.

The null hypothesis is that there are no difference between the median of the treatment techniques. The null hypothesis can be rejected for p-value$<\alpha$. As the mean is very vulnerable to outliers the use of the mean and t-test was validated by utilizing a q-q plot. The q-q plot allows for viewing if there are any deviations from normality.

3.6.2 Calculating toxicity risk for the simulated treatments

In order to evaluate and compare the treatments the toxicity risk of the bowel was quantified. This was done utilizing the model from Holyake et al. [38]. This is a meta study of the published data of small bowel dose-volume and acute diarrhea of Grade 3 in rectal cancer (see table 2.15). The study presented a model that quantifies the risk for acute toxicity from a dose-response relationship for rectal cancer with 10 Gy of the bowel as input. The V10Gy and toxicity risk relationship is given by logistic regression in equation 3.1. The t(x) is the toxicity risk, the x is V10 Gy, the β_0 = -2.63 is the intercept, and the β_{1x} = 0.005 is the B for V10 Gy. The model is illustrated in figure 3.8.

The model is based on conventionally-fractionated RT data but as there are no created models for SCRT this model was utilized to give an quantified indication of the difference between IGRT and online re-planning ART. As there was generated a new treatment plan for each fraction, the toxicity risk was calculated for all fractions not only for the planning CT. Each fraction was scaled up to 25 Gy to fit the model input. For each session CBCT the absolute bowel-volume receiving 10 Gy was acquired from the DVH. The input to the model was the median of five fractions volumes. The toxicity risk was calculated for IGRT and online ART for both the CS and EQUI beam setup.

$$t(x) = \frac{1}{(1 + e^{\beta_0 + \beta_1 x})} \tag{3.1}$$

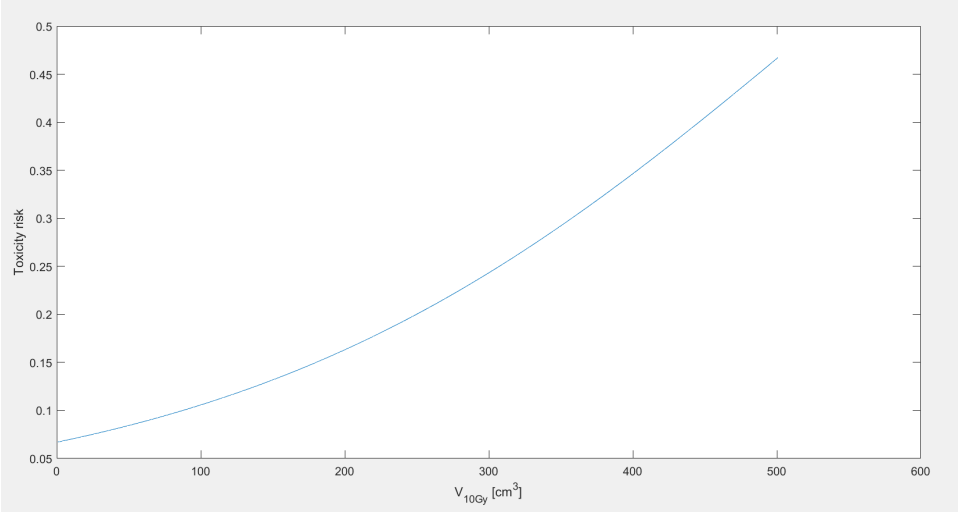

Figure 3.8: Toxicity risk for the amount of volume of the small bowel receiving 10 Gy

Chapter 4

Results

4.1 Preparing for online re-planning ART

4.1.1 Margins

We found three studies of margins that were relevant for this master thesis. A summary of the input motion, quantification of margin, and the intrafraction time of these are given in table 4.1.

*Table 4.1: Summary of the quantification of margins from the selected studies. The patients from the studies of Kleijnekamp et al., Eijkelenkamp et al. underwent short course RT. The study by van den Ende et al. also included patients that underwent LCRT. *Center of gravity (COG)*

	Patients	Input motion	Quantification of margin	Intrafraction time
Kleijnen 2016 [58]	16	Intrafractional: cine-MRI sequences at three times. Interfractional: T2-weighted MRI day 1-4.	PTV margins estimate defined as the 95% in 90% of the observed cases.	0, 9:30 and 18:00 min
Eijkelenkamp 2021 [59]	15	T2-weighted MRIs, one pre-treatment and five scans each fraction. Intrafractional: Trial and error with margins relative to GTV with ART. Interfractional: Trial and error with margins relative to the bone structure.	95% of the voxels has geometrical coverage. The margin is ok if this is fulfilled for 90% of the GTV both for inter- and intrafractional.	Mean 35 min (24-54 min)
van den Ende 2019 [45]	19	COG_{GTV}* relative to movement of fiducial markers in GTV. Movement of markers relative to bone. Interfractional: Two MRI examinations. Intrafractional: Daily pre-and post CBCT for the first five fractions.	van Herk margin recipe.	$\bar{t} = 9 \pm 1$ min

Van den Ende et al. studied the use of fiducial markers as a substitute for the GTV positioning [45]. The fiducial markers were placed in the tumor and the mesorectum. The patients that were included in this study had either SCRT or LCRT. For the first five fractions, there were acquired pre- and post-CBCTs of the patients. The margins for inter-fraction displacement and intra-fraction displacement for the different setups are presented in table 4.2. The center of gravity of the GTV (COG_{GTV}) displacement was extracted from the MRIs, and the displacement of the fiducial markers was extracted

from the CBCTs.

*Table 4.2: The systematic (Σ) and random (σ) errors for inter-fraction motion w.r.t bony anatomy based on both COG_{GTV} and fiducial markers. The systematic and random errors for intra-fraction displacement based on fiducials [45]. LR = left-right, AP= anterior-posterior, CC=craniocaudal, Σ = systematic error, σ = random error. *Center of gravity (COG).*

	LR [mm]	**AP [mm]**	**CC [mm]**
Inter-fraction motion w.r.t bony anatomy $(COG_{GTV})*$			
Σ	2.9	7.3	8.2
σ	1.4	1.7	2.1
Inter-fraction motion w.r.t bony anatomy (fiducial)			
Σ	3.7	5.0	4.9
σ	3.0	4.5	5.1
Intra-fraction displacement based on fiducial substitute of GTV			
Σ	0.8	1.4	1.6
σ	1.4	1.7	2.1

Kleijnen et al. studied how the PTV margin is affected by motion over time within a scan session [58]. The estimate of the PTV margins was expressed in percentages. For each individual patient, the maximum displacement in time was set to the 100% PTV margin reference. The patients underwent SCRT and were scanned daily with an MRI. Within the one-minute time interval the motion was very stable. The motion uncertainty was reduced by 71% for the CTV and 75% for the tumor volume compared to non-adaptive treatment. Kleijnen et al. also found that 90% of the time the average distance that included 95% of the surface voxels remained below 3.6 mm for the CTV and 2.3 mm for the GTV within the one-minute time interval. Kleijnen et al. argued that if ART were to be efficient, then the time intervals needed to stay under 18 minutes.

Eijkelenkamp et al. studied margins that are needed to cover the inter- and intrafraction motion of the GTV, expressing their results in mm [59]. They showed that the margins needed for sufficient GTV coverage were 17 mm for non-adaptive RT and 6 mm for adaptive RT. When the treatment fraction period was lower than 15 minutes, the margin could be reduced to 4 mm. The reduction of 17 mm to 6 mm and 4mm, simulating ART, makes up a reduction of 64.7% and 76.5% respectively.

Based on these studies, the margin we chose to proceed with for the online re-planning workflow was 4 mm isotropic. This expansion is justifiable when the execution of the online ART workflow is time-efficient [58], [59]. According to Van den Ende et al., the systematic and random errors of the intra-fraction displacement must be $\leq$2 mm for a 4 mm margin to be sufficient. This amounts to a reduction of 50% and 60% from the standard margins used in the clinic at HUH, which is within the same reduction range as the studies presented in table 4.1. The reduction is slightly less than Eijkelenkamp et al. and Kleijnen et al., but this reflects different margins in the non-adaptive RT. All results shown for ART in this chapter are hence based on a 4 mm isotropic expansion of the CTV.

4.2 Selecting the number of IMRT beams to use for ART

The 9-field IMRT plans and the 12-field IMRT plans were statistically compared in terms of bowel exposure and PTV coverage. Bowel exposure was compared for the volume receiving 7.5 Gy and 20 Gy, and the PTV coverage by D98%. The absolute volume of the bowel receiving 7.5 Gy and 20 Gy, and the achieved PTV D98% for six patients are listed in table 4.3. For V7.5 Gy (p = 0.688) and V20 Gy (p = 0.844) there were no significant difference. There was no significant difference (p=0.0625) between the PTV coverage for the 9-field and the 12-field IMRT plans. However, target coverage was more difficult to obtain using 9-beam angels. Despite several attempts, the 9-field CS plans did not fulfill the D98%>95% for patient 6. The median PTV D98% for the 9-field CS plans was 95.5%, and the median PTV D98% for the 12-field CS plans was 96.4%. The dose distribution for EQUI and CS for both 9-beam angles and 12-beam angles are shown in figure 4.1. It was not generated a 9-field CS plan for patient 7, since the evaluation was performed after this patient gave informed consent to participation. We decided to use 12-field IMRT plans in the ART workflow and for comparisons with IGRT.

Table 4.3: An overview of the bowel receiving 7.5 Gy and 20 Gy and the achieved D98% with 9-field CS plans for six patients.

CS 9-fields	PTV D98% [%]	Absolute volume bowel 7.5 Gy [cm^3]	Absolute volume bowel 20 Gy [cm^3]
Patient 1	96	174	140
Patient 2	96	417	121
Paient 3	96	1556	29
Patient 4	95	106	44
Patient 5	97	126	43
Patient 6	93	150	75

Table 4.4: An overview of the bowel receiving 7.5 Gy and 20 Gy and the achieved D98% with 12-field CS plans for six patients.

CS 12-fields	PTV D98% [%]	Absolute volume bowel 7.5 Gy [cm^3]	Absolute volume bowel 20 Gy [cm^3]
Patient 1	97	173	139
Patient 2	97	436	118
Patient 3	97	143	29
Patient 4	96	132	46
Patient 5	96	138	42
Patient 6	96	136	77

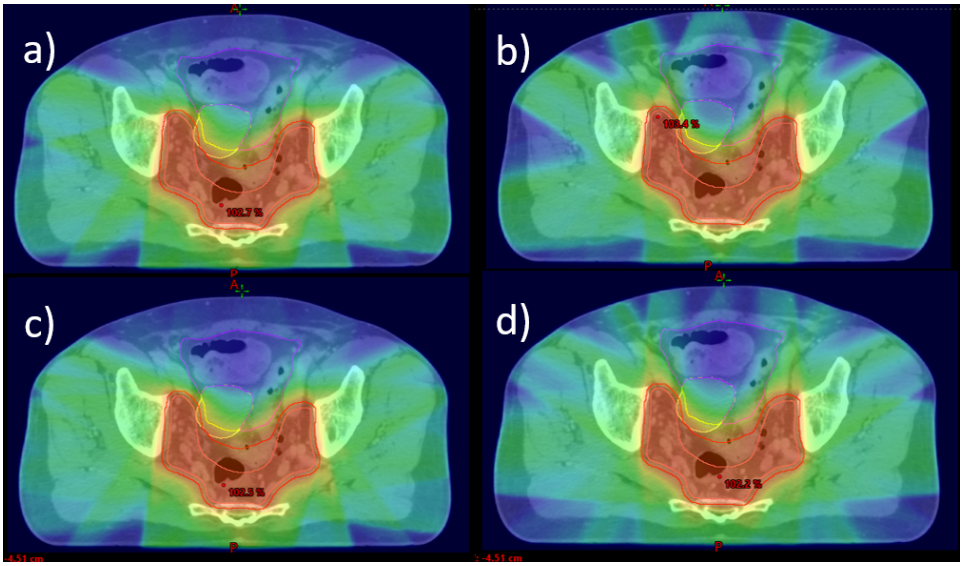

Figure 4.1: a) Dose distribution of 9-angles CS beam angle setup. b) Dose distribution of 9-angles EQUI beam angle setup. c) Dose distribution of 12-field CS beam angle setup. d) Dose distribution of 12-angles EQUI beam angle setup.

4.3 Evaluating the Ethos treatment planning

4.3.1 Defining clinical goals for the bowel

The 9 dose levels were plotted for both the treatment plans with line objectives generated in Eclipse TPS and the treatment plans with no clinical goals to bowel generated in the Ethos TPS. There were variations between the patients. Figure 4.2 shows almost no variation between the values obtained from the Eclipse TPS using the line objectives and the values obtained from Ethos TPS. Both figure 4.3 and figure 4.4 indicate that there is room for further improvement on the bowel sparing in Ethos TPS. Since the volume receiving 7.5 Gy show considerable deviation as compared to plans optimized with the line objective in Eclipse TPS, a clinical goal was set for this dose level and for a high dose of 20 Gy. The values for V7.5 Gy and V20 Gy obtained from the Ethos TPS for the seven patients are listed in table 4.5.

Table 4.5: The values for V7.5 Gy and V20 Gy for the 7 patients that were obtained from the plans generated in Ethos TPS before any clinical goals for bowel were implemented.

	Patient 1	**Patient 2**	**Patient 3**	**Patient 4**	**Patient 5**	**Patient 6**	**Patient 7**
V7.5 Gy [cm3]	174	496	277	149	122	132	291
V20 Gy [cm3]	141	121	25	46	42	67	68

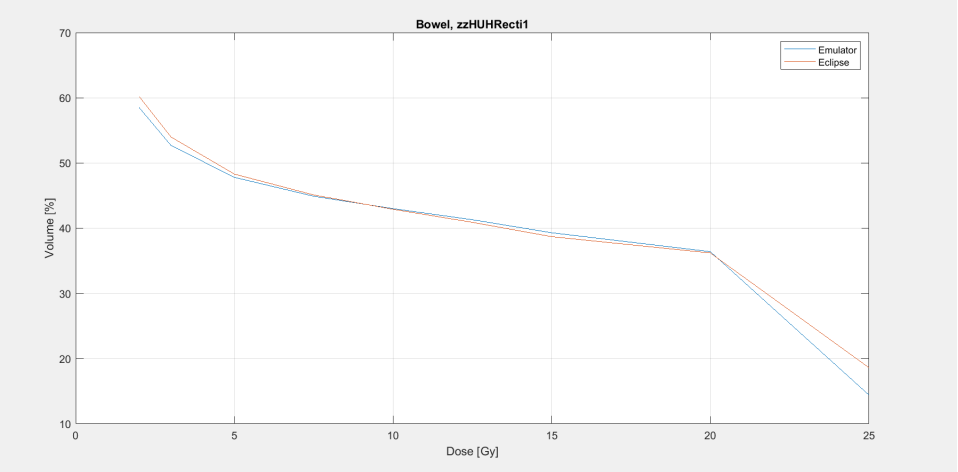

Figure 4.2: Dose volume graph for the PTV of patient 1. The graph shows that there are not much variation in the percentage of volume from when simulating the plan in Eclipse TPS and Emulator.

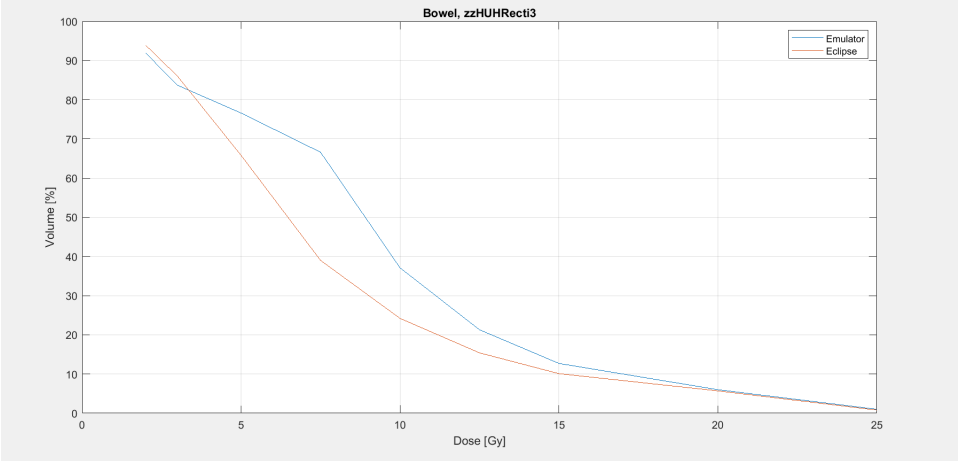

Figure 4.3: Dose volume graph for the PTV of patient 3. The graph shows a large variation in the percentage of volume from when simulating the plan in Eclipse TPS and Emulator.

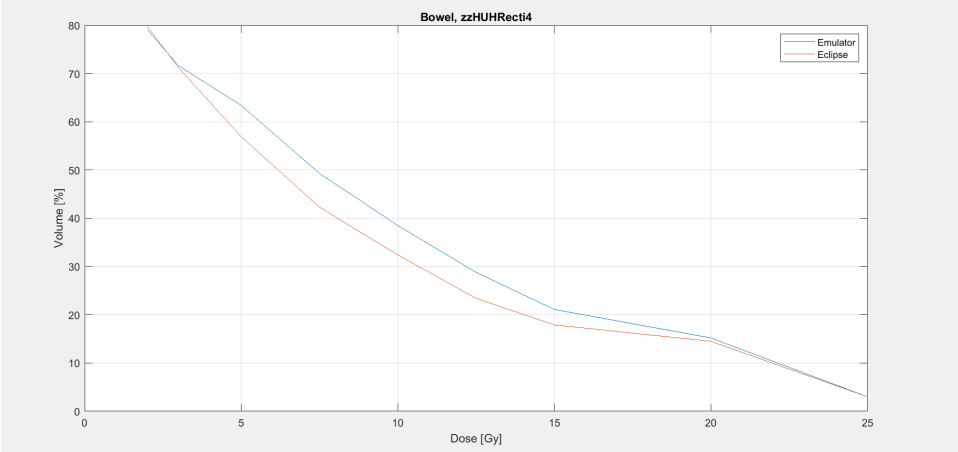

Figure 4.4: Dose volume graph for the PTV of patient 4. The graph shows a variation in the percentage of volume from when simulating the plan in Eclipse TPS and Emulator.

Initially, identical clinical goals were set for male and female patients. The mean of V7.5 Gy from the Eclipse plans and Ethos plans was calculated for each patient, in addition to the mean of the V20Gy from the Eclipse plans and the Ethos plans. The initial clinical goals were based on the median of the seven means of V7.5 Gy, and the median of the seven means of V20 Gy. The median value for absolute bowel volume receiving 7.5 Gy was 173 cm^3 and the median value for absolute bowel volume receiving 20 Gy was 68 cm^3. During the simulations of the first fractions with these clinical goals, two male patients got hot spots as. An example of this is figure 4.5.

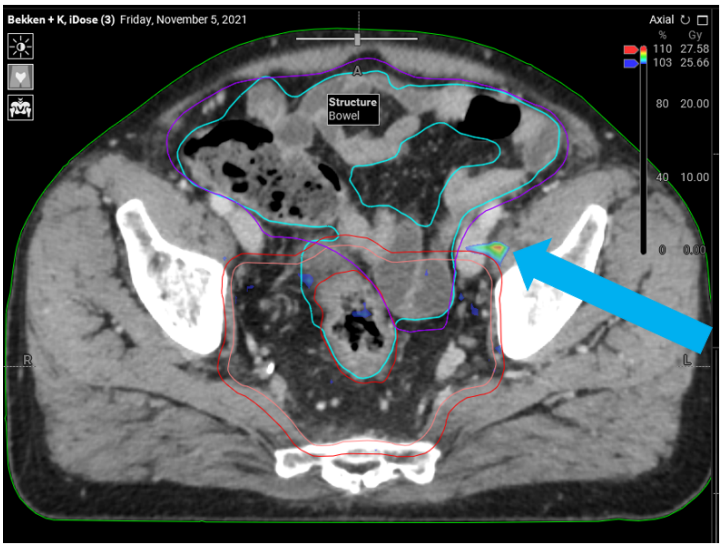

Figure 4.5: The initial clinical goals resulted in hotspot for some of the male patients. Here an example of patient 2 which got a hot spot > 107%.

Figure 4.6 and figure 4.7 shows how the internal anatomy of male and females are different. Most female patients have a cervix that will push the bowel upwards. Where the cervix is located for females, the bowel is located for men. This results in men receiving more high dose to the bowel during treatment as more bowel is located closer to the target volume. To account for this, two different sets of clinical goals for the bowel were defined. One for female patients and one for male patients. The clinical goals for the female patient group were based on the median value and therefore set to $173cm^3$ for the 7.5 Gy dose level and $68cm^3$ for the 20 Gy dose level. By trial and error the clinical goals for the male patient group were set to $450cm^3$ and $120cm^3$ for the 7.5 Gy and 20 Gy dose levels, respectively. After adjusting the clinical goals to the bowel the dose maximum was always under 105% for all patients. The clinical goals that were implemented in the Ethos TPS are listed in table 4.6.

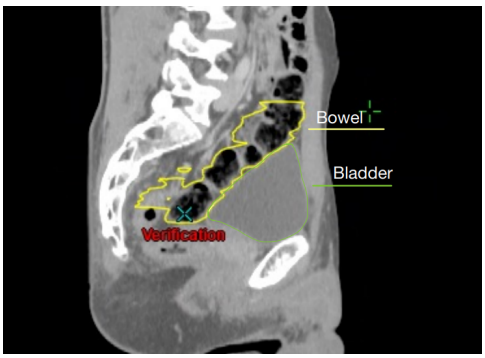

Figure 4.6: CT scan of a male patient

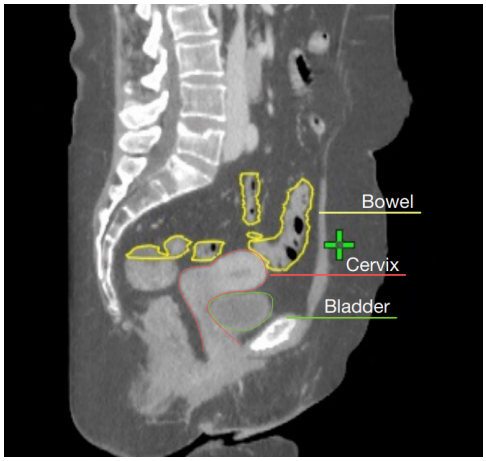

Figure 4.7: CT scan of a female patient

Table 4.6: The clinical goals for PTV, CTV, bowel and bladder, implemented in Ethos TPS

Structure	Clinical goal	Acceptable variation	Priority
PTV_25	D98% $\geq$95%	D98% $\geq$94%	Most Important
PTV_25	Dmax(0.10cm^3) < 105%	Dmax(0.10cm^3) $\leq$107%	Very Important
CTV_25	D99.5 % > 98%	D99.5% $\geq$95%	Very Important
Bowel (Male patients)	V7.5 Gy < 450 cm^3	V7.5 Gy $\leq$570 cm^3	Very Important
Bowel (Male patients)	V20 Gy < 120 cm^3	V20 Gy $\leq$145 cm^3	Very Important
Bowel (Female patients)	V7.5 Gy < 173 cm^3	V7.5 Gy $\leq$260 cm^3	Very Important
Bowel (Female patients)	V20 Gy < 68 cm^3	V20 Gy $\leq$105 cm^3	Very Important
Bladder	Dmean $\leq$20 Gy	Dmean $\leq$25 Gy	Important

4.3.2 Benchmarking plan optimization for bowel sparing in Ethos

The line objective plans from Eclipse TPS were used as a benchmark for bowel sparing. These were compared to the Ethos generated plans with the clinical goals in table 4.6. There was no significant difference between EQUI plans optimized with the line objective in Eclipse TPS and EQUI plans from the step-by-step optimization in the Ethos TPS for V7.5 Gy (p=0.30) or V20 Gy (p=0.81). There was a significant difference in PTV coverage (p=0.031) where the PTV for the Ethos plans had a median of D98% of 96.8% and PTV for plans obtained with the line objective had a median of D98% of 96.0%. Ethos TPS manages to press down the dose to the bowel while simultaneously fulfilling the PTV coverage.

Table 4.7: An overview of the PTV D98%, V7.5 Gy and V20 Gy for all patients, for both the line objective plans generated in Eclipse TPS and the treatment plans generated in Ethos TPS.

Patient 1		
	EQUI_Line (Eclipse TPS)	**EQUI_ART (Ethos TPS)**
PTV D98% [%]	96.0	97.1
V7.5 Gy [cm^3]	173	187
V20 Gy [cm^3]	139	136
Patient 2		
	EQUI_Line (Eclipse TPS)	**EQUI_ART (Ethos TPS)**
PTV D98% [%]	95.9	97.4
V7.5 Gy [cm^3]	477	409
V20 Gy [cm^3]	119	121
Patient 3		
	EQUI_Line (Eclipse TPS)	**EQUI_ART (Ethos TPS)**
PTV D98% [%]	96.0	96.6
V7.5 Gy [cm^3]	161	197
V20 Gy [cm^3]	24	25
Patient 4		
	EQUI_Line (Eclipse TPS)	**EQUI_ART (Ethos TPS)**
PTV D98% [%]	95.9	97.0
V7.5 Gy [cm^3]	125	149
V20 Gy [cm^3]	43	46
Patient 5		
	EQUI_Line (Eclipse TPS)	**EQUI_ART (Ethos TPS)**
PTVD98% [%]	96.2	96.9
V7.5 Gy [cm^3]	160	143
V20 Gy [cm^3]	42	43
Patient 6		
	EQUI_Line (Eclipse TPS)	**EQUI_ART (Ethos TPS)**
PTV D98% [%]	95.9	97.0
V7.5 Gy [cm^3]	150	152
V20 Gy [cm^3]	70	67
Patient 7		
	EQUI_Line (Eclipse TPS)	**EQUI_ART (Ethos TPS)**
PTV D98% [%]	96.1	97.2
V7.5 Gy [cm^3]	237	155
V20 Gy [cm^3]	70	64

4.4 Comparison of online re-planning ART and IGRT

4.4.1 Plan comparisons

The dose distributions based on the planning CTs were compared to study what difference to expect between the IGRT plans generated in Eclipse TPS and the online ART plans generated in Ethos TPS. Results from the planning CTs showed that the D98%>95% for the PTV was fulfilled for all IGRT and ART plans. For the EQUI beam setup there was a significant reduction (p=0.016) in the median V10 Gy for the ART plans compared to the IGRT plans. The median V10 Gy for the IGRT plans with the EQUI beam setup was 183 cm^3 and the corresponding median for ART was 130 cm^3. This translated to a small but significant (p=0.016) reduction of estimated acute diarrhea for the EQUI beam setup with 15% for IGRT and 12% for ART. The median V10 Gy for the IGRT plan utilizing CS beams was significantly (p=0.031) smaller compared to the IGRT using EQUI beams. There was no significant difference between the ART plans for CS beam angle setup and EQUI beam angle setup. The CS beam angle setup with ART resulted in the lowest toxicity risk for 3 of 7 patients. The EQUI beam angle setup resulted in the lowest toxicity risk for 2 of 7 patients. The ART plans resulted in the lowest toxicity risk for 5 of 7 patients. For 2 of 7 patients, the ART plan with EQUI beam setup and the IGRT plan with CS beam setup both gave the lowest toxicity risk.

Table 4.8: The V10 Gy and calculated toxicity risk for the IGRT and Ethos treatment plans for both the EQUI beams setup and CS beam setup.

Patient 1				
	EQUI_IGRT	**EQUI_ART**	**CS_IGRT**	**CS_ART**
V10Gy [cm^3]	183	177	175	159
Toxicity risk [%]	15	15	15	14
Patient 2				
	EQUI_IGRT	**EQUI_ART**	**CS_IGRT**	**CS_ART**
V10Gy [cm^3]	425	337	431	293
Toxicity risk [%]	38	28	38	24
Patient 3				
	EQUI_IGRT	**EQUI_ART**	**CS_IGRT**	**CS_ART**
V10Gy [cm^3]	187	144	140	176
Toxicity risk [%]	16	13	13	15
Patient 4				
	EQUI_IGRT	**EQUI_ART**	**CS_IGRT**	**CS_ART**
V10Gy [cm^3]	138	104	125	68
Toxicity risk [%]	13	11	12	9
Patient 5				
	EQUI_IGRT	**EQUI_ART**	**CS_IGRT**	**CS_ART**
V10Gy [cm^3]	173	84	103	104
Toxicity risk [%]	15	10	11	11
Patient 6				
	EQUI_IGRT	**EQUI_ART**	**CS_IGRT**	**CS_ART**
V10Gy [cm^3]	168	122	131	199
Toxicity risk [%]	14	12	12	16
Patient 7				
	EQUI_IGRT	**EQUI_ART**	**CS_IGRT**	**CS_ART**
V10Gy [cm^3]	253	130	202	163
Toxicity risk [%]	20	12	17	14

4.5 Simulation of treatment delivery

4.5.1 Time assessment of the simulations

The simulation was a time-consuming part of this project. The mean time per fraction was 33 minutes. When delineating structures the plan CT was used to help identify and locate different structures. The experience was that the structures were easier to study in Eclipse TPS compared to in the Emulator, as the Emulator apparently puts on an additional filter on the CBCT images. Approximately 70% of the fraction time was used to delineate the structures, the main part being delineating the bowel, depending on how well the emulator managed to delineate the structures itself. There were some instances where the emulator did not identify any bowel loops.

The influence of imaging artifacts

An accurate delineation of structures relies on good image quality. The image quality varied for each individual patient. Image a) in figure 4.8 shows a CBCT image slice of a patient where the amount of artifacts is limited giving a clear sight of the bowel loops. Image b) in figure 4.8 shows a CBCT slice of the same patient but higher up in the cranial direction. In this CBCT slice, it is hard to identify the bowel loops. All kVCBCT had the tendency that the amount of artifact increased when moving up in the cranial direction. When the bowels could no longer be identified they were included in a bowel bag structure as shown in figure 4.8. Thus, the bowel structure consisted of bowel loops when they were easy to identify and then also a BowelBag structure when the artifacts made it too hard to identify them.

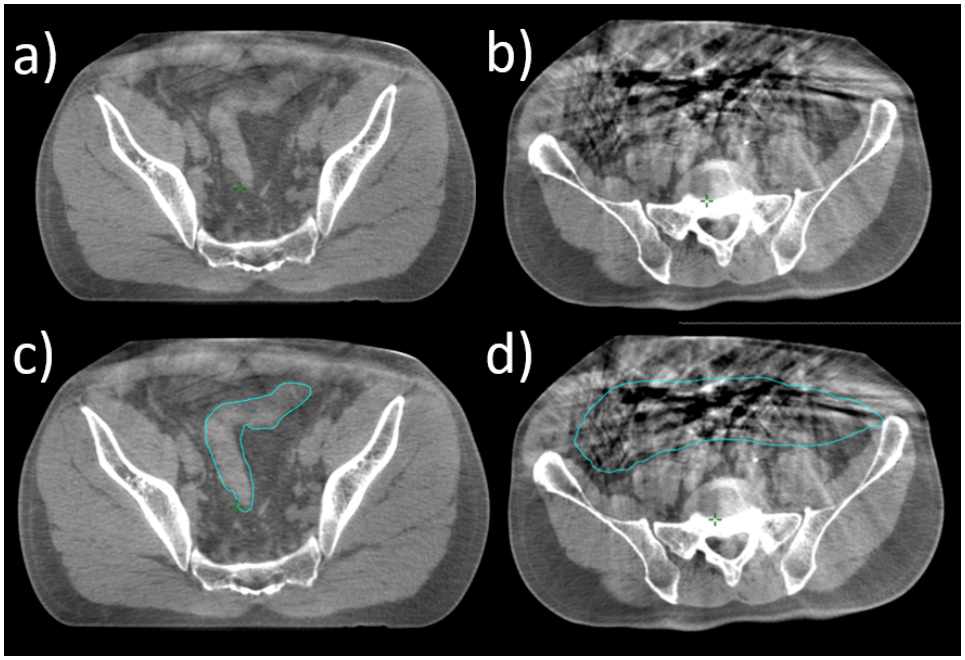

Figure 4.8: a) CBCT image slice of a patient where the amount of artifacts are limited, giving a clear sight of the bowel loops. b) CBCT of the same patient but higher ut in the cranial direction. This CBCT image is more affected by artifacts making it hard to identify the bowel loops. c) Delineation of bowel loop. d) The bowel included in a bowel bag structure due to artifacts.

4.5.2 Dosimetric comparison of ART versus IGRT

Results from D99.5% of the CTV for the simulated ART treatment and the simulated IGRT treatment for both EQUI beam setup and the CS beam setup are given in figure 4.9. There was a significant difference (p=0.0005) in CTV coverage between the IGRT and ART treatments for the EQUI beam angle setup. The median of the ART treatments with the EQUI beam setup was 98.2%, and the median for IGRT treatments with the EQUI beam setup was 97.7%. The boxplot shows that the IGRT plans, both for EQUI and CS, have outliers that result in the CTV goal not being fulfilled. One of the outlying values for the CS beam setup is within acceptable variation that was sat for the CTV coverage (D99.5% $\geq$95%). Whereas for the EQUI beam angle setup both of the outliers are beyond what is considered an acceptable variation. These outliers all belong to patient 6. The simulated ART treatment with EQUI beam setup has also an outlier, but this value is within the acceptable variation that was set for the CTV coverage. This indicates that the CTV coverage in ART treatments is more stable.

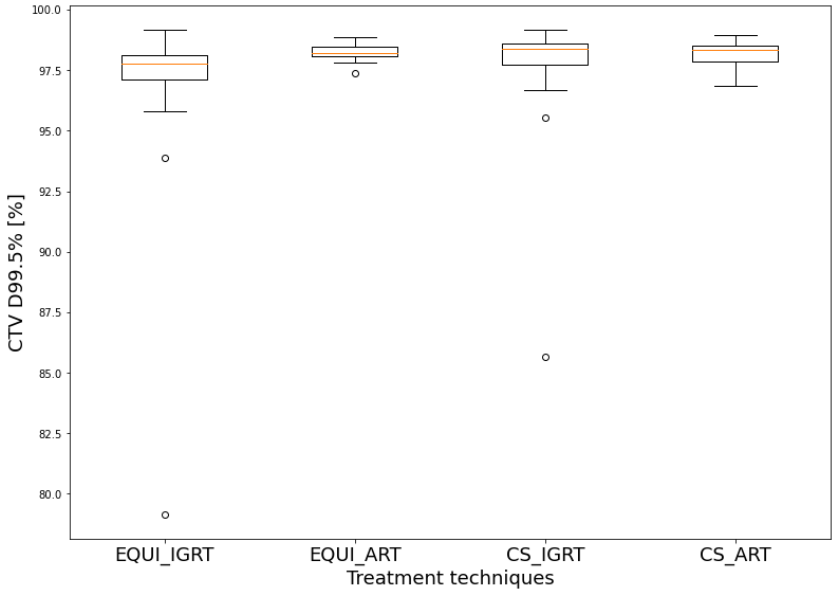

Figure 4.9: Box plot of D99.5% of CTV. The box represents the interquartile range, and the yellow line represents the median. The "whiskers" extends to minimum and maximum data points that are not outliers. The circles are outliers, which means they are more than 1.5 box width from the edge of the box.

The boxplot that illustrates the mean dose to the bladder shows that the IGRT treatments have a lower median value compared to the simulated ART treatments. However, there were no significant difference between the treatment techniques. There is a large difference in the minimum and maximum value for all four treatment techniques.

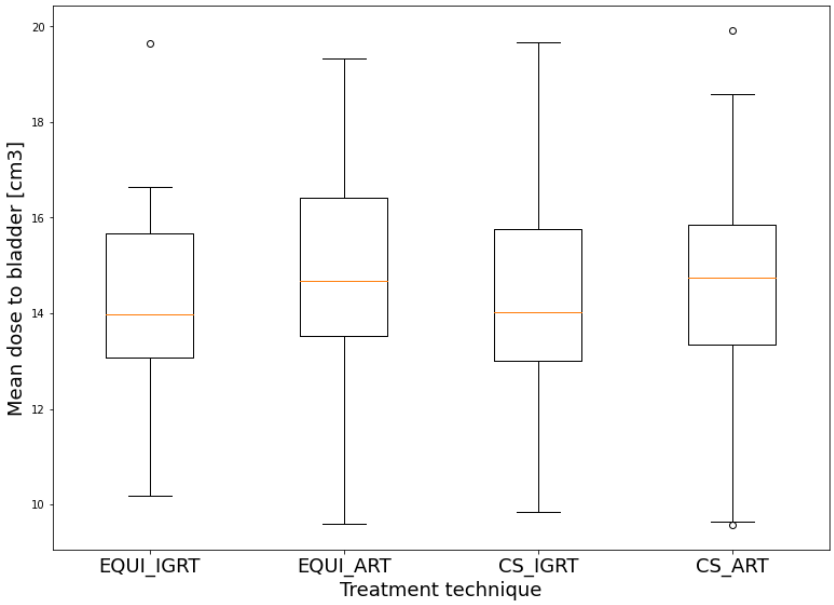

Figure 4.10: Box plot of mean dose to bladder. The box represents the interquartile range, and the yellow line represents the median. The "whiskers" extends to minimum and maximum data points that are not outliers. The circles are outliers, which means they are more than 1.5 box width from the edge of the box.

The simulated treatment with CS beams setup for both ART and IGRT has a smaller median for the V10 Gy value for bowel compared to the corresponding simulated treatments with EQUI beam setup. The V10 Gy of the simulated ART treatments with the EQUI beam setup was significantly lower (p=0.01) compared to the V10 Gy of the simulated IGRT treatments with the EQUI beam setup. The median V10 Gy for the IGRT treatments was 173 cm^3, and the median V10 Gy of the ART treatments was 145 cm^3. There was also a significant difference (p=0.01) between the CS ART treatments and the CS IGRT treatments. The median V10 Gy of the ART treatments was 123 cm^3, compared to the median V10 Gy of the IGRT treatments which was 127 cm^3. The V10 Gy for the simulated ART treatments with the CS beam setup was significantly lower (p=0.01) compared to the simulated ART treatment with the EQUI beam setup. The IGRT plans have several outliers meaning that there is a great variation of the V10 Gy value in the patient group.

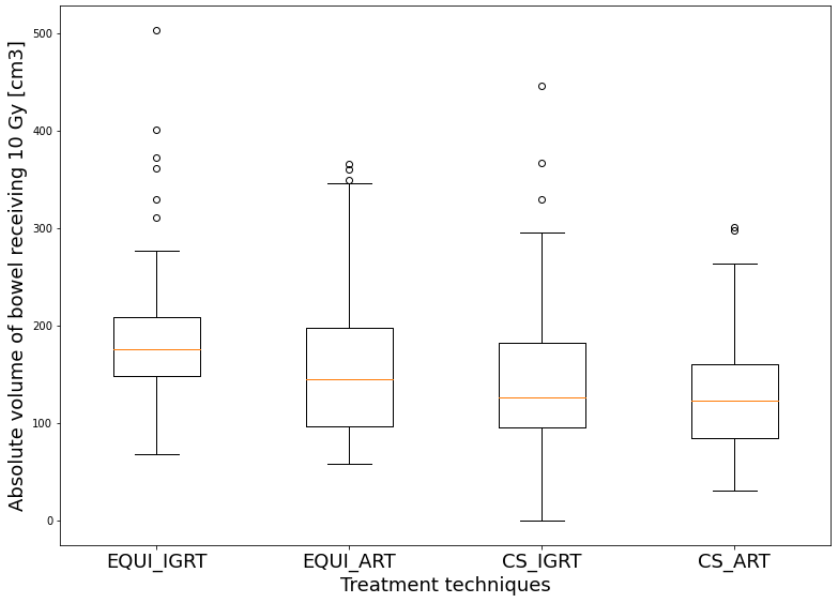

Figure 4.11: Box plot of V10Gy for bowel. The box represents the interquartile range, and the yellow line represents the median. The "whiskers" extends to minimum and maximum data points that are not outliers. The circles are outliers, which means they are more than 1.5 box width from the edge of the box.

4.5.3 Risk of severe acute diarrhea for the simulated treatments

The toxicity for the simulated treatments was based on the median V10 Gy across all fractions in each patient. The median V10 Gy and the calculated toxicity risk are listed in table 4.9. For all patients except patient 3, the ART treatments resulted in the lowest V10 Gy value and thus the lowest risk of severe acute diarrhea. For 3 of 7 patients, the CS beam angle setup with ART gave the lowest toxicity risk. For 2 of 7 patients, the EQUI beam angle setup with ART resulted in the lowest toxicity risk. For patient 5 both ART treatments gave the lowest toxicity risk.

Table 4.9: The median V10 Gy of the five fraction for each patient and the toxicity risk calculated based on the median V10 Gy for the simulated treatments.

Patient 1				
	EQUI_IGRT	**EQUI_ART**	**CS_IGRT**	**CS_ART**
V10Gy [cm^3]	208	177	192	158
Toxicity risk [%]	17	15	16	14
Patient 2				
	EQUI_IGRT	**EQUI_ART**	**CS_IGRT**	**CS_ART**
V10Gy [cm^3]	372	349	329	252
Toxicity risk [%]	32	29	27	20
Patient 3				
	EQUI_IGRT	**EQUI_ART**	**CS_IGRT**	**CS_ART**
V10Gy [cm^3]	132	192	81	114
Toxicity risk [%]	12	16	10	11
Patient 4				
	EQUI_IGRT	**EQUI_ART**	**CS_IGRT**	**CS_ART**
V10Gy [cm^3]	138	71	121	52
Toxicity risk [%]	13	9	12	9
Patient 5				
	EQUI_IGRT	**EQUI_ART**	**CS_IGRT**	**CS_ART**
V10Gy [cm^3]	190	80	95	80
Toxicity risk [%]	16	10	10	10
Patient 6				
	EQUI_IGRT	**EQUI_ART**	**CS_IGRT**	**CS_ART**
V10Gy [cm^3]	156	116	128	159
Toxicity risk [%]	14	11	12	14
Patient 7				
	EQUI_IGRT	**EQUI_ART**	**CS_IGRT**	**CS_ART**
V10Gy [cm^3]	184	81	124	114
Toxicity risk [%]	15	10	12	11

Each fraction for ART and IGRT and the two beam setups were considered as paired observations. Due to this many observations, the t-test was considered. Since the observations violated normality, as shown in figure 4.13, the Wilcoxon sign-rank test was utilized for this statistical comparison as well. Between the EQUI beam angle setup for IGRT and ART, there was a significant difference (p=0.0003). The median value of the toxicity risk for the IGRT treatment with the EQUI beam setup was 15%, and for the corresponding ART treatment, the median value of the toxicity risk was 11%. Between the two IGRT treatments with the EQUI beam setup and the CS beam setup, there was also a significant difference in the toxicity risk (p=0.0000002), with the median value of the toxicity risk being 15% for the EQUI beam setup and 12% for the CS beam setup. There was also a significant difference (p=0.01) between the simulated IGRT and ART treatments for the CS beam setup. The median toxicity risk was 12% for both the simulated IGRT treatments and the simulated ART treatments with the CS beam setup. There was no significant differences between the two ART treatments.

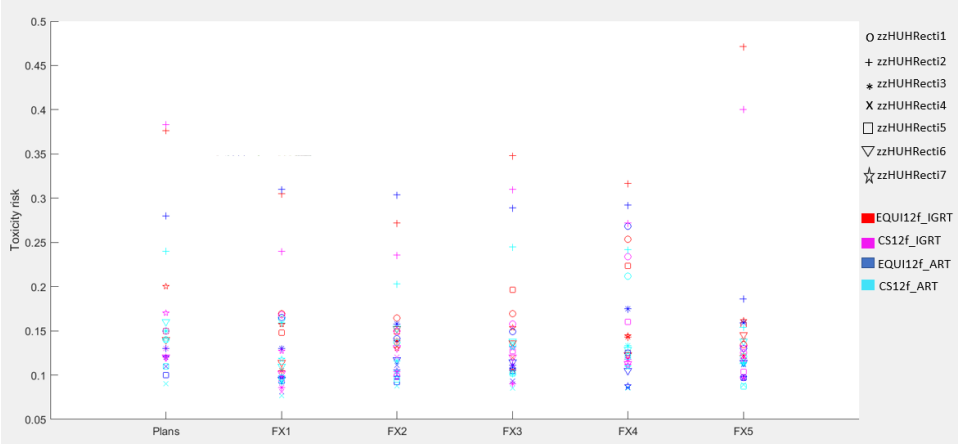

Figure 4.12: Plot of the toxicity risk values for each fraction for each patient. Each patient has its individual mark, and the treatment technique its individual color.

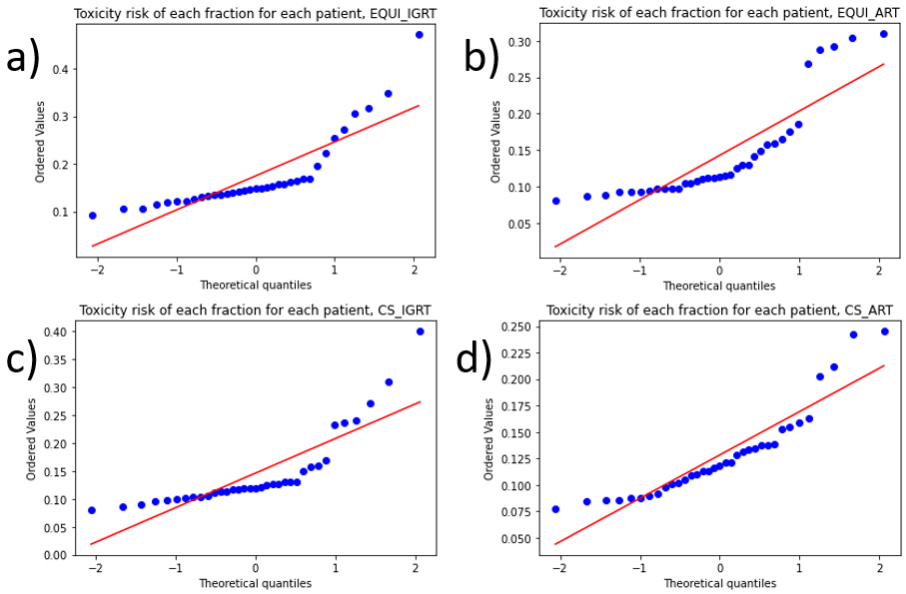

Figure 4.13: a) Q-Q plot of the toxicity risks for IGRT EQUI beam setup. b) Q-Q plot of the toxicity risks for ART EQUI beam setup .c) Q-Q plot of the toxicity risks for IGRT CS beam setup. d) Q-Q plot of the toxicity risks for ART CS beam setup

Chapter 5

Discussion

The main motivation behind this project has been to facilitate for a clinical implementation of online re-planning in rectal cancer. Preparing for the online re-planning workflow included finding PTV margins and clinical goals. The work included investigation of the different amount of beam angles to use for IMRT. Here 12 fields were chosen to be used in the adaptive workflow since, with this option, it was easier to fulfill target coverage. This work also introduced treatment simulations using the Emulator as a method to study dosimetric differences between ART and IGRT. Performing treatment simulation on the Emulator was the time-consuming part of this project and we had a steep learning curve. Dosimetric comparisons of ART versus IGRT were done for the plans to study what to expect from the different treatment strategies. Statistical comparisons were also done for the simulated treatments of ART and IGRT.

5.1 Preparing an online re-planning workflow

5.1.1 Margins

When studying possible margins it was hard to compare different literature. There were also relatively few patients included in the studies. The articles about rectal motion included in this master quantified the margins in their own individual way. Eijkelenkamp et al. and Van den Ende et al. both presented GTV margins. Even so, these were useful as they both showed the potential in reducing margin when utilizing online ART. The two articles that were most corresponding to my workflow were the studies done by de

Jong et al. Initially they compared plan selection with online adaptive RT with simulation [50]. The CTV was expanded with 3 mm. The conclusion of the paper was that the 3 mm margin was a potential margin to be used within online ART but in need of further studies. For the first online adaptive treatment with the Ethos treatment system de Jong et al. however, implemented a 5 mm PTV margin in all directions except for 8 mm in the cranial direction [54]. Our choice of 4 mm for the online ART is therefore smaller than their implementation. Their PTV margin in the cranial direction is actually identical to the clinical margins applied today at HUH for IGRT treatments.

The margin that was chosen to proceed with is the lower spectrum of what can be evaluated as a sufficient margin. The 4 mm isotropic margin was a pragmatic solution chosen in order to study the effect of maximal dose sparing to the bowel. Online ART adjusts for the inter-fractional displacements. The amount of intra-fraction motion however, is dependent on the time it takes to execute the treatment fraction. Kleijnen et al. discovered that for 90% of the time, the average distance that included 95% of the surface voxels never extended over 3.6 mm for the CTV during a one-minute time interval. Another discovery by Kleijnen et al. was that the plan of the day technique is only efficient if the time of treatment is kept to under 18 minutes. Extending the time of fraction to over 18 minutes is equal to delivering the treatment plan up to four days after the CBCT accumulation. With smaller margins these adjustments will need to be executed faster. Utilizing larger margins will not require as fast adjustments, but then again the purpose and advantage with online ART may diminish.

The mean time-use for us from the delineation to the treatment delivery was 33 minutes. As this was the first time using the Emulator there is good reason to believe that the treatment time will be reduced with practice and when given the right competence. The 4 mm PTV margin will need to be validated before a clinical implementation.

5.1.2 Clinical goals

The clinically implemented BowelBag clinical goal at HUH is a mean dose. The currently applied dose objective for SCRT at HUH can be modified to further reduce dose

to the bowel (see section 5.1.3). In the clinically implemented IGRT workflow, the BowelBag structure is delineated on the CT-planning image and then the same structure is used for the whole treatment process. However, in the online re-planning workflow the bowel structure is delineated on the daily-session image for each fraction based on the anatomy of the day. The studies that are published about dose-volume effects of the bowel are mainly from conventional treatment such as daily 2 Gy fractions [35]. As this meta-study focuses on 5 Gy x 5 fractions we decided not to look at the clinical goals recommended by QUANTEC but establish clinical goals by a trial and error method based on SCRT. The reason for choosing the DVH rather than studying the dose distribution when constructing clinical goals is because the DVH is more implemented in the clinical. In addition to that, the DVH gives easier access to quantified dose-volume data.

To study the dose delivery to the bowel structure, 9 dose levels were chosen as report values for the initial ART plans. These gave a good overview of the different dose levels for the bowel structure. The clinical goals were only tested for one ART fraction. To construct better clinical goals it would have been useful to simulate one or several fractions for all patients with only the 9 reported values as the daily adapted bowel structure deviates from the planning structure. It would also have been useful to study the alternations in the bowel structure for the different fractions. However, this method would have been more time-consuming, and the clinical goals defined in this master thesis were found to be efficient when compared to the benchmarking plans.

Holyoake et al. discovered that V10 Gy was the DVH parameter with the strongest prediction of toxicity risk (p=0.004) [38]. The clinical goals in this project were assigned to the dose levels 7.5 Gy and 20 Gy. The 7.5 Gy dose level was chosen by comparing the DVH for the benchmarking plans and the ART plans. The majority of the patients showed room for further improvement around 7.5 Gy for the ART plans. In addition to this V10 Gy was not chosen as a clinical goal to avoid this dose level being biased as this was used to study the toxicity risk. The V20 Gy dose level was chosen to study a high dose, as well as it is considered a dose level predictive of toxicity [38].

The clinical goals were set by studying the DVHs in a trial and error method. The test simulations that were done with the initial clinical goals resulted in hot spots > 107% for some of the male patients. If this were to happen during treatment it would cause for postponing of the treatment as a new treatment plan with adjusted clinical goals needed to be generated. This would result in more use of resources in the clinic and also further strain on the patient. Therefore the absolute volume dose criteria for the male patient group was increased even further.

In the clinical implemented workflow at HUH there is no differences in the treatment of rectal cancer for men and women. The question of whether or not having separate clinical goals for men and women needs to be further studied. The patient group, with only two women, included in this project is not broad enough for a conclusion in regard to exact values for the clinical goals. The reasoning behind having separate clinical goals is based on anatomy differences. Where the bowel is located for men, the cervix is located for women. This results in the bowel being pushed further away from the PTV and the high dose. The median delineated bowel volume for the two female patients were 499 cm^3 and 389 cm^3 compared to the median delineated bowel volume for the male patients with 246 cm^3, 958 cm^3, 437 cm^3, 601 cm^3 and 662 cm^3. The initial clinical goals for the majority of the males were too strict. This is the reason for keeping the initial calculated clinical goals for the two female patients, as they did not result in hot spots.

The sat clinical goals for bowel in absolute volume may not be as effective for all patients as even within gender patient groups there is a great variation in bowel volume. The median delineated bowel volume for patient 3 for the five fractions was 437 cm^3. As the median value was 437 cm^3 the clinical goal for V7.5 Gy sat to 450 cm^3 might not be as effective as for patients with a larger volume. Due to this fact, the mean clinical goal used for IGRT may be more efficient for patient 3. Nevertheless, the clinical goals found in this master thesis did give an indication on that online re-planning with the Ethos TPS is efficient when optimizing sparing dose to the bowel.

As the goal of this thesis was to study the possibility of reducing the toxicity of the bowel there has not been a focus on the bladder or cervix. Therefore, the clinical goal of the bladder in the Ethos TPS was sat to Dmean $\leq$ 20 Gy. The consequences of this are discussed in section 5.3. No clinical goal was given to the cervix. The amount of radiation to the cervix for women might be something that should be addressed in further studies.

5.1.3 Benchmarking bowel dose using a line objective

The dose-volume data on the line objective versus a mean clinical goal are not included in this master thesis. However, as I developed the line objective in Eclipse TPS, I studied the differences in dose-volumes for these two techniques. The line objective was an effective tool for pressing down the bowel dose and is a good alternative to use in Eclipse TPS. The line objective was used to benchmark bowel dose as it is a more restricting method compared to using a few independent points, and we wanted to study the maximal bowel sparing. As the optimization process is different in Ethos TPS we also wanted to assure its performance. The reason why the line objective was not utilized in the Ethos TPS is that it would prolong the optimization process. The duration of the optimization process increases when adding many clinical goals. By default it would also be prioritized last of the other clinical goals, meaning that it would not be as effective as wanted [communication with Ethos representative from Varian]. As saving time is crucial in an online re-planning workflow two clinical goals of the bowel were implemented and the line objective optimized plans were used for benchmark bowel sparing instead.

The comparisons of the treatment plans with the line objectives and the plans generated in Ethos TPS with two clinical goals for bowel showed no significant difference for the two dose levels V7.5 Gy and V20 Gy. An important difference was however the PTV coverage. There was a significant difference in the D98% for the PTV. The Ethos TPS managed to press down the dose to the bowel and still maintain a good PTV coverage, where 5 of 7 plans achieved D98% $\geq$97%. For the line objective plans 4 of 7

plans achieved D98% $\geq$96%, the highest being 96.2%. As the goal for the PTV coverage is D98%>95%, both the line objective and Ethos TPS do a good job to fulfill this criterion.

5.2 Simulating treatments

5.2.1 Using the Emulator

This was the first work where the Emulator was used to develop an online re-planning workflow and a lot of unexpected obstacles occurred. This master thesis was based on the ability to transfer data between the Eclipse TPS and Ethos TPS. One complication that occurred was the fact that the calibration of Eclipse and the Emulator did not correspond. Importing the treatment plans from Eclipse TPS to the Emulator gave several errors. This required contacting Varian to modify the calibration settings of the Emulator used by the clinic at HUH. Another complication occurred when transferring the data from each fraction from the Emulator to Eclipse TPS. This required a workaround with import-export of data to and from the Eclipse TPS which was time-consuming.

The Emulator was not compatible with importing a second plan for the same patient. Therefore a workaround was done to enable duplicate treatments for a given patient in the Emulator, and separate CS and EQUI simulations were made. The structures from the test simulations that were run for all five fractions for all patients were used as a template when simulating the alternative beam setup. The template structures were studied in Eclipse TPS and I tried to copy them as precisely as possible. However, as they could not be copied directly into the Emulator there are some deviations in the structure volumes from the simulation done for the EQUI beam angle setup and the CS beam angle setup. For patient 3 the bowel volume for one fractions with the EQUI beam angle setup was 480.3 cm^3, compared to the bowel volume for the CS beam angle setup with 486.1 cm^3. In another fraction the consistency was high for the delineations, the difference between them constituted to 0.6 cm^3. This will therefore most likely not influence the results between ART and IGRT for the neither the CS beam setup nor the EQUI beam setup.

Simulating treatment with the Emulator was a steep learning curve. The Emulator system was relatively stable, but there were some instances where the system crashed and the whole session was restarted. Also when delivering the treatment the system crashed and loaded for a long time. The simulations were done with my supervisor available for guidance. There was a big difference between simulating the first patient and the last. The first simulation took the longest time. With more practice, we got more and more confident in the decisions and learned what to recognize of different anatomy structures in the CBCT images. When the online re-planning workflow is implemented clinically there will also be a clinical learning curve as one becomes more familiar with the Ethos TPS and the workflow. The clinical in-room time for the clinical implementation of online ART done by De Jong et al was 34 minutes. Their method was to streamline the workflow from the start. The radiotherapists who participated in the clinical implementation of online ART at their institution were already experienced in CBCT-based online IGRT. They also needed to participate in a delineation course and a target definition workshop. In addition to this, the radiotherapists had 40 hours of self-study on the research version of the clinical software.

All treatment simulations utilized the rectum, bladder and, bowel as influencers. As the cervix had not been delineated on the planning CT this was not suggested as an influencer by the Emulator. The bladder was the structure that needed the least adjustments. How well the emulator delineated the bowel was very dependent on the patient, and the amount of artifacts. There were also some incidents where the Emulator detected none of the bowel structure. This resulted in a longer delineation time. The part of the rectum that needed the most modification was the transition from the rectum to bowel. Otherwise, the rectum was delineated well by the Emulator.

No oncologist verified the CTVs that were delineated in the Emulator, only the CTVs on the planning CT. Therefore we chose to copy the CTV on the planning CT. This was done by using internal markers as reference, such as blood vessels, surrounding organs, and calcium deposits within the pelvis. The expansion of the CTV can be different from LCRT and SCRT as the patients are in different stages. Still, we chose to proceed with the CTVs defined for LCRT as these were delineated by the oncologists. Both LCRT and SCRT are recommended by ESMO as preoperative treatment [10]. The patients that will have maximum benefit of LCRT and SCRT are still not defined internationally and this is being investigated in multiple trials. One of these trials being RAPIDO.

5.2.2 Considerations for bowel segmentation

As the goal was to study the toxicity risk of the bowel the initial plan was to delineate only the bowel loops. However, as shown in 4.5.1 the artifacts became dominant moving up in the cranial direction. Therefore, the bowel became a combination of bowel loops and BowelBag. Some patients with a greater amount of bowel bag than others. There was a great variation in the amount of artifacts for the individual patients. Patient 5 had especially many artifacts. This resulted in most of the bowel for patient 5 being included in a BowelBag structure. In addition to it being hard to identify the bowel loops the implementation of the partial BowelBag structure was also done to make the delineation more efficient. Still, delineation of the bowel was the most time-consuming part of the simulation. As shown by Kleijnen et al., and Eijkelenkamp et al., fraction times needs to be short in order to limit organ motion. In the areas where the bowel loops are easy to identify, delineating the bowel loop is not more time-consuming compared to delineating a BowelBag structure. This method allows for delineating the bowel loops that are most affected by high dose. Both de Jong et al. and Sibholt et al. included the bowel in a bowel cavity structure in the planning CT [47], [50]. However, the bowel was not included in the daily adaption based on CBCTs in their clinical implementations. At HUH for prostate, the bowel is not defined in the daily CBCTs. As no one has included bowel in their online adaptive Ethos workflow it has been difficult to compare the results of this master thesis.

5.3 Comparison of online ART and IGRT

The D99.5% > 98% was given as the clinical goal for the CTV. The simulated IGRT treatments both had outliers where this clinical goal is not fulfilled. The results in regard to bowel sparing showed that the median bowel volume is lowest for the CS beam angle setup treatments, both for IGRT and ART. The CS beam angle selection has no entering beams in the ventral direction in contrary to the EQUI beam selection. This results in a lower dose to the bowel structure. All investigated deliveries and beam setup had outliers, however, the EQUI beam setup for IGRT has the greatest amount of outliers. This indicates that the EQUI beam setup with IGRT restricts the amount of bowel volume receiving 10 Gy least effective.

De Jong et al. discovered a significant reduction for dose to both bowel bag and bladder for all DVH parameters when comparing the simulated plan selection and simulated online strategy [50]. However, they utilized a smaller margin around the CTV (3 mm). They also used the same clinical goals and prioritization for the OARs in the online ART treatment as the ones used in the plan selection strategy. The clinical goals for the OARs and their prioritization were also the same in the online ART treatment and the plan selection strategy. The simulation data for bladder presented in the box plot in figure 4.10 shows that the median for the IGRT treatments is lower compared to the ART treatments. This is due to that this project focused on optimization for bowel sparing in Ethos. The clinical goal of the bladder in Ethos TPS was therefore sat to Dmean $\leq$ 20 Gy. More restrictive clinical goals were tested but this affected the amount of bowel sparing. The threshold stated by Quantec for Grade $\geq$3 late toxicity for the bladder is Dmax < 65 Gy [33]. Meaning that the Dmean $\leq$ 20 Gy, the equivalent dose in 2 Gy fractions is EQD_2 = 40 Gy, is still within what is considered an acceptable dose to the bladder.

5.3.1 Risk of severe acute diarrhea

In order to translate dosimetric differences of the investigated treatments into clinical relevance, a dose-response model for severe acute diarrhea was used. When wanting

to quantify the clinical consequence of dose to bowel there is a lack of models developed for SCRT. In addition to this, the models for predicting the biological effect are based on the dose to the bowel in the planning CT wheras we had input for all treatment fractions as well. The model utilized to quantify the toxicity risk in this thesis is based on conventional fractionation. Therefore this model may not provide a precise quantification of the severe acute diarrhea but is used to give an indication of the differences in delivery techniques. The model is also based on the DVH data of small bowel delineated as bowel loops. In this project, it became necessary to combine the bowel structure as both bowel loops and a bowel bag structure. This means that in reality, the absolute toxicity risk could be lower and more bowel volume than anticipated is being spared. This will however not influence the comparisons between online ART and IGRT since the delineation of the bowel structure was identical for every patient. The absolute risk estimated between different patients should be interpreted with care since some patients have more artefacts resulting in larger bowel volume (and V10 Gy). In the RAPIDO trial there were a higher frequency of severe acute toxicity in the patient group with SCRT and intensified chemotherapy compared to CRT. This may also alter the toxicity risk estimates found in this project.

When the risk for acute severe diarrhea was calculated based on the median V10 Gy of the five fractions for one patient the results showed that the CS beam angle setup resulted in the lowest toxicity risk for most cases with 3/7 compared to EQUI with 2/7. The IGRT treatments resulted in a lower V10 Gy value and followed a lower toxicity risk only for patient 3. In table 4.9 it appears as both IGRT treatments were better compared to the ART treatment with CS beam angle setup for patient 6. However, patient 6 is the outlier in figure 4.9, meaning that in the case of the IGRT treatments the sparing of bowel affected the CTV coverage negatively. For two of the fractions it resulted in the CTV coverage not being fulfilled.

Figure 4.12 gives a good indication that the toxicity risk is not equal for all fractions. Some alternations in the bowel volume occur because of the delineation with artifacts, but also due to bowel movements in between different fractions. Of the seven patients,

patient 2 was the one with the largest amount of bowel volume which may explain why this patient is so distinctively different. This patient is a good example of how effective ART may be compared to IGRT. The toxicity risk for fraction five for the EQUI beam angle setup is 47% in contrast to the 15% achieved with the CS beam angle setup with ART.

5.4 Future work

During simulation of the treatment and when delineating the CTV, the discovery was that some of the bowel volume could be spared from high dose if the CTV were to be restricted in the areas it overlapped with the bowel. The same applies to the bladder. Delineating the bowel as individual bowel loops instead of a BowelBag structure may also allow for increased sparing of individual loops. One limitation to this is the amount of artifacts that can occur on a CBCT. However, for the majority of the patients the artifacts close to the PTV were limited, giving a decent visibility of the bowel loops. Thus, delineating the bowel close to the target volume as individual loops and including the bowel in a BowelBag structure when the artifacts become too distinctive, may allow for sparing the bowel loops of high dose.

The delineation of the bowel structure and importantly also the validation of PTV margins should be further investigated. A good tool for evaluating the margins is to utilize post fraction CBCTs. This allows for studying how the organs have shifted during the treatment delivery.

Including more patients in future work will make it possible to optimize more effective clinical goals for the patient group. Gender differences should be continued to be studied in future work.

In order to quantify the benefit of the ART treatment more accurately, there needs to be developed a toxicity model based on SCRT data for rectal cancer. In addition to a toxicity model, the use of dose accumulation models that takes organ motion and the

actual delivered fractionation dose into account should be implemented in the clinical workflow to achieve knowledge about the actual biologic effect. As the use of daily imaging increases, hopefully the focus on obtaining valuable data follows, and this can be achieved in the near future.

Chapter 6

Conclusions

In this master, treatment simulations for an online re-planning workflow was developed and successfully implemented on the Emulator. There is not enough data to conclude that the 4 mm PTV margin used in the adaptive workflow in this master thesis is the optimal margin for ART. Yet, 4 mm is an option if the time for execution of an adaptive fraction is 15 min or less.

Clinical goals were successfully found for the bowel for an online re-planning strategy by benchmarking against line objective plans. Findings in this master thesis indicated that creating gender-specific treatments may lead to more efficient optimization of sparing dose to the bowel and avoidance of elevated dose outside of the target volume. Treatment planning with these clinical goals together with the reduced PTV margins spared the bowel without compromising the target coverage as compared to IGRT. The sparing of bowel in the online ART plans, did not depend on the choice of beam angles setup.

The dosimetric differences were analyzed by simulating treatments based on online re-planning and IGRT. This master thesis gives a solid indication that online re-planning ART can improve treatment of LARC by reducing RT dose to healthy bowel. In addition to sparing the dose to the bowel, the treatments with ART gave a better and more stable PTV and CTV coverage. However, for bladder, the treatments with ART resulted in an elevated dose to the bladder compared to the IGRT strategy.

The bowel sparing in online re-planning ART translated to lower risks of severe acute diarrhea, for both beam setups. These results show that ART, irrespective of beam angles, gives a significantly lower risk for toxicity compared to the IGRT treatments.

Bibliography

[1] W. H. O. International agency for research on cancer, *Rectum, Source: Globocan 2020*, https://www.helsedirektoratet.no/retningslinjer/kreft-i-tykktarm-og-endetarm-handlingsprogram, 2020.

[2] Helsedirektoratet, "Nasjonalt handlingsprogram med retningslinjer for diagnostikk, behandling og oppfølging av kreft i tykktarm og endetarm," Dec. 2020.

[3] Kreftregisteret, "Nasjonalt kvalitetsregister for tykk- og endetarmskreft, Årsrapport 2020.," 2021.

[4] R. Berman, V. Lee, and D. Ryan, *Rectal Cancer Treatment Health Professional Version - National Cancer Institute*, https://www.cancer.gov/types/colorectal/hp/rectal-treatment-pdq, Feb. 2022.

[5] B. M. Wolpin, J. A. Meyerhardt, H. J. Mamon, and R. J. Mayer, "Adjuvant Treatment of Colorectal Cancer," *CA Cancer J. Clin.*, vol. 57, no. 3, pp. 168–185, May 2007, ISSN: 0007-9235. DOI: 10.3322/canjclin.57.3.168.

[6] R. Glynne-Jones, L. Wyrwicz, G. B. E. Tiret, C. Rödel, A. Cervantes, and D. Arnold, *Clinical Practice Guidelines Slideset Rectal Cancer*, https://www.esmo.org/content/download/178876/3265837/1/Clinical-Practice-Guidelines-Slideset-Rectal-Cancer.pdf, 2018.

[7] *Definition of metastasis - NCI Dictionary of Cancer Terms*. [Online]. Available: https://www.cancer.gov/publications/dictionaries/cancer-terms/def/metastasis.

[8] *Rectal Cancer Treatment - Patient Version - National Cancer Institute*, https://www.cancer.gov/types/colorectal/patient/rectal-treatment-pdq, Sep. 2021.

[9] T. A. Hope, M. J. Gollub, S. Arya, *et al.*, "Rectal cancer lexicon: consensus statement from the society of abdominal radiology rectal & anal cancer disease-focused panel," *Abdom. Radiol.*, vol. 44, no. 11, pp. 3508–3517, Nov. 2019, ISSN: 2366-0058. DOI: 10.1007/s00261-019-02170-5.

[10] R. Glynne-Jones, L. Wyrwicz, E. Tiret, *et al.*, "Rectal cancer: ESMO Clinical Practice Guidelines for diagnosis, treatment and follow-up†," *Ann. Oncol.*, vol. 28, pp. iv22–iv40, Jul. 2017, ISSN: 0923-7534. DOI: 10.1093/annonc/mdx224.

[11] R. R. Bahadoer, E. A. Dijkstra, B. van Etten, *et al.*, "Short-course radiotherapy followed by chemotherapy before total mesorectal excision (TME) versus preoperative chemoradiotherapy, TME, and optional adjuvant chemotherapy in locally advanced rectal cancer (RAPIDO): a randomised, open-label, phase 3 trial," *Lancet Oncol.*, vol. 22, no. 1, pp. 29–42, Jan. 2021, ISSN: 1474-5488. DOI: 10.1016/S1470-2045(20)30555-6. eprint: 33301740.

[12] *Radikaloperasjon Store medisinske leksikon*, Sep. 2018. [Online]. Available: https://sml.snl.no/radikaloperasjon.

[13] J. Erlandsson, T. Holm, D. Pettersson, *et al.*, "Optimal fractionation of preoperative radiotherapy and timing to surgery for rectal cancer (Stockholm III): a multicentre, randomised, non-blinded, phase 3, non-inferiority trial," *Lancet Oncol.*, vol. 18, no. 3, pp. 336–346, Mar. 2017, ISSN: 1470-2045. DOI: 10.1016/S1470-2045(17)30086-4.

[14] J. Wang, Y. Long, K. Liu, Q. Pei, and H. Zhu, "Comparing neoadjuvant long-course chemoradiotherapy with short-course radiotherapy in rectal cancer," *BMC Gastroenterol.*, vol. 21, no. 1, pp. 1–7, Dec. 2021, ISSN: 1471-230X. DOI: 10.1186/s12876-021-01851-0.

[15] J. B. Yuval, S. Patil, and J. Garcia-Aguilar, "Interpreting the RAPIDO trial: factors to consider," *Lancet Oncol.*, vol. 22, no. 3, e87–e88, Mar. 2021, ISSN: 1470-2045. DOI: 10.1016/S1470-2045(21)00061-9.

[16] N. A. Mayles. P and J. Rosenwald, *Handbook of Radiotherapy Physics: Theory and Practice (1st ed.)* Taylor & Francis Ltd, 2007.

[17] *External Beam Radiation Therapy for Cancer - National Cancer Institute*, https://www.cancer.gov/about-cancer/treatment/types/radiation-therapy/external-beam, May 2018.

[18] F. M. Khan and J. P. Gibbons, *Khan's the physics of radiation therapy*. Lippincott Williams & Wilkins, 2014.

[19] H. Cember and T. Johnson, *Introduction to Health Physics (Fourth edition)*. New York: McGraw-Hill Education., 2009.

[20] W. Strydom, W. Parker, and M. Olivares, *Review of Radiation Oncology Physics: A Handbook for Teachers and Students*, 2009. [Online]. Available: https://www.irsn.fr/fr/professionnels_sante/documentation/documents/syllabus_chapitre_8.pdf.

[21] E. J. Hall, A. J. Giaccia, *et al.*, *Radiobiology for the Radiologist 7th edition*. Philadelphia, 2006, vol. 6.

[22] D. Hanahan and R. A. Weinberg, "Hallmarks of Cancer: The Next Generation," *Cell*, vol. 144, no. 5, pp. 646–674, Mar. 2011, ISSN: 0092-8674. DOI: 10.1016/j.cell.2011.02.013.

[23] F. W. McKenna and S. Ahmad, "Isoeffect calculations with the linear quadratic and its extensions: An examination of model-dependent estimates at doses relevant to hypofractionation," *Journal of Medical Physics / Association of Medical Physicists of India*, vol. 36, no. 2, p. 100, Apr. 2011. DOI: 10.4103/0971-6203.79689.

[24] N.-S. Hegemann, M. Guckenberger, C. Belka, U. Ganswindt, F. Manapov, and M. Li, "Hypofractionated radiotherapy for prostate cancer," *Radiation Oncology (London, England)*, vol. 9, 2014. DOI: 10.1186/s13014-014-0275-6.

[25] S. Levernes, "Volumer og og doser i ekstern stråleterapi," Nov. 2012, ISSN: 0804-4910.

[26] N. G. Burnet, S. J. Thomas, K. E. Burton, and S. J. Jefferies, "Defining the tumour and target volumes for radiotherapy," *Cancer Imaging*, vol. 4, no. 2, p. 153, 2004. DOI: 10.1102/1470-7330.2004.0054.

[27] M. van Herk, "Errors and margins in radiotherapy," *Semin. Radiat. Oncol.*, vol. 14, no. 1, pp. 52–64, Jan. 2004, ISSN: 1053-4296. DOI: 10.1053/j.semradonc.2003.10.003.

[28] J. C. Stroom and B. J. M. Heijmen, "Geometrical uncertainties, radiotherapy planning margins, and the ICRU-62 report," *Radiother. Oncol.*, vol. 64, no. 1, pp. 75–83, Jul. 2002, ISSN: 0167-8140. DOI: 10.1016/S0167-8140(02)00140-8.

[29] H.-G. Menzel, "International commission on radiation units and measurements," *Journal of the ICRU*, vol. 14, no. 2, pp. 1–2, 2014.

[30] D. Xu, G. Li, H. Li, and F. Jia, "Comparison of IMRT versus 3D-CRT in the treatment of esophagus cancer: A systematic review and meta-analysis," *Medicine*, vol. 96, no. 31, Aug. 2017. DOI: 10.1097/MD.0000000000007685.

[31] L. W. Brady, H. Heilmann, and M. Molls, *New technologies in radiation oncology*. Springer, 2006, vol. 86.

[32] M. R. Young and B. Y. James, "Intensity modulated radiotherapy and image guidance," in *Prostate Cancer*, Elsevier, 2016, pp. 413–426.

[33] L. B. Marks, E. D. Yorke, A. Jackson, *et al.*, "Use of Normal Tissue Complication Probability Models in the Clinic," *International Journal of Radiation Oncology∗Biology∗Physics*, vol. 76, no. 3, Supplement, S10–S19, Mar. 2010, ISSN: 0360-3016. DOI: 10.1016/j.ijrobp.2009.07.1754.

[34] *Common Terminology Criteria for Adverse Events (CTCAE) | Protocol Development | CTEP*, Nov. 2017. [Online]. Available: https://ctep.cancer.gov/protocoldevelopment/electronic_applications/ctc.htm.

[35] B. D. Kavanagh, C. C. Pan, L. A. Dawson, *et al.*, "Radiation DoseVolume Effects in the Stomach and Small Bowel," *International Journal of Radiation Oncology∗Biology∗Physics*, vol. 76, no. 3, Supplement, S101–S107, Mar. 2010, ISSN: 0360-3016. DOI: 10.1016/j.ijrobp.2009.05.071.

[36] K. L. Baglan, R. C. Frazier, D. Yan, R. R. Huang, A. A. Martinez, and J. M. Robertson, "The dose-volume realationship of acute small bowel toxicity from concurrent 5-FU-based chemotherapy and radiation therapy for rectal cancer," *International Journal of Radiation Oncology∗Biology∗Physics*, vol. 52, no. 1, pp. 176–183, Jan. 2002, ISSN: 0360-3016. DOI: 10.1016/S0360-3016(01)01820-X.

[37] J. C. Roeske, D. Bonta, L. K. Mell, A. E. Lujan, and A. J. Mundt, "A dosimetric analysis of acute gastrointestinal toxicity in women receiving intensity-modulated whole-pelvic radiation therapy," *Radiother. Oncol.*, vol. 69, no. 2, pp. 201–207, Nov. 2003, ISSN: 0167-8140. DOI: 10.1016/j.radonc.2003.05.001.

[38] D. L. P. Holyoake, M. Partridge, and M. A. Hawkins, "Systematic review and meta-analysis of small bowel dosevolume and acute toxicity in conventionally-fractionated rectal cancer radiotherapy," *Radiother. Oncol.*, vol. 138, pp. 38–44, Sep. 2019, ISSN: 0167-8140. DOI: 10.1016/j.radonc.2019.05.001.

[39] W. C. Scarfe and A. G. Farman, "What is Cone-Beam CT and How Does it Work?" *Dent. Clin. North Am.*, vol. 52, no. 4, pp. 707–730, Oct. 2008, ISSN: 0011-8532. DOI: 10.1016/j.cden.2008.05.005.

[40] *KV Imaging Systems for Linear Accelerators | Radiology Oncology Systems*, Feb. 2020. [Online]. Available: https://www.oncologysystems.com/blog/kv-imaging-systems-for-linear-accelerators.

[41] L. A. Dawson and D. A. Jaffray, "Advances in Image-Guided Radiation Therapy," *J. Clin. Oncol.*, vol. 25, no. 8, pp. 938–946, Mar. 2007, ISSN: 0732-183X. DOI: 10.1200/JCO.2006.09.9515.

[42] *Definition of fiducial marker - NCI Dictionary of Cancer Terms*, Apr. 2022. [Online]. Available: https://www.cancer.gov/publications/dictionaries/cancer-terms/def/fiducial-marker.

[43] S. Thornqvist, L. B. Hysing, L. Tuomikoski, *et al.*, "Adaptive radiotherapy strategies for pelvic tumors a systematic review of clinical implementations," *Acta Oncol.*, vol. 55, no. 8, pp. 943–958, Aug. 2016, ISSN: 0284-186X. DOI: 10.3109/0284186X.2016.1156738.

[44] D. Yan, F. Vicini, J. Wong, and A. Martinez, "Adaptive radiation therapy," *Phys. Med. Biol.*, vol. 42, no. 1, pp. 123–132, Jan. 1997, ISSN: 0031-9155. DOI: 10.1088/0031-9155/42/1/008.

[45] R. P. J. van den Ende, E. M. Kerkhof, L. S. Rigter, *et al.*, "Feasibility of Gold Fiducial Markers as a Surrogate for Gross Tumor Volume Position in Image-Guided Radiation Therapy of Rectal Cancer," *International Journal of Radiation*

Oncology∗Biology∗Physics, vol. 105, no. 5, pp. 1151–1159, Dec. 2019, ISSN: 0360-3016. DOI: 10.1016/j.ijrobp.2019.08.052.

[46] A. Vestergaard, L. P. Muren, H. Lindberg, *et al.*, "Normal tissue sparing in a phase II trial on daily adaptive plan selection in radiotherapy for urinary bladder cancer," *Acta Oncol.*, vol. 53, no. 8, pp. 997–1004, Aug. 2014, ISSN: 0284-186X. DOI: 10.3109/0284186X.2014.928419.

[47] P. Sibolt, L. M. Andersson, L. Calmels, *et al.*, "Clinical implementation of artificial intelligence-driven cone-beam computed tomography-guided online adaptive radiotherapy in the pelvic region," *Physics and Imaging in Radiation Oncology*, vol. 17, pp. 1–7, Jan. 2021, ISSN: 2405-6316. DOI: 10.1016/j.phro.2020.12.004.

[48] Hoag, *Viewray mridian linear accelerator*, Aug. 2021. [Online]. Available: https://www.hoag.org/specialties-services/cancer/treatments-services/radiation-oncology/state-of-the-art-equipment/viewray-mridian-linear-accelerator.

[49] Elekta, *Elekta unity, mr linac*, Feb. 2022. [Online]. Available: https://www.elekta.com/products/radiation-therapy/unity/#slide2.

[50] R. de Jong, K. F. Crama, J. Visser, *et al.*, "Online adaptive radiotherapy compared to plan selection for rectal cancer: quantifying the benefit," *Radiat. Oncol.*, vol. 15, no. 1, pp. 1–9, Dec. 2020, ISSN: 1748-717X. DOI: 10.1186/s13014-020-01597-1.

[51] Y. Archambault, C. Boylan, D. Bullock, *et al.*, "Making on-line adaptive radiotherapy possible using artificial intelligence and machine learning for efficient daily re-planning," *Med Phys Intl J*, vol. 8, no. 2, 2020.

[52] P. H. Winston, *Artificial intelligence*. Addison-Wesley Longman Publishing Co., Inc., 1992.

[53] V. M. Systems, *Ethos Algorithms Reference Guide*, https://www.myvarian.com/s/productdocumentationdetail?lang=en&Id=0690h00000AcAu6AAF, Jun. 2021.

[54] R. de Jong, J. Visser, N. van Wieringen, J. Wiersma, D. Geijsen, and A. Bel, "Feasibility of Conebeam CT-based online adaptive radiotherapy for neoadjuvant treatment of rectal cancer," *Radiat. Oncol.*, vol. 16, no. 1, pp. 1–11, Dec. 2021, ISSN: 1748-717X. DOI: 10.1186/s13014-021-01866-7.

[55] R. Bijman, L. Rossi, T. Janssen, *et al.*, "MR-Linac Radiotherapy The Beam Angle Selection Problem," *Front. Oncol.*, vol. 11, 2021. DOI: 10.3389/fonc.2021.717681.

[56] V. E. M. Systems, *Ethos Therapy Clinical Cases*, 2020. [Online]. Available: https://varian.widen.net/view/pdf/bwhifcscii/EthosTherapyClinicalCases.pdf?u=bmxzem.

[57] M. J. Campbell, D. Machin, and W. S. J., *Medical Statistics Fourth Edition*. 2007.

[58] J.-P. J. E. Kleijnen, B. van Asselen, J. P. M. Burbach, *et al.*, "Evolution of motion uncertainty in rectal cancer: implications for adaptive radiotherapy," *Phys. Med. Biol.*, vol. 61, no. 1, pp. 1–11, Nov. 2015, ISSN: 0031-9155. DOI: 10.1088/0031-9155/61/1/1.

[59] H. Eijkelenkamp, M. R. Boekhoff, M. E. Verweij, F. P. Peters, G. J. Meijer, and M. P. W. Intven, "Planning target volume margin assessment for online adaptive MR-guided dose-escalation in rectal cancer on a 1.5 T MR-Linac," *Radiother. Oncol.*, vol. 162, pp. 150–155, Sep. 2021, ISSN: 0167-8140. DOI: 10.1016/j.radonc.2021.07.011.

Appendix A

Comparison DVH for both the IGRT and ART plan with the EQUI beam setup.

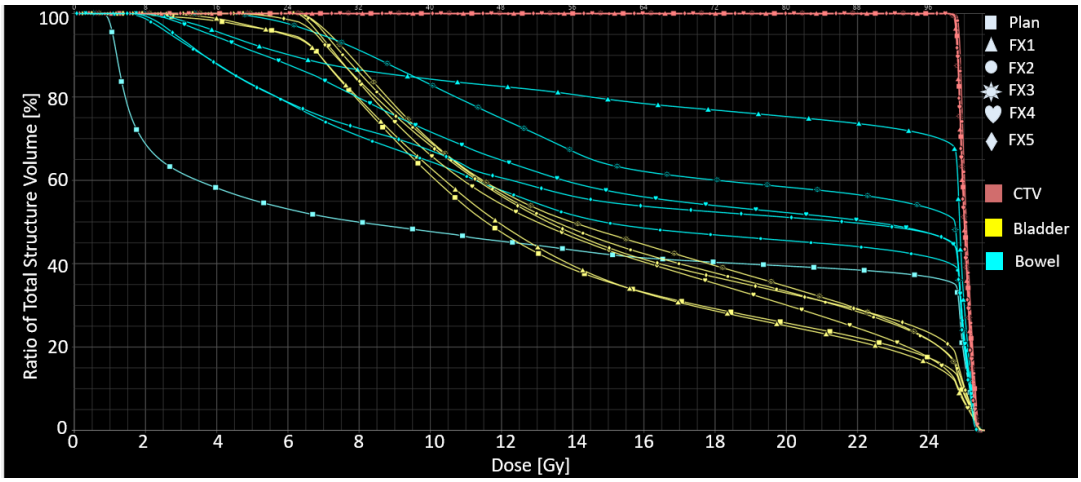

Figure 6.1: Comparison DVH of the plan and the five fractions for Patient 1 with the EQUI IGRT treatment. This patient is an example on when there were a small difference between the IGRT and ART treatments.

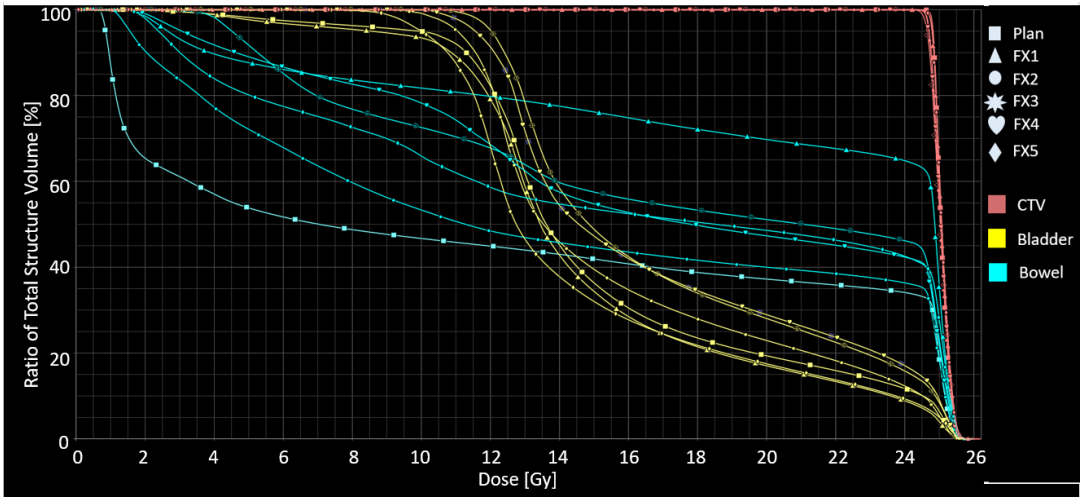

Figure 6.2: Comparison DVH of the plan and the five fractions for Patient 1 with the EQUI ART treatment. This patient is an example of when there were a small difference between IGRT and ART treatments.

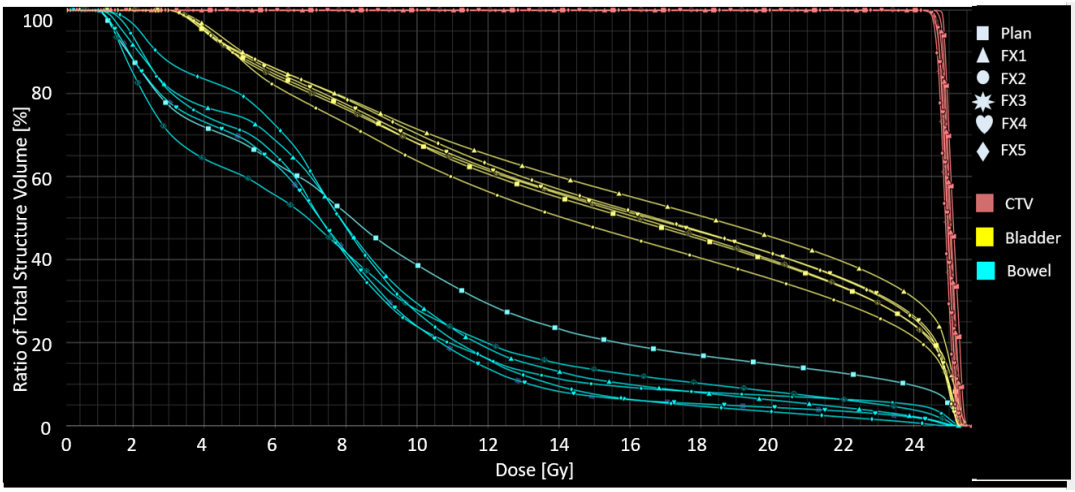

Figure 6.3: Comparison DVH of the plan and the five fractions for Patient 7 with the EQUI IGRT treatment. This patient is an example of when there were a greater difference between IGRT and ART treatments.

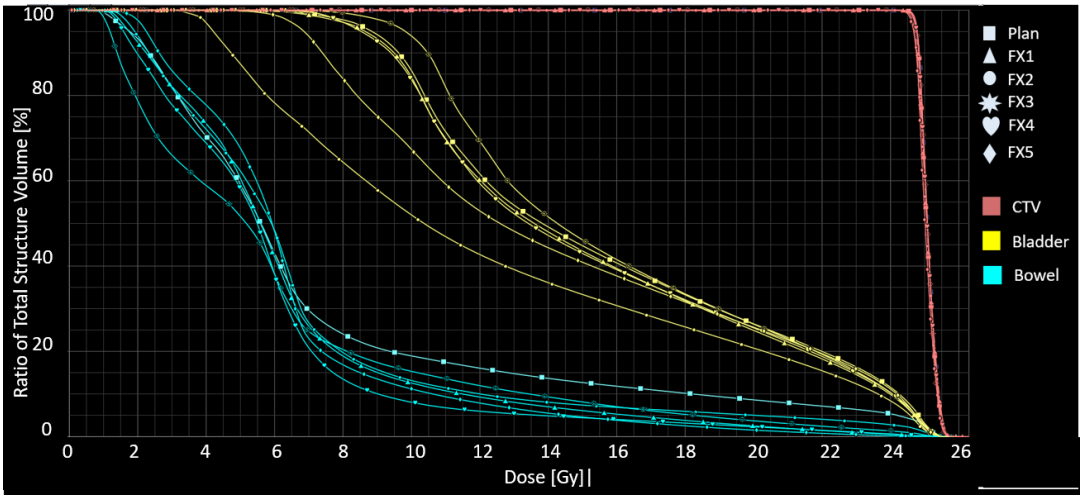

Figure 6.4: Comparison DVH of the plan and the five fractions for Patient 7 with the EQUI ART treatment. This patient is an example of when there were a greater difference between IGRT and ART treatments.

Appendix B

Plan Dose Report for a CS plan from Ethos TPS

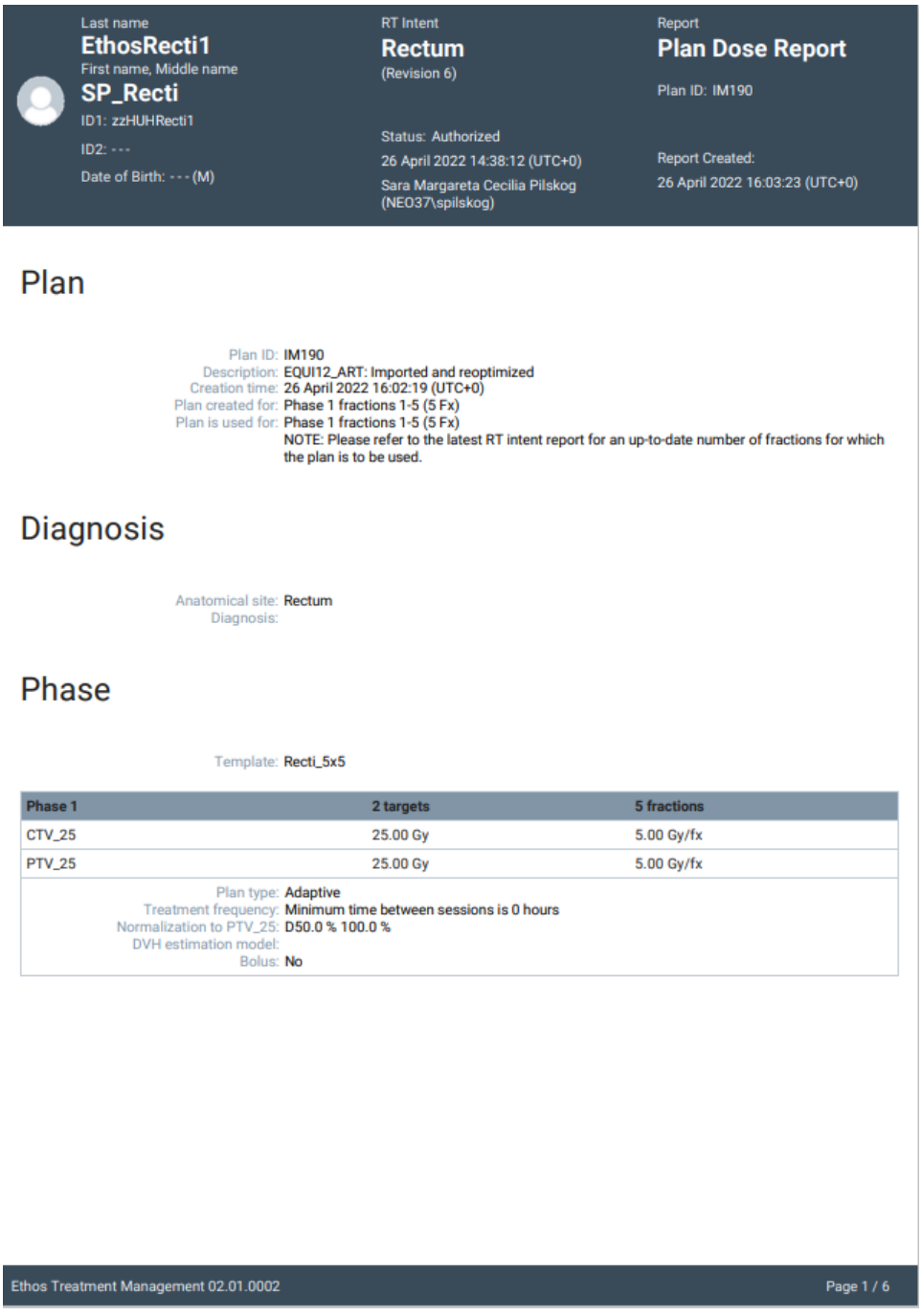

Last name
EthosRecti1
First name, Middle name
SP_Recti
ID1: zzHUHRecti1
ID2: - - -
Date of Birth: - - - (M)

RT Intent
Rectum
(Revision 6)
Status: Authorized
26 April 2022 14:38:12 (UTC+0)
Sara Margareta Cecilia Pilskog (NE037\spilskog)

Report
Plan Dose Report
Plan ID: IM190
Report Created:
26 April 2022 16:03:23 (UTC+0)

Plan

Plan ID: IM190
Description: EQUI12_ART: Imported and reoptimized
Creation time: 26 April 2022 16:02:19 (UTC+0)
Plan created for: Phase 1 fractions 1-5 (5 Fx)
Plan is used for: Phase 1 fractions 1-5 (5 Fx)
NOTE: Please refer to the latest RT intent report for an up-to-date number of fractions for which the plan is to be used.

Diagnosis

Anatomical site: Rectum
Diagnosis:

Phase

Template: Recti_5x5

Phase 1	2 targets	5 fractions
CTV_25	25.00 Gy	5.00 Gy/fx
PTV_25	25.00 Gy	5.00 Gy/fx

Plan type: Adaptive
Treatment frequency: Minimum time between sessions is 0 hours
Normalization to PTV_25: D50.0 % 100.0 %
DVH estimation model:
Bolus: No

Ethos Treatment Management 02.01.0002 Page 1 / 6

Clinical Goals and Achieved Values

Targets

CTV_25

	Goal	Achieved Value	Goal status
P2	D99.5 % (660.57 cm3) > 98.0 % (24.50 Gy) Var: D99.5 % (660.57 cm3) ≥ 95.0 % (23.75 Gy)	97.8 % (24.44 Gy)	Within variation

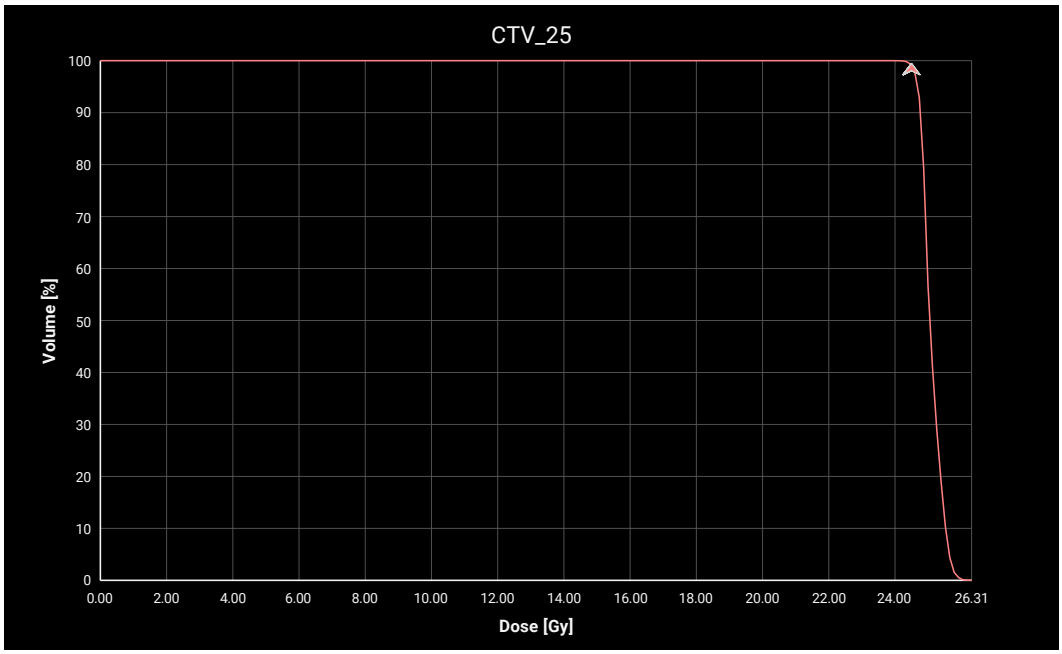

PTV_25

	Goal	Achieved Value	Goal status
P1	D98.0 % (924.93 cm3) ≥ 95.0 % (23.75 Gy) Var: D98.0 % (924.93 cm3) ≥ 94.0 % (23.50 Gy)	97.1 % (24.28 Gy)	Met
P2	Dmax(0.10 cm3) < 105.0 % (26.25 Gy) Var: Dmax(0.10 cm3) ≤ 107.0 % (26.75 Gy)	105.1 % (26.29 Gy)	Within variation

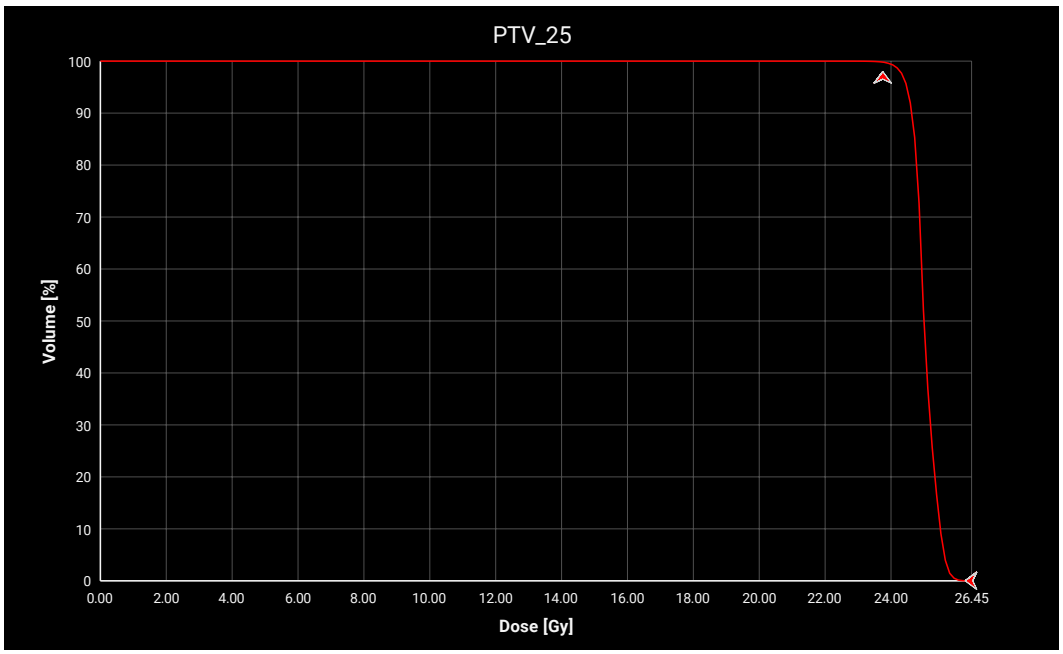

Organs

Bladder

	Goal	Achieved Value	Goal status
P3	Dmean ≤ 20.00 Gy Var: Dmean ≤ 25.00 Gy	12.15 Gy	Met

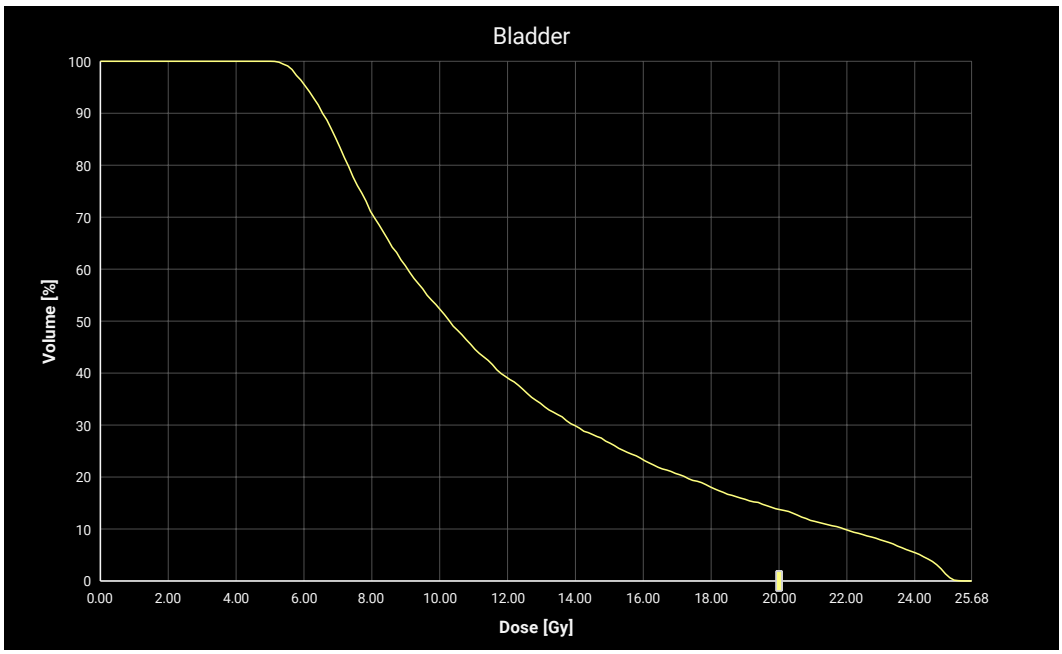

Bowel

	Goal	Achieved Value	Goal status
P2	V7.50 Gy < 173.00 cm3 Var: V7.50 Gy ≤ 260.00 cm3	87.88 cm3	Met
P2	V20.00 Gy < 68.00 cm3 Var: V20.00 Gy ≤ 105.00 cm3	44.81 cm3	Met
PR	V2.00 Gy < 100.0 % (302.82 cm3)	85.1 % (257.81 cm3)	Met
PR	V3.00 Gy < 100.0 % (302.82 cm3)	77.4 % (234.42 cm3)	Met
PR	V5.00 Gy < 100.0 % (302.82 cm3)	63.0 % (190.70 cm3)	Met
PR	V7.50 Gy < 100.0 % (302.82 cm3)	29.0 % (87.88 cm3)	Met
PR	V10.00 Gy < 100.0 % (302.82 cm3)	22.6 % (68.40 cm3)	Met
PR	V12.00 Gy < 100.0 % (302.82 cm3)	20.2 % (61.17 cm3)	Met
PR	V15.00 Gy < 100.0 % (302.82 cm3)	18.1 % (54.76 cm3)	Met
PR	V20.00 Gy < 100.0 % (302.82 cm3)	14.8 % (44.81 cm3)	Met
PR	V25.00 Gy < 100.0 % (302.82 cm3)	4.5 % (13.69 cm3)	Met

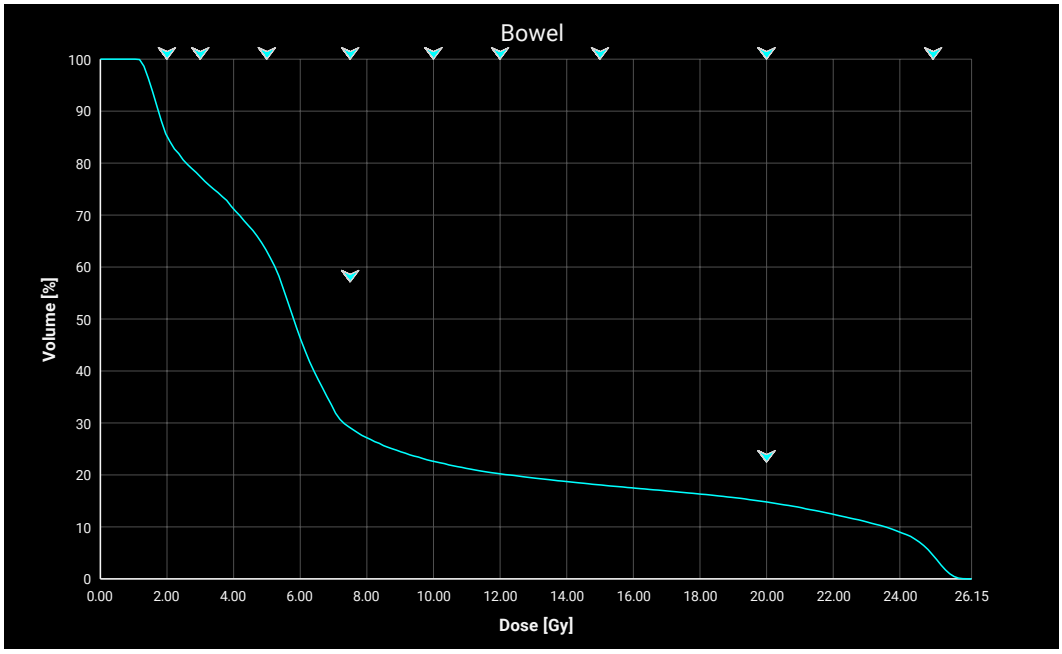

Global Maximum Dose: 26.58 Gy

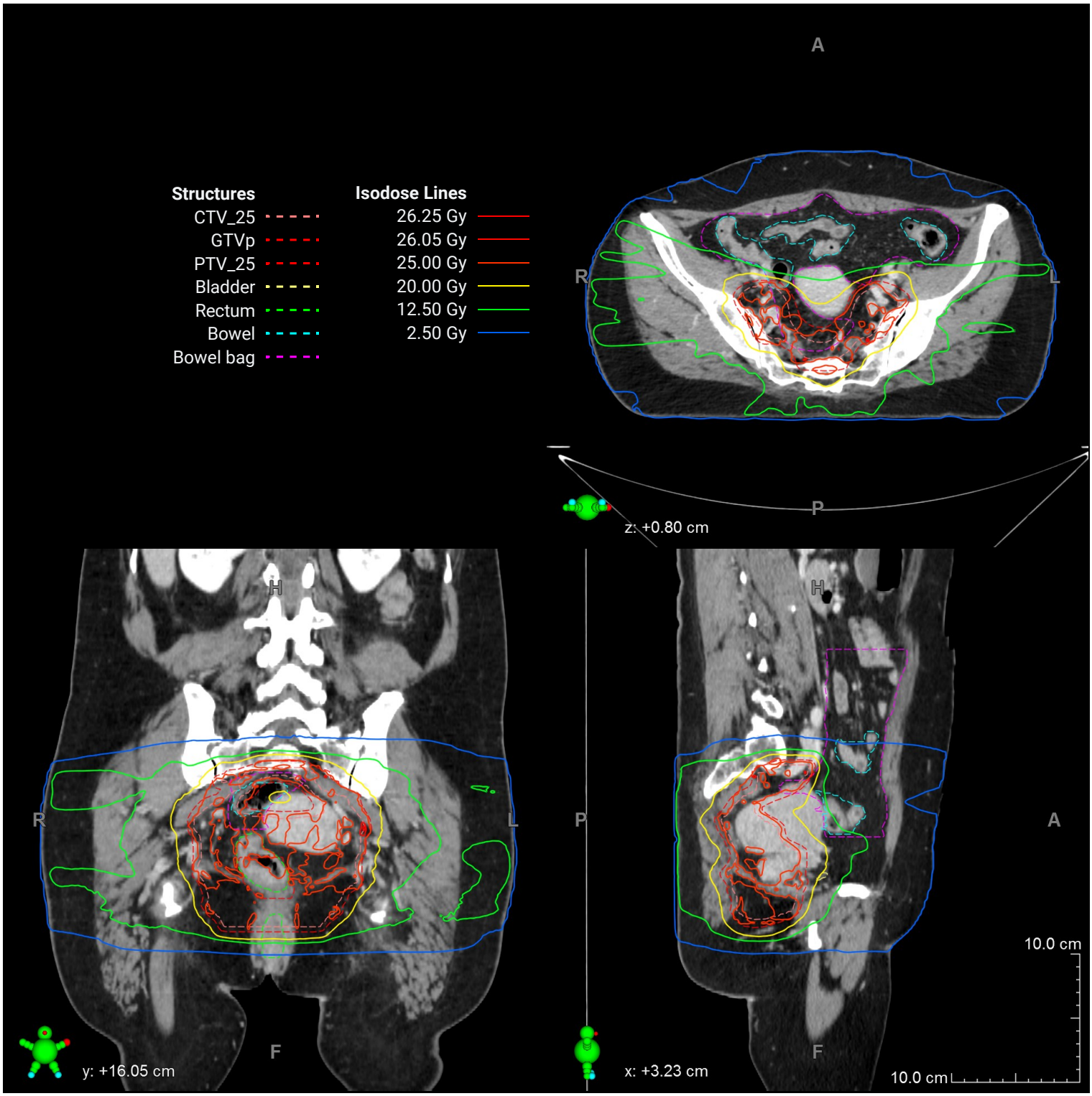

Warnings and errors

Plan validation

Warnings

1. The image CT scanner Philips Brilliance Big Bore 760038 HBEHUSAKMF02CT has not been calibrated. Using calibration curves from default CT scanner Philips Big Bore instead.

Plan

Planning directive

Phase 1	5 fx	2 targets
PTV_25	25.00 Gy	5.00 Gy/Fx
CTV_25	25.00 Gy	5.00 Gy/Fx

Normalization goal: PTV_25: DVH point 50.0% 25.00 Gy
Normalization factor: 0.997

Treatment unit

TPS name:	Ethos Treatment Planning	Particle type:	Photon
Treatment units:	RDSMCH1	Energy:	6 MV
Dose calibration depth:	1.30 cm	Primary fluence mode:	FFF

Fields

Treatment orientation: HFS

Isocenter 1
Position (DICOM) X: -0.53 cm Y: 14.80 cm Z: -4.53 cm
Scale IEC61217

Field name		Gantry [°]	Collimator [°]	MU
Field 1	IMRT	64.0°	10.0°	475.7 MU
Field 2	IMRT	84.0°	10.0°	304.2 MU
Field 3	IMRT	100.0°	10.0°	248.2 MU
Field 4	IMRT	140.0°	10.0°	408.1 MU
Field 5	IMRT	160.0°	10.0°	372.3 MU
Field 6	IMRT	192.0°	10.0°	473.7 MU
Field 7	IMRT	220.0°	10.0°	392.4 MU
Field 8	IMRT	260.0°	10.0°	286.3 MU
Field 9	IMRT	272.0°	10.0°	301.6 MU
Field 10	IMRT	280.0°	10.0°	313.3 MU
Field 11	IMRT	292.0°	10.0°	303.2 MU
Field 12	IMRT	300.0°	10.0°	475.4 MU

Total	4354.4 MU

Isocenter 1

Isocenter 1

X: -0.53 cm Y: 14.80 cm Z: -4.53 cm

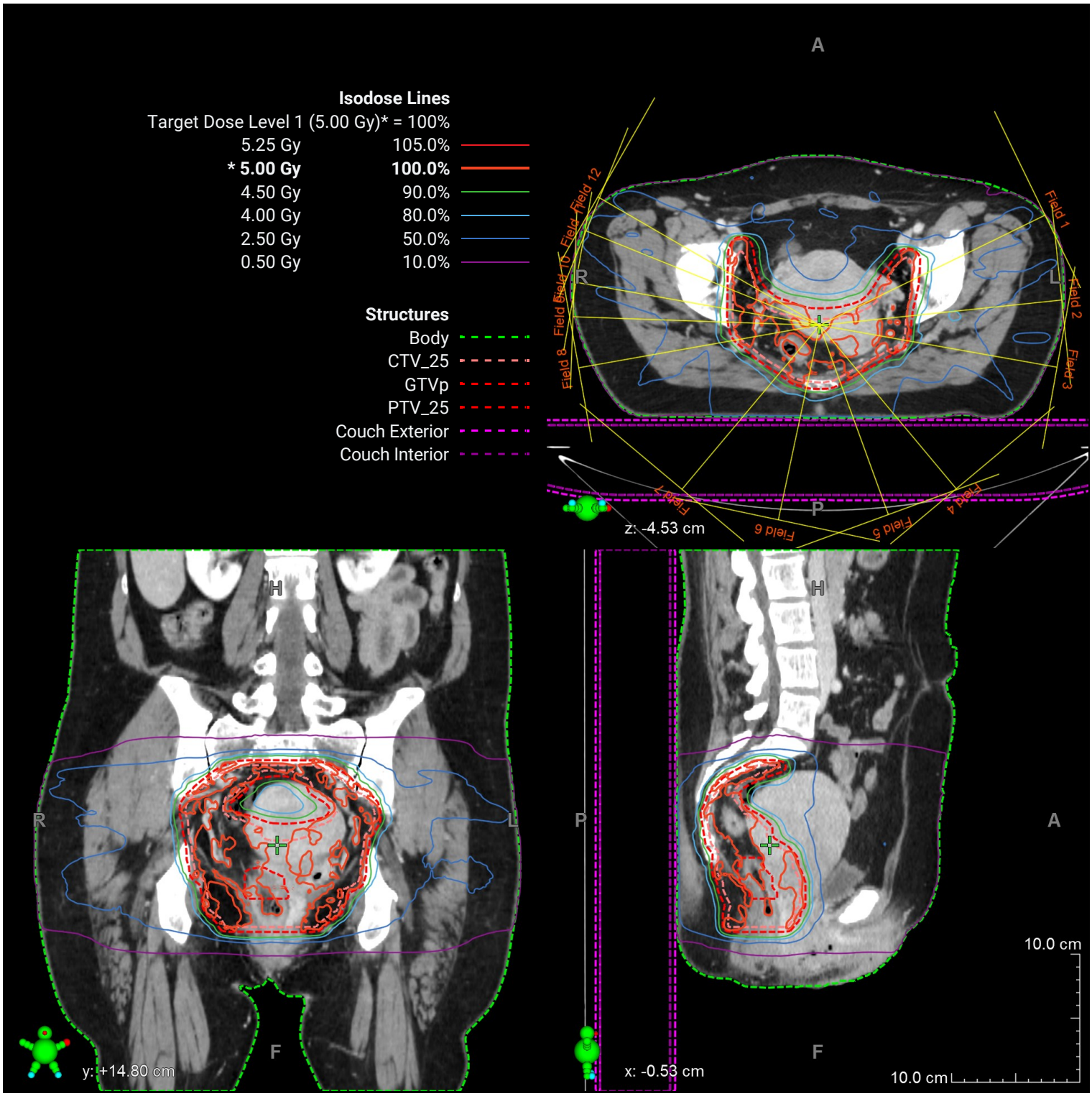

Summary

Dose

Grid size:	X: 158 Y: 91 Z: 211
Grid resolution:	X: 0.25 cm Y: 0.25 cm Z: 0.20 cm
Dose reporting condition:	Dose to medium, transport in medium

Primary image

ID:	Bekken + K, iDose (3)
Size:	X: 512 Y: 512 Z: 211
Resolution:	X: 0.09 cm Y: 0.09 cm Z: 0.20 cm
Acquisition time:	10 December 2021 11:24:25 (UTC+0)
CT scanner:	Philips Big Bore
Last approved by:	Carol Huang
Last approved on:	16 March 2021 10:43:48 (UTC+0)

Plan

DICOM UID:	1.2.246.352.800.572637956882289586 8.3417750095259815351

Technical structures

Simulation isocenter

Position (DICOM)	X: 0.47 cm Y: 11.92 cm Z: -0.20 cm

Couch plane

Position (DICOM)	X: -22.04 cm Y: 22.17 cm Z: -23.60 cm
Couch type:	Halcyon couch

Calculation logs

Plan optimization

Algorithm version: 1.1.2.44

Language of dose calculation log messages: EN.
Device used for GPU acceleration: Tesla P100-PCIE-16GB
Planning Algorithm Library version 2.3.0.43 62a4bb88fee885c296caf938d6677eace1bf324e
Device used for GPU acceleration: Tesla P100-PCIE-16GB
Beam data directory:
C:\ProgramData\SF\Calculation\Fabric\work\Applications\CalculationQueueWorker_App20\CalculationQueueWorkerServiceManifest.Algorithms.1.1.2.44.1.0.0\AutomatedPlanning.1.1.0001\BeamData//PO
Dose calculation algorithm = FTDCGPU
MLC Tongue and Groove width set to: Distal 0.040 cm, Proximal 0.056 cm.
Inhomogeneity correction = On
Air cavity correction = Off
Automatic feathering = Off
Field-grouping z-threshold = 30.00 mm
Dose calculation resolution = 2.50 mm
Structure resolution = 2.50 mm
Target projection margin = 6.00 mm
Automatic lower dose objective control = Off
Automatic target overlap control = On
IMRT minimum fluence factor = 0.000
Field 1: Fixed jaws on.
Field 2: Fixed jaws on.
Field 3: Fixed jaws on.
Field 4: Fixed jaws on.
Field 5: Fixed jaws on.
Field 6: Fixed jaws on.
Field 7: Fixed jaws on.
Field 8: Fixed jaws on.
Field 9: Fixed jaws on.
Field 10: Fixed jaws on.
Field 11: Fixed jaws on.
Field 12: Fixed jaws on.
Patient support device 'Structure: 9' used in dose calculation, material: 'Water', density: 0.724773 g/cm3.
Patient support device 'Structure: 10' used in dose calculation, material: 'Air', density: 0.001100 g/cm3.
Highest mass density in dose calculation: 2.049 g/cm3.
Volume of mass density higher than 2.0 g/cm3 used in automatic material assignment: 8.169 cm3.
Reporting dose to medium.
IMRT field normalization
Machine directory:
C:\ProgramData\SF\Calculation\Fabric\work\Applications\CalculationQueueWorker_App20\CalculationQueueWorkerServiceManifest.Algorithms.1.1.2.44.1.0.0\AutomatedPlanning.1.1.0001\BeamData//AXB/dmx/
Treatment unit: RDS_DMX, energy: 6X-FFF
Calculation is using Preconfigured Beam Data version 4.0.
MLC Tongue and Groove width set to: Distal 0.040 cm, Proximal 0.056 cm.
The automated planning task took 99.178 seconds.

Dose calculation

Algorithm version: 1.1.2.44

Messages
Structure with type "PatientSupportDevice" and name "Couch Exterior" is used in dose calculation. The density of the structure is 0.725 g/cm3 and the material is "Water".
Structure with type "PatientSupportDevice" and name "Couch Interior" is used in dose calculation. The density of the structure is 0.001 g/cm3 and the material is "Air".
The image size is expanded to fully include the patient support device structures.
Language of dose calculation log messages: EN.
AcurosCalculationOptions.AutomaticHighDensityMaterial__ = Bone
AcurosCalculationOptions.CalculationGridSizeInCM = 0.250
AcurosCalculationOptions.DoseReportingMode = Dose to medium
AcurosCalculationOptions.FieldNormalizationType = No field normalization
AcurosCalculationOptions.HeterogeneityCorrection = ON
AcurosCalculationOptions.MaximumAutomaticHighDensityVolumeInCM3__ = 1.000
AcurosCalculationOptions.PlanDoseCalculation = ON
AcurosCalculationOptions.UseGPU = Yes
Machine directory:
C:\ProgramData\SF\Calculation\Fabric\work\Applications\CalculationQueueWorker_App20\CalculationQueueWorkerServiceManifest.Algorithms.1.1.2.44.1.0.0\DoseCalculationTask.1.1.0001\AcurosBeamData\/dmx/
Treatment unit: RDS_DMX, energy: 6X-FFF
Calculation is using Preconfigured Beam Data version 4.0.
Patient support device 'Couch Exterior' used in dose calculation, material: 'Water', density: 0.724773 g/cm3.
Patient support device 'Couch Interior' used in dose calculation, material: 'Air', density: 0.001100 g/cm3.
The following MLC dosimetric parameters read from MLC add-on beam data are used in dose calculation.
Distal MLC TnG step width = 0.040 cm.
Proximal MLC TnG step width = 0.056 cm.
MLC dosimetric leaf gap = 0.010 cm.
MLC leaf transmission factor = 0.005 .
MLC Tongue and Groove width set to: Distal 0.040 cm, Proximal 0.056 cm.
Fluence Pixel Size 1.250x1.250 mm2.
Effective interleaf gap = 0.00079 cm.
Modulation factor: 1.6831.
Modulation factor: 2.5691.
Modulation factor: 1.9724.
Modulation factor: 2.4143.
Modulation factor: 1.7990.
Modulation factor: 2.4733.
Modulation factor: 2.4684.
Modulation factor: 2.3109.
Modulation factor: 2.5299.
Modulation factor: 1.1246.
Modulation factor: 1.8542.
Modulation factor: 1.7230.
Highest mass density in dose calculation: 2.049 g/cm3.
Volume of mass density higher than 2.0 g/cm3 used in automatic material assignment: 8.023 cm3.
Reporting dose to medium.
Flattening MLC sequence recognized on a Halcyon machine. IMRT normalization is not used, but instead the field normalization follows the regular normalization rules for a static field.
No field normalization
The dose calculation task took 44.606 seconds.

Current Plan Approval Status

Clinical Approval: Approved. 29 April 2022 08:46:44 (UTC+0), Sara Margareta Cecilia Pilskog, NEO37\spilskog

Technical Approval: Approved. 29 April 2022 08:46:58 (UTC+0), Sara Margareta Cecilia Pilskog, NEO37\spilskog

Plan Approval Log

29 April 2022 08:46:58 (UTC+0) — Technical approval added. Sara Margareta Cecilia Pilskog (NEO37\spilskog)
Note:

29 April 2022 08:46:44 (UTC+0) — Clinical approval added. Sara Margareta Cecilia Pilskog (NEO37\spilskog)
Note:

Appendix C

Abstract submitted to MedFys 2022.

Reducing bowel toxicity for rectal cancer with CBCT-based online adaptive radiotherapy

Karoline Lewinsen[1], Liv Bolstad Hysing[1,2], Johanna Austrheim Hundvin[2], Sara Pilskog[1,2]

[1]Institute of Physics and Technology, University of Bergen, Bergen, Norway, kle018@uib.no

[2]Department of Oncology and Medical Physics, Haukeland University Hospital, Bergen, Norway

Purpose: Daily motion of the rectum requires large PTV margins for patients undergoing radiotherapy (RT) for their rectal cancer. Online adaptive RT (ART) uses daily CBCT for adjusting the plan to the anatomy of the day, and therefore has potential to reduce PTV margins. In this master, the purpose is to investigate online ART to spare the bowel and bladder. Initially, we focus on beam angles to spare bowel.

Methods: All IMRT dose plans were derived for short course RT 5x5Gy, motivated by the update in the national guidelines for rectal cancer. The CTV for standard RT was expanded with 8mm in all directions except in the ventral direction where it was 10mm. The PTV margin with online ART was 5mm in all directions. We used a 9-field class solution (CS) with gantry angles set to 64,84,100,140,160,192,220,260, and 292° and a 9-fields IMRT with equidistant (EQUI) angles, where the first gantry is sat to 20°, with 40° intervals. These two field configurations were applied to online ART and standard delivery. We compared the dose to the bowel bag and the bladder in the 4 IMRT plans. The risk for grade 3 (G3) diarrhea was quantified from a dose-response relationship for rectal cancer with 10Gy of the bowel bag as input.

Results: Preliminary results are given for one patient. The $D_{98\%}$>95% and D_{max}<107% of the PTV were fulfilled for all IMRT plans. For the 9-field EQUI with standard RT the risk of G3 diarrhea was calculated to 16%, and reduced to 14% for online ART. For the 9-field CS the toxicity was 15% and 14% for standard and adaptive delivery.

Conclusion: CBCT-based online ART shows potential in reduction of the toxicity risk. Small reductions were achieved from altered beam angles. We will next add more patients and assessment of delivery doses.